Structural basis for differential electron flux in human methionine synthase reductase and cytochrome P450 reductase

by

Carla Erin Meints

B.Sc., University of British Columbia, 2010

A THESIS SUBMITTED IN PARTIAL FULFILLMENT OF
THE REQUIREMENTS FOR THE DEGREE OF

DOCTOR OF PHILOSOPHY

in

THE COLLEGE OF GRADUATE STUDIES

(Biochemistry and Molecular Biology)

THE UNIVERSITY OF BRITISH COLUMBIA

(Okanagan)

April 2015

Abstract

Human diflavin oxidoreductases, methionine synthase reductase (MSR) and cytochrome P450 reductase (CPR), share overall structural organization, substrate specificity, and direction of electron flow. However, MSR exhibits repressed catalytic activity and weak substrate binding compared to CPR. In this study, we identified structural features that control the differential kinetic properties of these flavoenzymes. Single point mutations in the MSR and CPR active sites were studied by steady state and pre-steady state absorbance spectrophotometric techniques to reveal structure-function relationships.

In the research first chapter, we investigated the role of a conserved tryptophan in MSR that lies coplanar with the FAD cofactor. Reducing the side chain size resulted in a 1.5- and >400-fold tighter NADPH binding affinity in W697H and W697S and lowered the preference for NADPH over NADH. W697H also accelerated flavin reduction by 4.6-fold. Thus, the energetic cost of Trp697 displacement by the nicotinamide ring presents an energy barrier to NADPH binding. Consequently, Trp697 regulates coenzyme affinity, and coenzyme preference by ensuring initial recognition of the 2',5'-ADP moiety. The second research chapter evaluated the effect of more conservative mutations, W697Y and W697F, that resulted in improved coenzyme binding affinity and 9-fold accelerated flavin reduction. Equivalent mutations in CPR slowed flavin reduction. Thus, Trp697 gates hydride transfer in MSR, but not in CPR. Instead, following hydride transfer, electron flow in CPR is limited by displacement of the oxidized nicotinamide ring. This is supported by the 46-fold faster flavin reduction of the 2'-phosphate-binding site variant K602AV603K which weakened coenzyme affinity.

In the third research chapter, we analyzed the role of FAD proximal His322 which is within hydrogen bonding distance to the catalytic triad residue Asp674 in CPR. The equivalent residue in MSR is Ala312. Through reciprocal mutagenesis, we found that H322A had stronger affinity for NADPH but slower flavin reduction, while A312H weakened coenzyme affinity. His322 is proposed to weaken coenzyme binding affinity by competing with the nicotinamide ring for electrostatic interaction with Asp674, thereby accelerating $NADP^+$ release and electron flow through CPR.

The final research chapter shifted to the conserved FAD-stacking tryptophan residue (Trp704) in plant CPR from *Artemisia annua* (AaCPR) for an additional perspective on

overall CPR catalysis. The steady state and pre-steady state data revealed that Trp704 also triggers $NADP^+$ release, however this step is not as critical for electron flux in AaCPR compared to human CPR.

Preface

The work presented in Chapter 2 has been published: [Carla E. Meints], Frida S. Gustafsson, Nigel S. Scrutton, and Kirsten R. Wolthers (2010). Tryptophan 697 modulates hydride and interflavin electron transfer in human methionine synthase reductase. Biochemistry. 50: 11131-11142. I designed, expressed, and purified the enzyme variants. I also measured all the steady state and pre-steady state kinetics for each variant via UV-visible spectrophotometry and stopped-flow experiments. Frida Gustafsson was an undergraduate student working with me on the project. The manuscript was drafted by Dr. Kirsten R. Wolthers with editorial comments by Dr. Nigel Scrutton.

A portion of Chapter 3 has been published with the exception of the coenzyme-binding residue mutations: [Carla E. Meints], Svetlana Simtchouk, Kirsten R. Wolthers (2013). Aromatic substitution of the FAD-shielding tryptophan reveals its differential role in regulating electron flux in methionine synthase reductase and cytochrome P450 reductase. FEBS Journal. 280: 1460-1474. Svetlana Simtchouk generated and expressed the tryptophan variants of CPR and conducted some of the kinetic experiments. I carried on the work by designing, expressing and purifying all other variants. I measured all the steady state and pre-steady state kinetics for each variant via UV-visible spectrophotometry and stopped-flow methods. I also measured the redox potentials of specified CPR variants. I analyzed the results and contributed to the discussion and overall preparation of the manuscript with Dr. Kirsten R. Wolthers.

The work of Chapter 4 has been published with the exception of the MSR hinge data. [Carla E. Meints], Sarah M. Parke, and Kirsten R. Wolthers (2014). Proximal FAD histidine residue influences interflavin electron transfer in cytochrome P450 reductase and methionine synthase reductase. Archives of Biochemistry and Biophysics. 547: 18-26. Sarah M. Parke was an undergraduate student that assisted me on the project. I designed, expressed, and purified each variant. I also conducted the steady state and pre-steady state kinetic experiments. With the assistance of Sarah, the redox potentials of the specified variants were determined. I analyzed the results and contributed to manuscript preparation with Dr. Kirsten R. Wolthers.

Chapter 5 was based on work conducted by myself in Dr. Kirsten R. Wolthers' enzymology lab. I designed and expressed the variants as well as performed all the steady state

and pre-steady state kinetic experiments through UV-visible and stopped-flow spectrophotometric methods. I compiled, analyzed the results, and wrote the chapter with editorial comments from Dr. Kirsten R. Wolthers.

I also co-authored the following paper during my PhD study: Svetlana Simtchouk, Jordan L. Eng, [Carla E. Meints], Caitlyn Makins, and Kirsten R. Wolthers (2013). Kinetic analysis of cytochrome P450 reductase from *Artemisia annua* reveals accelerated rates of NADPH-dependent flavin reduction. FEBS Journal. 280: 6627-6642. I was involved in the pre-steady state kinetic experimentation and analysis, as well as figure preparation.

Table of Contents

List of Tables

List of Figures

List of Abbreviations

2',5'-ADP	adenosine 2',5'-diphosphate
AaCPR	cytochrome P450 reductase from *Artemisia annua*
ABS	Antley-Bixler Syndrome
AdoMet	S-adenosylmethionine
AMP	adenosine monophosphate
ATP	adenosine triphosphate
CH_3THF	methyltetrahydrofolate
CoA	coenzyme A
CPR	cytochrome P450 reductase
CT	charge-transfer
CYP71AV1	cytochrome P450 71AV1
DAAO	D-amino acid oxidase
DNA	deoxyribonucleic acid
dNTP	deoxyribonucleotide triphosphate
DTT	dithiothreitol
EDTA	ethylenediaminetetraacetic acid
ETF	electron-transferring flavoprotein
FAD	flavin adenine dinucleotide (quinone)
$FADH_2$	flavin adenine dinucleotide, reduced (hydroquinone)
FeCN	ferricyanide $Fe(CN)_6{}^{3-}$
FMN	flavin mononucleotide (quinone)
$FMNH_2$	flavin mononucleotide, reduced (hydroquinone)
FNR	ferredoxin NADP(H)-dependent reductase
GST	glutathione-S-transferase
Hepes	4-(2-hydroxyethyl)-1-piperazineethanesulfonic acid
IPTG	isopropyl β-D-1-thiogalactopyranoside
ITC	isothermal titration calorimetry
k_{cat}	catalytic turnover number
k_{cat}/K_m	catalytic efficiency

K_d	dissociation constant
kDa	kilodaltons
K_i	inhibition constant
KIE	kinetic isotope effect
K_m	Michaelis-Menten constant
KPi	potassium phosphate
LB	Luria-Bertani broth
MetH	methionine synthase from *Escherichia coli*
MS	methionine synthase
MSR	methionine synthase reductase
MTRR	gene encoding for MSR
NADH	nicotinamide adenosine dinucleotide, reduced
NAD^+	nicotinamide adenosine dinucleotide, oxidized
NADPD	(R)-[4-^{2}H]-NADPH
NADPH	β-nicotinamide adenosine diphosphate, reduced
$NADP^+$	β-nicotinamide adenosine diphosphate, oxidized
NMDA	N-methyl-D-aspartate
NMN	nicotinamide mononucleotide
NMR	nuclear magnetic resonance
NOS	nitric oxide synthase
NR1	human novel reductase 1
PCR	polymerase chain reaction
PDA	photodiode array
PDB	protein data bank
PM	photomultiplier
PMSF	phenylmethylsulfonyl fluoride
POR	gene encoding for CPR
SVD	singular value decomposition
TAPS	N-tris(hydroxymethyl)methyl-3-aminopropanesulfonic acid
THF	tetrahydrofolate
TPNH	triphosphopyridine nucleotide, reduced (NADPH)
Tris	tris(hydroxymethyl)aminomethane
UV	ultraviolet

Acknowledgments

I would first like to full-heartedly thank Dr. Kirsten Wolthers for providing invaluable guidance, advice, and patience throughout my graduate studies and, especially, during thesis writing. Thank you for giving me this opportunity, my academic career began and continues with your support and encouragement.

I would also like to thank my committee members: Drs. Al Vaisius, Jim Bailey, and Kevin Smith. Thank you all for taking the time to listen to my multiple mutagenesis adventures some of which were quite interesting, while others were only moderately interesting. Special thanks to Dr. Jim Bailey for allowing me to use the Ag/Cl and platinum electrodes for redox potentiometry studies and for helpful troubleshooting discussions. I am grateful to Dr. Kevin Smith for taking pity on me and letting me into his lab to pilfer liquid nitrogen on numerous occasions. I would also like to thank Dr. Al Vaisius for first getting me hooked on biochemistry and proteins during my undergraduate degree.

Finally, I would not have made it this far without the unwavering support of my parents Tim and Blanche, my stepdad Ken, and the other legs to the redheaded tripod Phillip and Sarah. Through all the stress, you were all there to encourage me to keep pushing forwards. Through all the success, you were all there to celebrate with me.

Dedication

This thesis is dedicated to the SF-61DX2 Stopped-flow System and glove box. Many nights were spent hand-in-hand with the glove box, attempting to deconvolute diflavoenzyme spectra...

Chapter 1

Introduction

1.1 Flavin-dependent Enzymes

1.1.1 Biological Prevalence and Diversity

Flavin-dependent enzymes are ubiquitous throughout nature and are necessary for maintaining the living condition of all known organisms. Approximately 1-3% of prokaryotic and eukaryotic genomes encode for proteins that use flavins.[1,2] Of the estimated 19 000 protein-encoding genes in humans, 89 genes have been identified that encode for flavin-binding proteins.[3–5] The majority of these flavoenzymes catalyze electron transfers between obligate two-electron donors (e.g. NADPH, NADH) and one-electron acceptors (e.g. metals, oxygen).[5] For this reason, flavoenzymes are common participants in the electron transport chain of major energy metabolic pathways such as oxidative phosphorylation and photosynthesis.[6] The ability for the flavin cofactor to harvest light energy also enables it to function in light-dependent reactions such as DNA repair and circadian rhythm regulation.[7,8] Flavoproteins are further utilized in the metabolism of carbohydrates, amino acids, lipids and nucleic acids, as well as a host of other biochemical processes as illustrated in Figure 1.1.[9,10]

1.1.2 Flavin Discovery

In 1879, an English chemist named Alexander Blyth isolated a yellow compound from cow's milk and named it lactochrome.[11] Over fifty years later, two independent research groups lead by chemists Richard Kuhn and Paul Karrer, solved the chemical structure of the yellow compound, and it was renamed riboflavin: ribo- for the ribityl side chain and -flavin from the Latin word for yellow *flavius*, Figure 1.2.[12–14] While the riboflavin chemical structure was still being determined, Otto Warburg isolated the first flavin-binding protein, Old Yellow Enzyme, during his work on the mechanism of biological respiration.[14,15] Following Warburg's work, Hugo Theorell treated this protein with ammonium sulfate at low pH, which produced a white protein precipitate and a yellow nonprotein supernatant. Both layers lost the NADPH oxidase activity observed in the untreated protein.[14,16] However, mixing the yellow supernatant with the resuspended protein at the physiological pH restored activity, indicating that both components are required for chemistry. Theorell

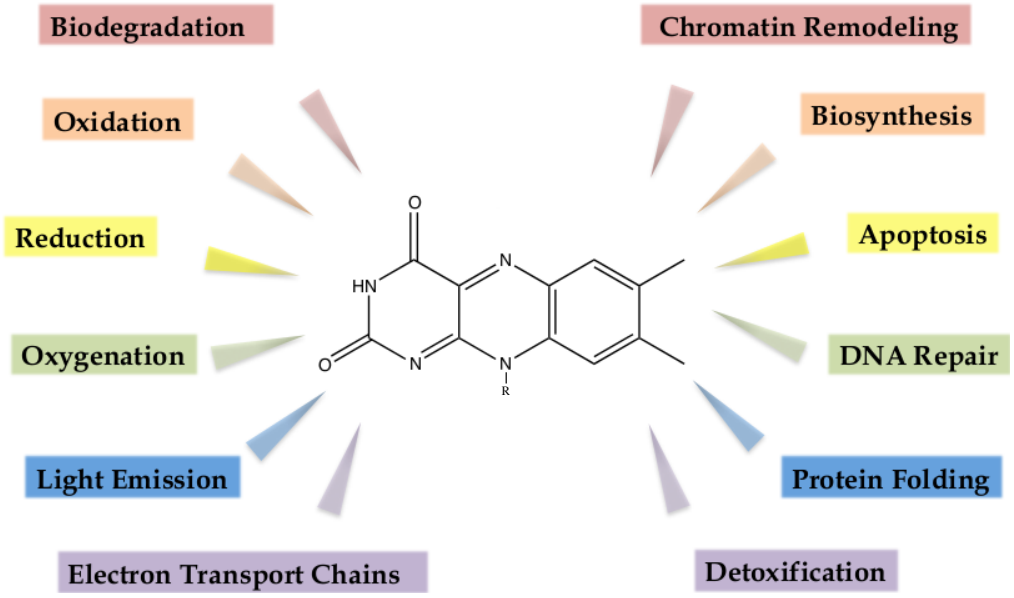

Figure 1.1: Diversity of flavin-dependent biochemical processes. Figure is adapted from van Berkel and Joosten.[9]

later identified the yellow component as a phosphorylated riboflavin, flavin mononucleotide (FMN), shown in Figure 1.2. Three years later, Warburg and Christian conducted a similar experiment on D-amino acid oxidase and determined the yellow nonprotein component to be the condensation product of FMN and adenosine monophosphate (AMP), flavin adenosine dinucleotide (FAD), as shown in Figure 1.2.[14,17]

1.1.3 Biological Sources of Flavins

Flavin cofactors, FMN and FAD, are derived from the water-soluble dietary precursor riboflavin, an essential growth factor also known as vitamin B_2. Plants and most microorganisms can synthesize riboflavin. However animals, rare prokaryotic and eukaryotic microorganisms cannot and must obtain it from exogenous sources.[18,19] Dietary sources include milk and dairy products, meats, fatty fish, and green vegetables. A secondary source of riboflavin is provided by natural microflora of the large intestine.[18] In foods, most of vitamin B_2 is derived from flavin-bound enzymes.[20] As the enzymes are digested, the flavin cofactors are hydrolyzed by nonspecific diphosphatases and liberated as free riboflavin in the intestinal lumen.[20,21] Free riboflavin is absorbed by small intestine enterocytes while colonocytes absorb riboflavin produced by large intestine microflora.[21,22] Once across the cellular membrane, riboflavin is phosphorylated by riboflavin kinase to yield FMN in the reaction shown in Figure 1.3. Phosphorylation serves as a metabolic trap to prevent dif-

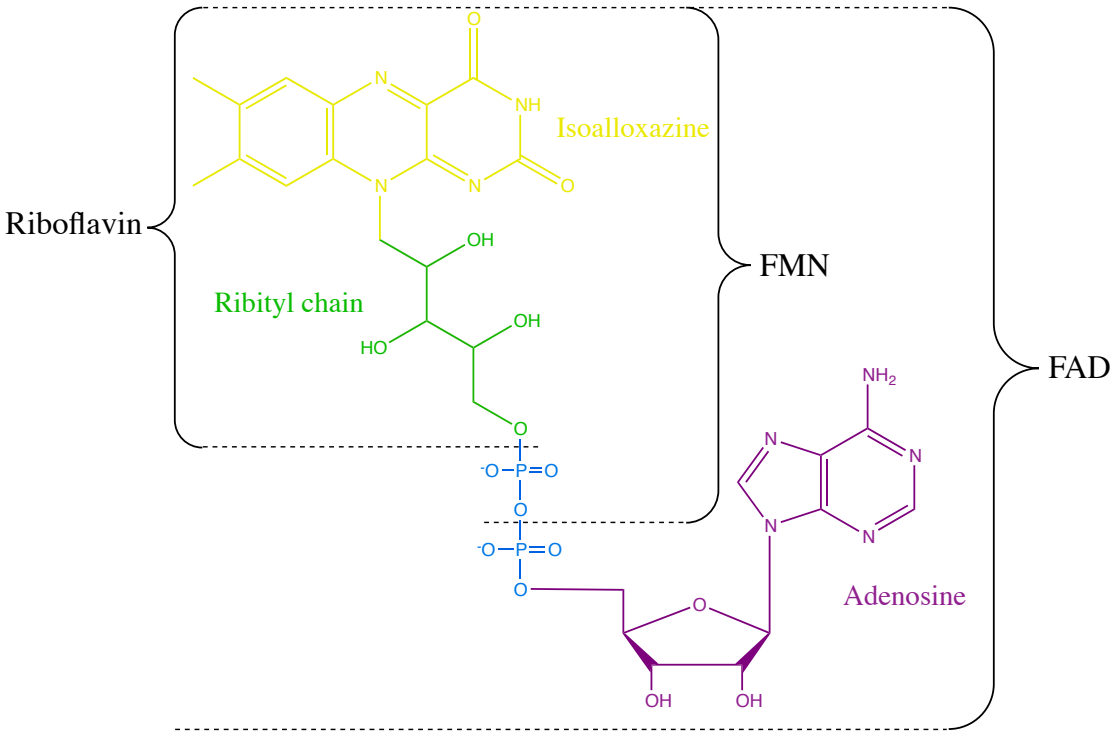

Figure 1.2: Chemical structure of riboflavin, flavin mononucleotide (FMN) and flavin adenosine dinucleotide (FAD). The isoalloxazine ring, the ribityl chain, phosphate groups, and adenosine are coloured in yellow, green, blue, and purple, respectively.

fusion of free riboflavin out of the cell, which can be quickly excreted through the urinary system.[20,21] Available FMN can be converted to FAD by an adenylylation catalyzed by FMN adenylyltransferase as shown in Figure 1.3. Blood plasma proteins, albumin and certain immunoglobins bind and protect riboflavin and its derivatives for transport within the bloodstream to target tissues.[21,23] Upon arrival, the flavins are incorporated into newly synthesized flavin-dependent enzymes.

1.1.4 Flavin Structure

The versatile chemistry of flavins arises from the chemically active isoalloxazine ring: 7,8-dimethylbenzo[g]pteridine-2,4(3H,10H)-dione. It can exist in three redox states: fully oxidized quinone, semiquinone (one-electron reduced), and hydroquinone (two-electron reduced), see Figure 1.4. Each of these states can exist in a pH-dependent protonated, deprotonated, or ionic form.[24] The oxidized quinone has a highly conjugated ring system that is responsible for its visible absorbance properties. It is a brilliant yellow colour with maximal absorbance peaks at 360 and 450 nm as shown in the spectral profile of a flavoenzyme in the oxidized state (Figure 1.5). The neutral semiquinone is blue with a broad absorbance maximum from 580-625 nm. The unpaired electron on the semiquinone is partially stabilized through delocalization in the conjugated ring.[25] Noncovalent or covalent interactions between the flavin and protein can act to destabilize or further stabilize the semiquinone form.[14] In the hydroquinone state, conjugation is interrupted and creates the leuco (bleached) form which causes an absorbance loss at 450 nm. This electron-rich flavin can participate as a one-electron donor, a two-electron donor via hydride transfer, or act as a nucleophile at N5 or C4a atoms (see Figure 1.4 for atom numbering).[2]

In most flavoenzymes, the flavin is bound through noncovalent interactions with local amino acids.[26] The binding affinity is typically in the nanomolar range or lower, so the flavin is considered a nondissociable prosthetic group rather than a dissociable coenzyme.[2] Catalytic function, substrate specificity, substrate stereochemistry and flavin redox potential have all been found to be influenced by the protein environment surrounding the cofactor.[2,14,26] For example, local protein interactions can finely tune the reactivity of the oxidized isoalloxazine ring, given that it is a highly polarizable molecule.

A few flavoenzymes form a covalent linkage with the C8a or C6 positions on the isoalloxazine ring. The side chains of histidine, cysteine or tyrosine residues participate in the covalent linkage.[27] Covalent linkage has been proposed to be involved in protein stability, oxygen reactivity, and controlling the cofactor redox potential. It has also been shown to suppress deleterious modifications of the flavin during catalysis. For example, the covalent linkage at C6 of FMN in trimethylamine dehydrogenase prevents formation of inactive 6-hydroxy FMN.[27]

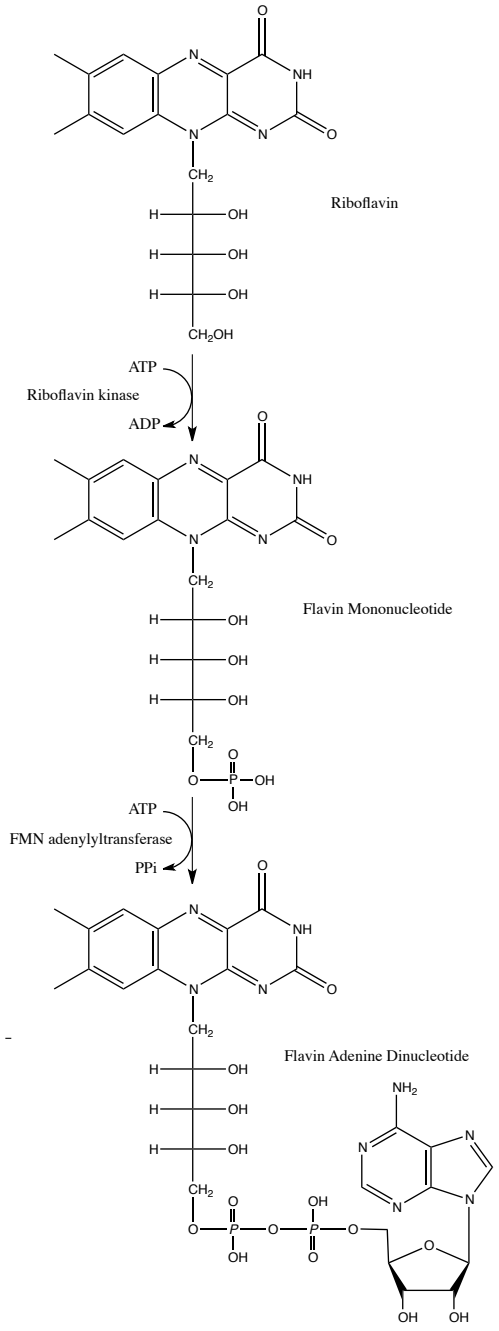

Figure 1.3: Biosynthetic pathway of FMN and FAD from the riboflavin precursor.

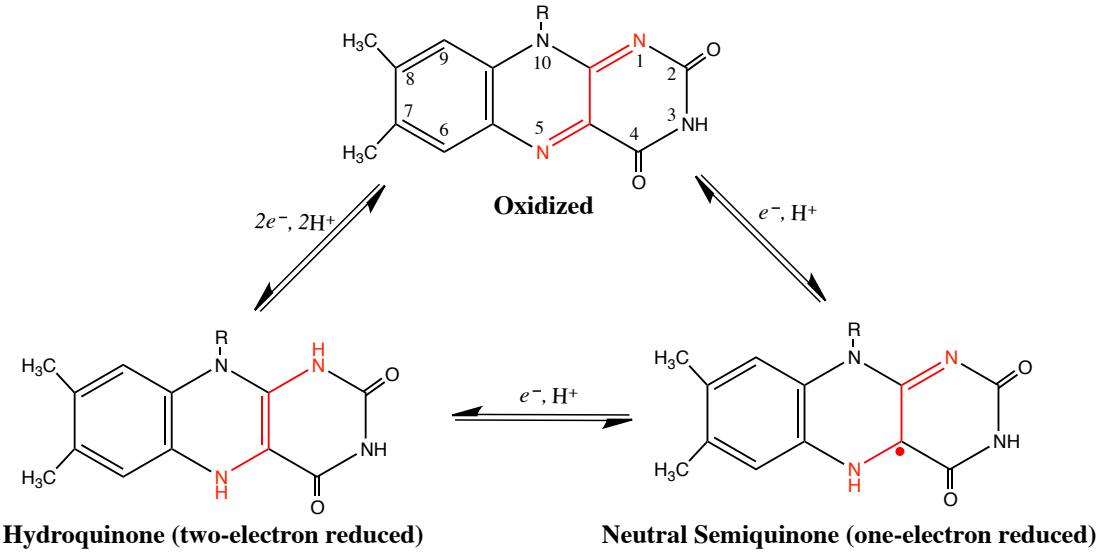

Figure 1.4: Reductive and oxidative half-reactions of flavin isoalloxazine ring. Red illustrates the bonds across which the electrons are redistributed.

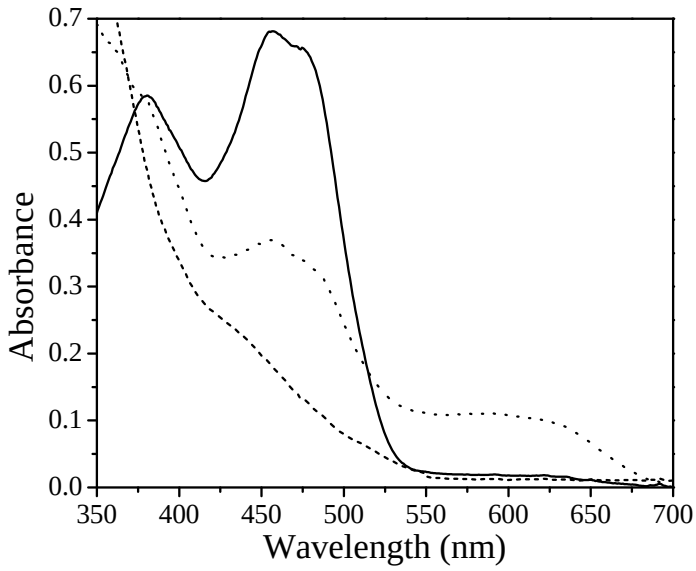

Figure 1.5: Spectral profile of the flavoenzyme cytochrome P450 reductase in the oxidized (solid), semiquinone (dotted) and fully reduced states (dashed).

1.1.5 Common Flavin-Catalyzed Reactions

Flavoenzyme catalysis typically consists of two separate half-reactions where the bound flavin alternates between oxidized and reduced states, shown in Figure 1.6. In the reductive half-reaction, an electron donor is oxidized and the flavin is reduced whereas in the oxidative half-reaction, an electron acceptor is reduced and the flavin is oxidized. In the oxidoreductase class of flavoenzymes, both the oxidative and reductive half-reactions involve one- or two-electron transfers between redox active groups, such as metal centers and pyridine nucleotides. An example of an oxidoreductase is ferredoxin-NADP(H) reductase, which be discussed in greater detail later in this chapter. Below are examples of how other classes of flavoenzymes, dehydrogenase, oxidase and monooxygenase, employ different mechanisms in their oxidative and reductive half-reactions to catalyze a great diversity of chemical reactions.

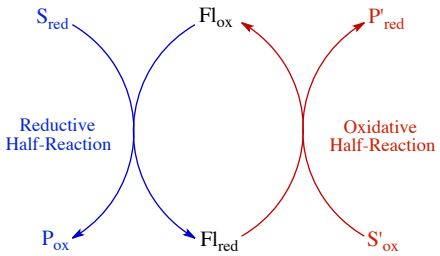

Figure 1.6: Oxidative and reductive half-reactions of typical flavoenzymes.

Mammalian acyl-Coenzyme A (CoA) dehydrogenase catalyzes the first step in fatty acid β-oxidation.[28] The enzyme introduces a *trans* double bond into short, medium, long and very long chain acyl-CoA thioester substrates. The reductive half-reaction illustrated in Figure 1.7 shows the concerted breakage of the αC-H and βC-H bonds where the first hydrogen is abstracted by an active site base and the second is transferred as a hydride to the flavin N5 atom to generate the reduced flavin and the trans-Δ^2-enoyl-CoA product. In the oxidative half-reaction, the flavoenzyme is regenerated by two consecutive transfers of reducing equivalents to electron transferring flavoproteins (ETF), which shuttle electrons into the respiratory chain.

Mammalian D-amino acid oxidase (DAAO) catalyzes the oxidative deamination of D-α-amino acids to the corresponding α-imino acids.[29] Neuronal DAAO has been implicated in regulating signaling in the brain through its action on D-serine, a ligand for N-methyl-D-aspartate (NMDA) receptors.[30] Figure 1.8 shows that binding of the appropriate D-α-amino acid substrate is followed by direct hydride transfer to the N5 atom of the oxidized flavin isoalloxazine ring in the reductive half-reaction.[29,31] The imino product is then released and nonenzymatically hydrolyzed to the corresponding keto acid. The reduced flavin is then

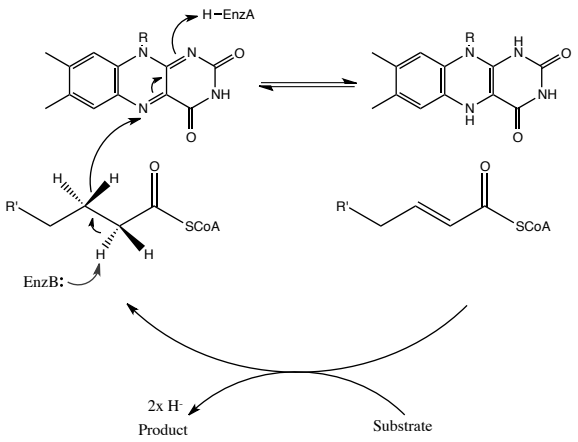

Figure 1.7: Proposed catalytic mechanism of acyl-CoA dehydrogenase.

oxidized in the oxidative half-reaction by molecular oxygen. Oxygen is released as hydrogen peroxide.

Bacterial *p*-hydroxybenzoate hydroxylase acts in the catabolism of aromatic compounds such as *p*-hydroxybenzoate that are liberated during the biodegradation of lignin, a major component of wood.[32] First, the oxidized enzyme binds both *p*-hydroxybenzoate and NADPH. A hydrogen-bond network then deprotonates *p*-hydroxybenzoate to the phenolate anion. This triggers protein rearrangements that lead to a pendulum-like movement of the isoalloxazine ring from a buried *'in'* conformation to a more solvent-exposed *'out'* conformation. The latter enables NADPH-FAD complex formation and reduction of the isoalloxazine ring. Following $NADP^+$ release, the ring returns to the *'in'* conformation.[32,33] In the oxidative half-reaction, the reduced FAD transfers a single electron to molecular oxygen to form a superoxide anion, which then rapidly reacts with the C4a atom to form a C4a-hydroperoxoflavin intermediate. The electrophilic properties of this intermediate enables transfer of a hydroxyl to the substrate, which generates 3,4-dihydroxybenzoate. The enzyme is restored following release of water and product.

1.1.6 Unusual Flavin-Catalyzed Reactions

DNA photolyases catalyze the reduction of cyclobutane pyrimidine dimers that are formed in UV irradiated DNA.[34] They are present in many organisms, including bacteria, plants and some animals such as the goldfish (*Carassius auratus*) and the marsupial rat kangaroo (*Potorous tridactylis*).[35] The flavoenzyme contains FAD and a light-harvesting chromophore, either 5,10-methenyltetrahydrofolate or 8-hydroxy-deazaflavin. In the first step of catalysis, the positively charged groove of the enzyme binds to the damaged DNA phosphodiester backbone and the pyrimidine dimer flips out of the helix into the enzyme

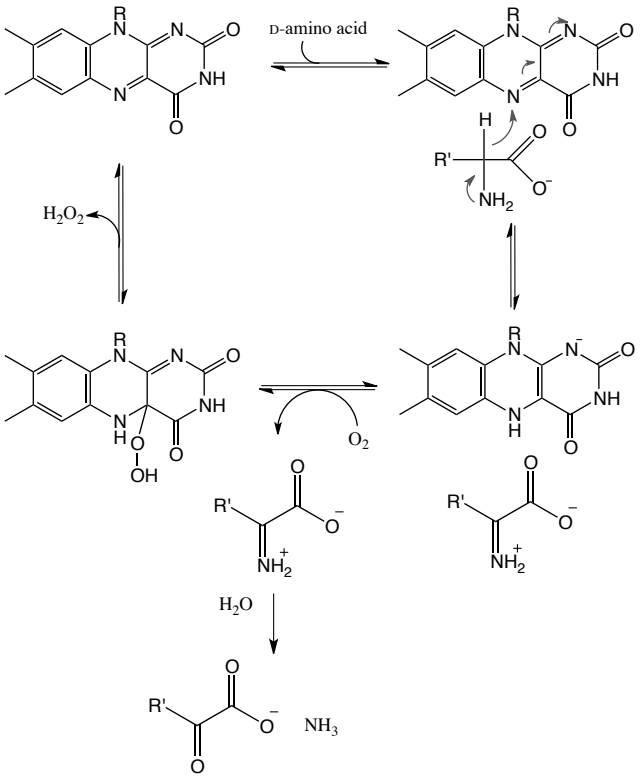

Figure 1.8: Proposed catalytic mechanism of D-amino acid oxidase.

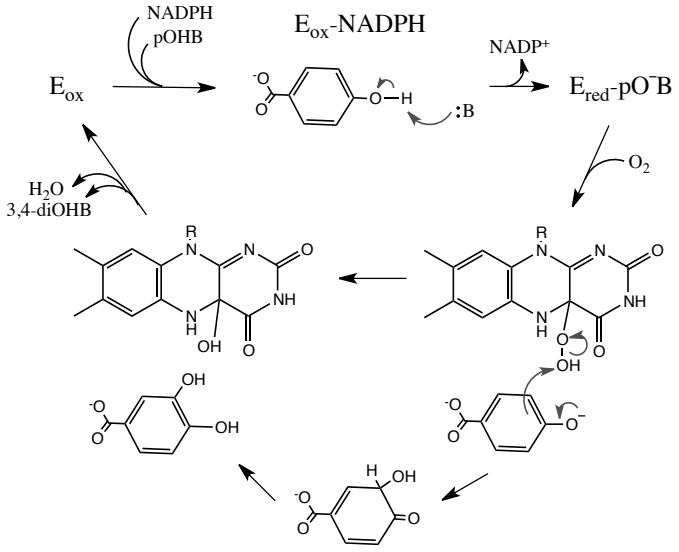

Figure 1.9: Proposed catalytic mechanism of *p*-hydroxybenzoate hydroxylase.

cavity.[36] Light is then absorbed by the chromophore and the excitation energy is transferred to the reduced flavin which is located near the interior of the cavity. Electron transfer from the reduced flavin to the pyrimidine dimer forms a ketyl radical, which decomposes stepwise to split the cyclobutane into a pyrimidine-pyrimidine anion radical pair.[37] Final electron transfer back onto the flavin semiquinone regenerates the reduced flavin and the repaired DNA is released.

Iodotyrosine deiodinase is the first identified mammalian member of the NADH oxidase/flavin reductase superfamily.[38] This enzyme relies on FMN to catalyze the reductive dehalogenation of byproducts of thyroid hormone synthesis to generate iodide and tyrosine.[39] These liberated products are then reused to produce more thyroid hormone. In the absence of this flavoenzyme, precious iodine sources are excreted and an iodine deficiency ensues.[39] Iodotyrosine deiodinase is an unusual enzyme since reductive dehalogenation is rarely observed in aerobic organisms, even less so in mammals.[38] Only one other reductive dehalogenase is known in humans, a nonflavoenzyme that involves the participation of thiol reductants and cysteine residues.[40] Although the mechanistic details are still not fully understood, iodotyrosine deiodinase catalysis has been determined to proceed without the use of thiols and cysteines.[38,41] Thus, this flavoenzyme is an excellent example of the ever-expanding repetoire of known flavin-mediated reactions.

1.1.7 Ferredoxin NADP(H)-dependent Reductase, an Oxidoreductase

In a recent review of over 300 flavoenzymes, it was determined that $\sim$ 90% of flavin-dependent enzymes belong to the catalytic class of oxidoreductase, which encompasses

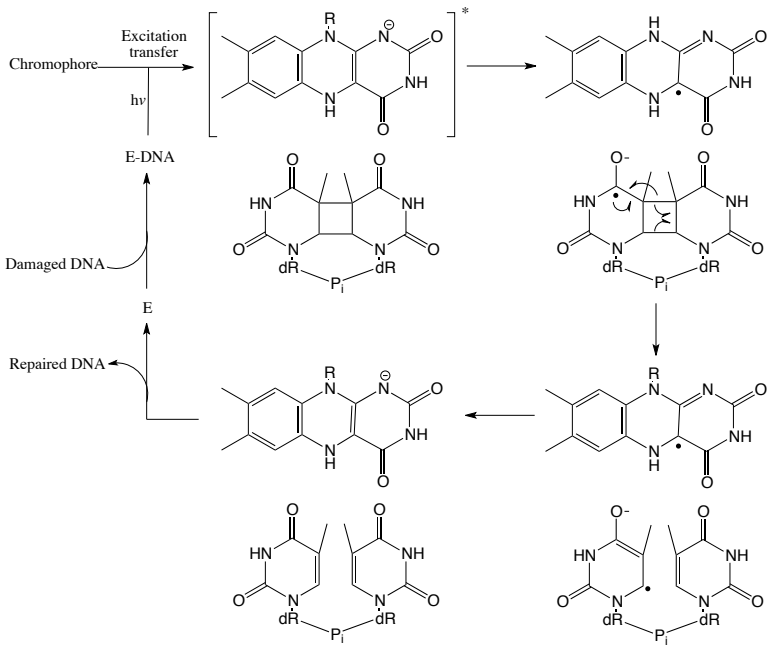

Figure 1.10: Proposed catalytic mechanism of DNA photolyase.

oxidation-reduction catalysis.[5] Ferredoxin NADP(H)-dependent reductases (FNR) form one of the largest families of oxidoreductases. They are monomeric, hydrophilic FAD-bound enzymes. The first FNR was isolated from spinach chloroplasts in 1956 by Avron and Jagendorf and given the name "TPNH diaphorase" for its ability to transfer electrons to or from NADP(H).[42] In the following decade, Arnon and colleagues confirmed the physiological role for FNR.[43] The enzyme catalyzes the final step of photosynthesis where electrons are transferred from ferredoxin, a small iron-sulphur protein, to $NADP^+$ to yield NADPH. In 1991, the X-ray crystal structure of spinach FNR was solved.[44] Figure 1.11 shows the structure is comprised of a two-domain motif. The FAD binds to an $\alpha\beta\alpha$-motif with a compact six-stranded anti-parallel flattened β-barrel. The NADP(H)-domain consists of a five-stranded β-sheet sandwiched by six α-helices with Rossman topology. Together, these domains are referred to as the FNR module.[44,45]

Many more enzymes in the FNR family have since been discovered with a myriad of physiological roles. For example, bacterial FNR transfers reducing equivalents from NADPH to flavodoxin, an FMN-bound structural analogue of ferredoxin. Flavodoxin has numerous redox partners that makes FNR indispensible for nitrogen fixation, steroid metabolism, terpenoid biosynthesis, oxidative-stress response, and iron-sulphur cluster biogenesis in heterotrophic bacteria and fungi.[46]

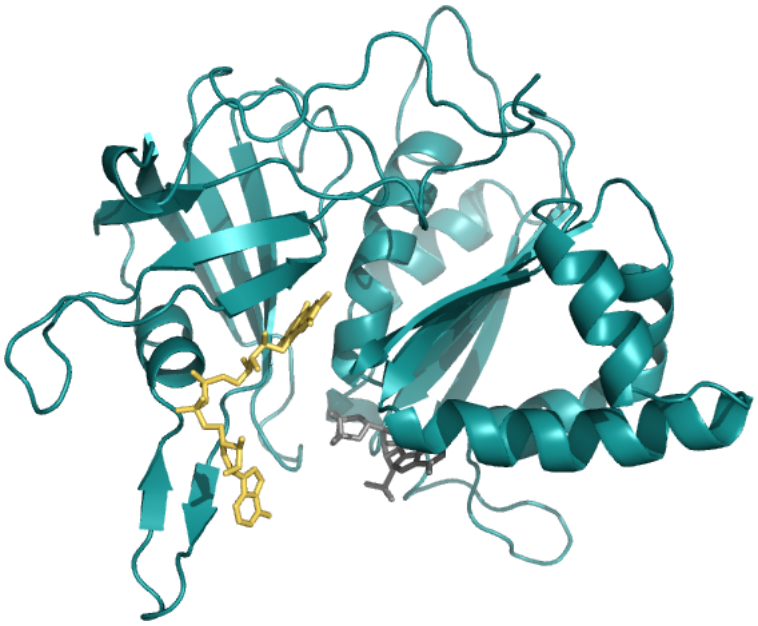

Figure 1.11: Crystal structure of spinach FNR with bound FAD (yellow) and 2',5'-adenosine diphosphate substrate moiety (grey). PDB 1FND.

1.1.8 The Diflavin Oxidoreductase Family

Members of the diflavin oxidoreductase family are multidomain enzymes that contain noncovalently bound molecules of FAD and FMN. The enzymes transfer reducing equivalents from NADPH to FAD to FMN and onto a physiological electron acceptor. Prokaryotic members include the α-subunit of sulphite reductase of *Escherichia coli* and the reductase domain of a fatty acid hydroxylase called flavocytochrome P450 BM3 from *Bacillus megaterium*.[47,48] Known eukaryotic members are cytochrome P450 reductase (CPR), the reductase domain of nitric oxide synthase (NOS), methionine synthase reductase (MSR), and human novel reductase 1 (NR1).[49–53] This family likely emerged from the early evolutionary fusion of ancestral genes of prokaryotic FNR and flavodoxin.[54] All members share the following structural arrangement from N- to C-terminal: i) a FMN-binding domain homologous to bacterial flavodoxin, ii) a flexible hinge region that joins with a bridging connecting domain, and iii) a FAD/NADPH-binding domain homologous to bacterial FNR. The overall domain organization of diflavin oxidoreductases, shown in Figure 1.14, is represented by the structure for the prototypic family member CPR. CPR and MSR share the greatest sequence similarity among the known diflavin oxidoreductases; a sequence alignment of human MSR, human CPR, and plant CPR are shown in Figure 1.12 and distinguishing structural features between CPR and MSR are highlighted in Figure 1.13.

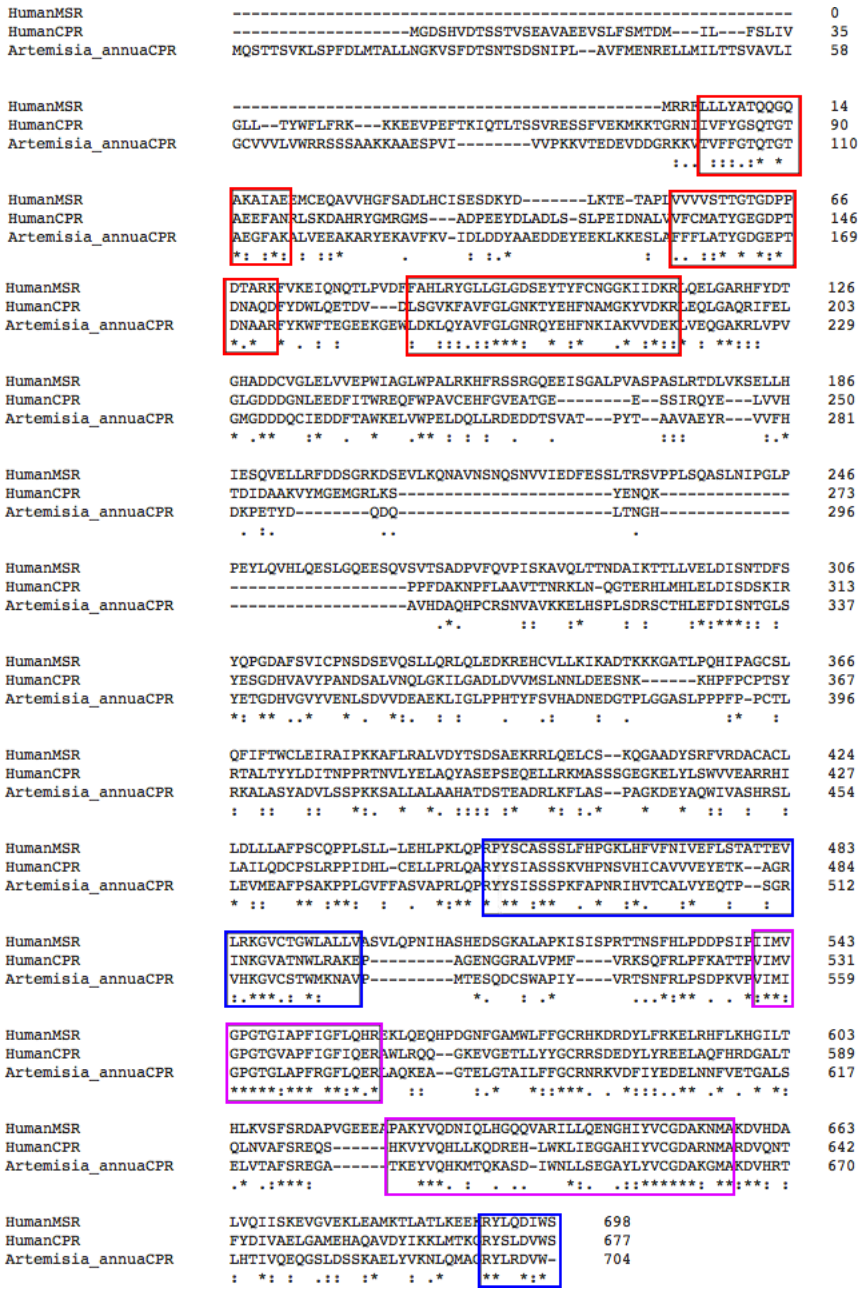

Figure 1.12: Sequence alignment of three diflavin oxidoreductases: human MSR, human CPR, and plant CPR derived from *Artemisia annua*. An asterisk denotes an identical residue, a colon denotes a conserved residue, and a period denotes a semiconserved residue. The FMN-binding residues are boxed in blue, the FAD-binding residues are boxed in red, and the NADPH-binding residues are boxed in purple.

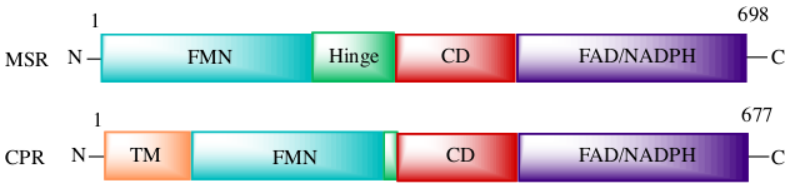

Figure 1.13: Primary sequence domain organization of human methionine synthase reductase and cytochrome P450 reductase. The FAD/NADPH-binding domain in purple, connecting domain (CD) in red, hinge region in green, FMN-binding domain in teal, and transmembrane (TM) domain in peach.

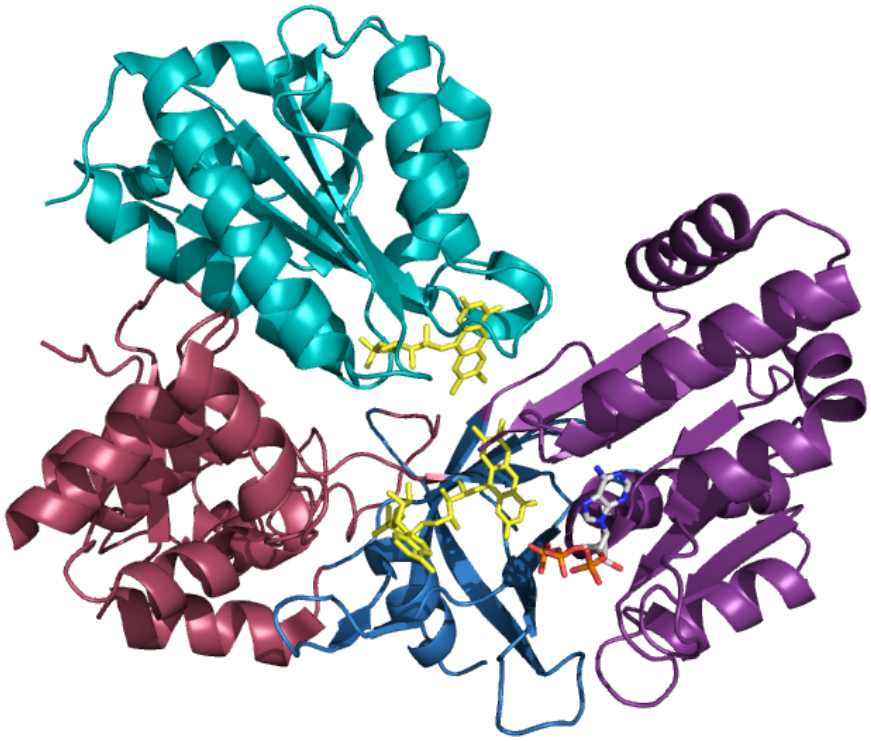

Figure 1.14: Crystal structure of the prototypical human isoform of cytochrome P450 reductase [PDB 3QE2]. Structures are shown in a cartoon model with the FAD/NADPH-binding domain, connecting domain, and FMN-domain coloured in purple, blue, and teal, respectively. FAD and FMN flavins are represented in yellow stick model and the NADPH molecule is in grey with the nitrogen, oxygen and phosphorous atoms coloured as blue, red, and orange, respectively.

1.2 Cytochrome P450 Reductase

1.2.1 Structure

CPR is a 78 kDa monomeric enzyme that is localized to the cytosolic side of the endoplasmic reticulum.[55] It is anchored to the endoplasmic reticulum membrane by a 6 kDa hydrophobic α-helical domain. To date, crystallization of full-length native human CPR has been unsuccessful. However, removal of the N-terminal membrane-spanning helix enabled expression and purification of a soluble form of CPR which formed crystals that diffracted in the X-ray beam.[49,56,57] Soluble CPR is a poor reductant for membrane-bound cytochrome P450s, but it can reduce the non-physiological electron acceptor cytochrome *c*.[58]

The protein structure of the FMN-binding domain of CPR is presented in Figure 1.15. It comprises a five-stranded parallel β-sheet sandwiched between five α-helices.[49] The planar FMN isoalloxazine ring is stacked between two aromatic residues, Tyr115 and Tyr77. The latter is tilted 40°with respect to the cofactor.[56] The crystal structure further reveals that the solvent-exposed dimethyl benzene edge of FMN is located within 4 Å of that of FAD. The FMN mononucleotide moiety is also stabilized by electrostatic interaction with a helix dipole formed at the N-terminal end of an α-helix.

A short 12 amino acid (Gly231-Arg242) hydrophilic hinge links the FMN domain to the connecting domain which tethers to the FAD/NADPH-binding domain.[49] Hamdane *et al.* observed that shortening the hinge length progressively impeded electron transfer from FAD to FMN and reduced enzyme activity.[59] The hinge provides the flexibility required for the FMN domain to form mutually exclusive complexes with i) the FAD/NADPH domain, and ii) the terminal electron acceptor.

By definition of the diflavin oxidoreductase family, the FAD/NADPH-binding domain is homologous to the FNR module; see Section 1.1.7.[49,57] The FAD isoalloxazine ring is surrounded by the 'catalytic triad' (residues Ser457, Cys629 and Asp675 - human CPR numbering), which facilitate the transfer of a hydride ion from the NADPH nicotinamide ring to the isoalloxazine ring.[60] The two conserved aromatic residues that stack against the FAD isoalloxazine ring in Figure 1.16 are Trp676 and Tyr455. With $NADP^+$ bound, Trp676 is partially stacked over the isoalloxazine ring. Due to steric clash, the indole side chain blocks the NADPH nicotinamide ring from moving into the FAD active site, which is necessary for direct hydride transfer. Deletion of the C-terminal residues Trp676 and Ser677 enabled the nicotinamide ring to stack over the isoalloxazine ring, as observed in the variant crystal structure.[61] Thus, conformational rearrangement of Trp676 is required to accommodate the incoming nicotinamide ring.

Interestingly, Figure 1.17 shows a second orientation of Trp676 that was captured in the $NADP^+$-free form of CPR where a disulfide bond was engineered between the FMN and

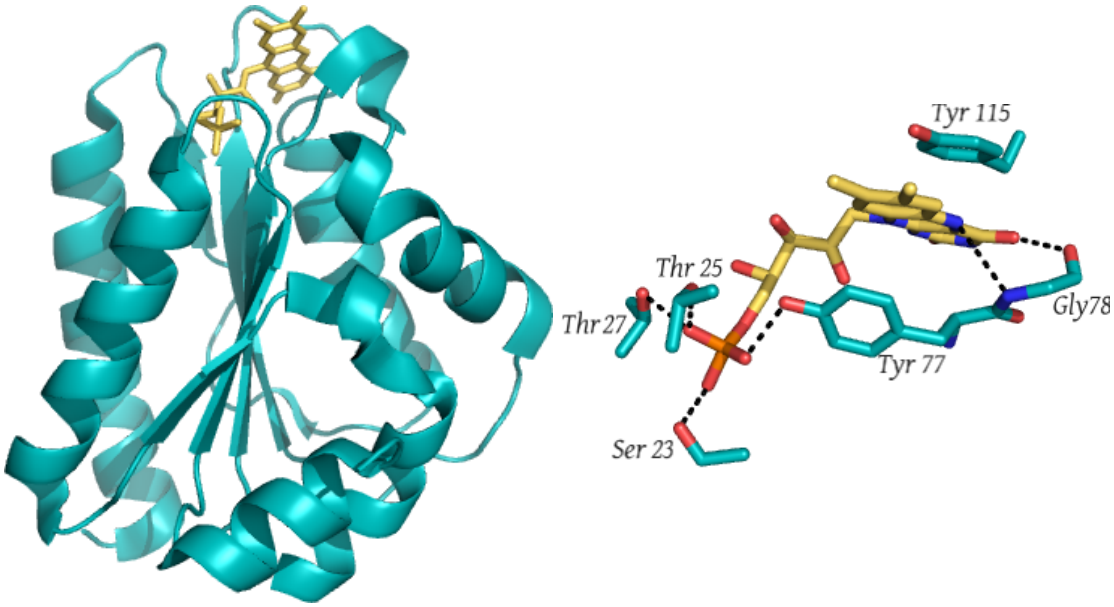

Figure 1.15: Crystal structure of CPR FMN-binding domain and FMN-stabilizing residues [PDB 3QE2]. *Left*: The FMN-binding domain represented in cartoon model in teal and the FMN cofactor shown in yellow stick model. *Right*: FMN-stabilizing residues. The FMN cofactor in yellow with the standard atom-coloured stick model, shown stacked against Tyr77 and 115 on the *re*- and *si*-sides, respectively. Hydrogen bonds are shown in black dashed between the flavin and hydroxyl groups of Ser23, Thr25, Thr27 and Tyr77. Possible contacts between the Gly78 and the isoalloxazine ring are also shown.

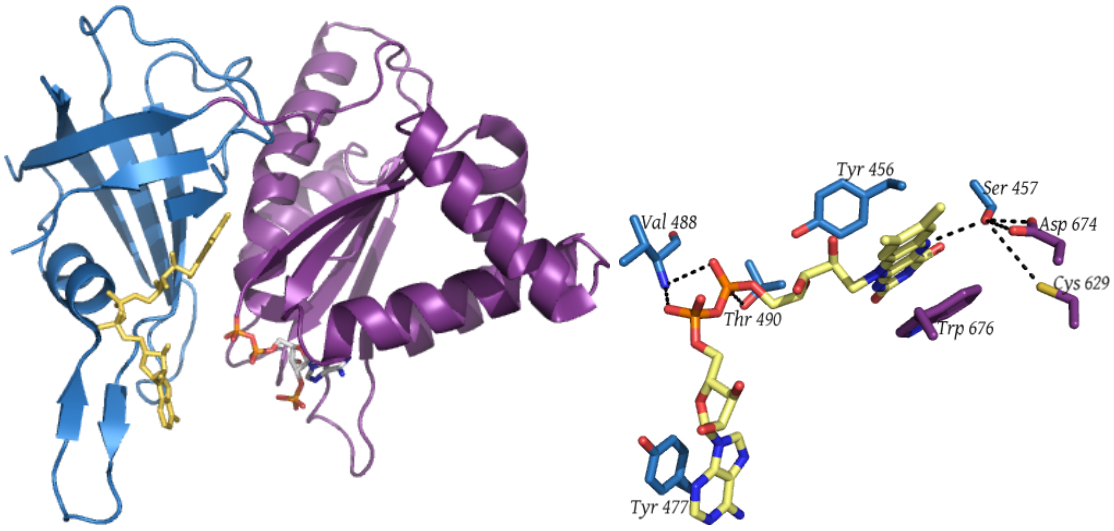

Figure 1.16: Crystal structure of CPR FAD/NADP(H)-binding domain and FAD-stabilizing residues. *Left* Human CPR FAD/NADP(H)-binding domain crystal structure [PDB 3QE2]. The FAD-binding domain is represented in blue cartoon model, NADPH-binding domain in purple, the FAD cofactor is shown in yellow stick model, and the NADPH is shown in grey with the standard atom colouring. *Right* FAD-stabilizing residues. The FAD cofactor is in yellow stick model with the standard atom colouring and potential hydrogen bonds are shown in black dashes.

FAD/NADPH domains ($NADP^+$-free CPR without the disulfide link is not available).[57] In this structure the Trp676 indole side chain is flipped and rotated by 90°, such that the entire indole ring lies planar to the isoalloxazine ring. This second structure suggests that Trp676 adopts multiple conformations during catalysis.[57] Trp676 is first fully stacked with the isoalloxazine ring, then undergoes a NADPH-induced conformational change to the partially stacked position, followed by displacement from the active site by the nicotinamide ring.

Further scrutiny of the active site reveals a loop adjacent to the FAD isoalloxazine ring with an aspartic acid (Asp634). Figure 1.17 displays the different orientations captured for this residue. In substrate-bound CPR, the side chain of Asp634 is rotated away from the active site.[49] However in rat variants, with an engineered disulfide link or deleted Trp676, the aspartic acid is projected between the isoalloxazine ring and the coenzyme-binding site, therefore this residue must also undergoes NADPH-induced conformational change.[57] Additional residues that form the coenzyme-binding site are shown in Figure 1.18. The residues (Tyr604, Lys602, Ser596, and Arg597) are positioned for hydrogen bonding with the 2'-phosphate of NADPH. Further stabilizing interactions are formed between Arg298 and Thr535 and the $NADP^+$ pyrophosphate.

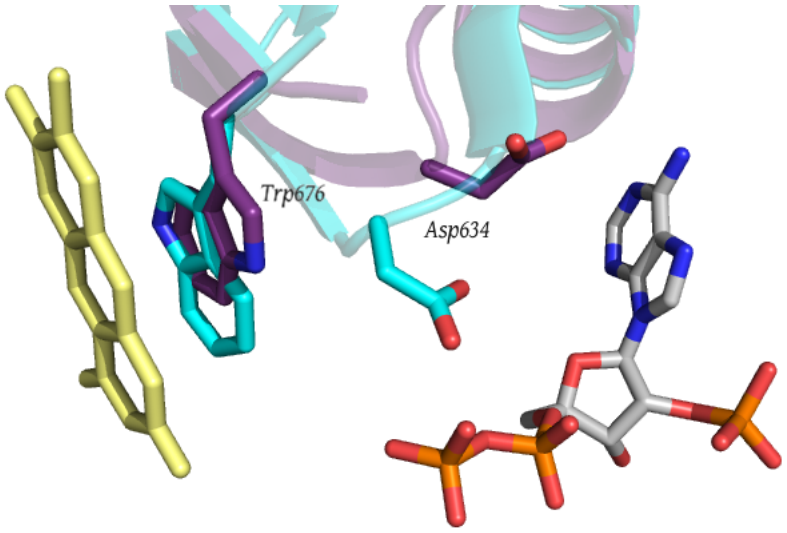

Figure 1.17: Different orientations of active site residues Trp676 and Asp634 in CPR. Wild-type human CPR is shown in purple while the disulfide linked rat variant is in cyan [PDB 3QE2 and 3OJW]. The 2',5'-ADP moiety of NADPH is shown in grey with the standard atom-coloured stick model. FAD isoalloxazine ring is in yellow with the ribityl adenosine tail removed for clarity.

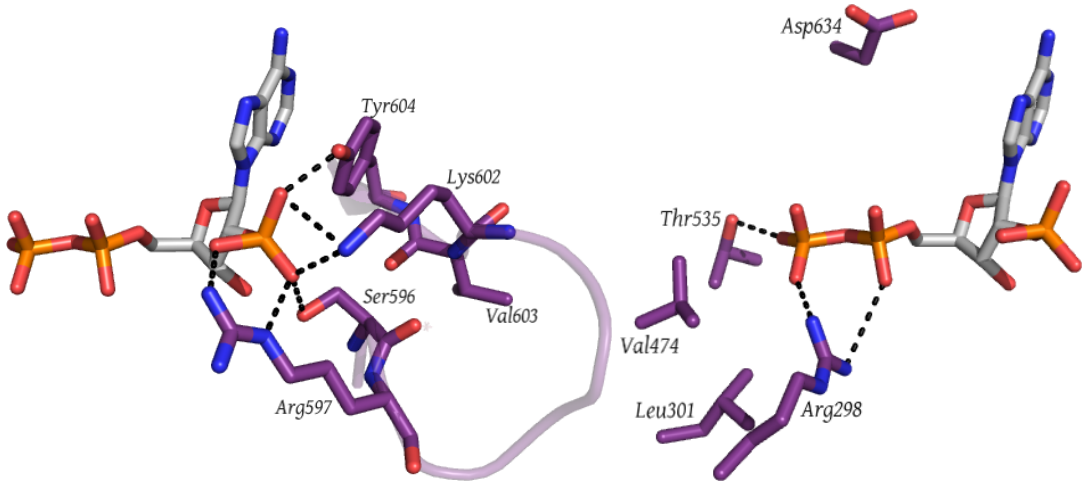

Figure 1.18: NADPH stabilizing residues at the coenzyme binding pocket for CPR [PDB 3EQ2]. *Right* Residues that interact with the NADPH 2'-phosphate. *Left* Residues that interact with the NADPH pyrophosphate. NADPH is shown in grey with the standard atom-coloured stick model. Potential hydrogen bonding interactions are shown in black dashes.

1.2.2 Enzymology

A general reaction scheme for the CPR reductive half-reaction has been proposed, and it is shown in Figure 1.19.[57,60,61] First, NADPH binds to the fully oxidized enzyme (Step I). In Step II, a hyride ion is transferred from NADPH to the FAD isoalloxazine to form the FAD hydroquinone. A single electron is then transferred from $FADH_2$ to FMN to yield the disemiquinone (III; FMNH• and FADH•)). In the fourth step (IV), the FMN is fully reduced to the hydroquinone by a second electron transfer. Dissociation of oxidized $NADP^+$ allows for a second molecule of NADPH to bind and further reduce the enzyme to the four-electron reduced dihydroquinone (V). Release of $NADP^+$ and transfer of two reducing equivalents to the appropriate acceptor completes the catalytic cycle.

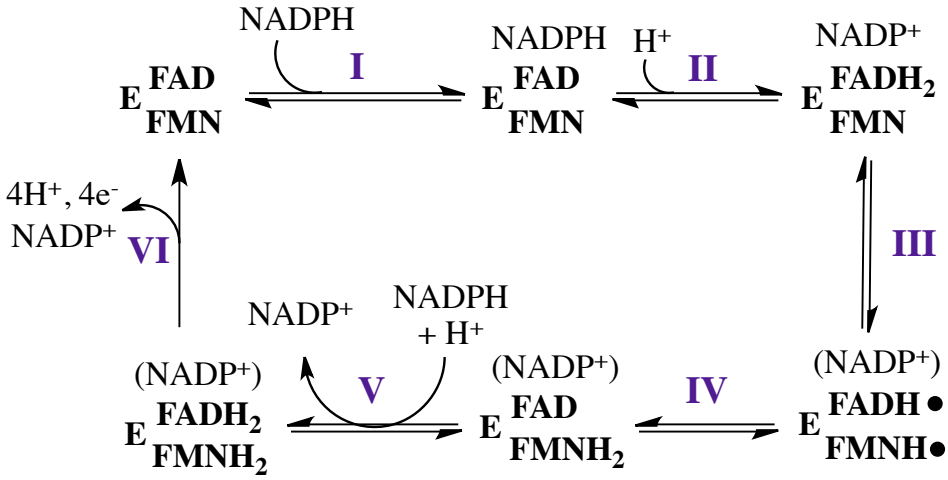

Figure 1.19: Proposed mechanism for NADPH-mediated reduction and oxidation of diflavin oxidoreductases. **I** NADPH binds. **II** Donation of hydride ion from NADPH to FAD. **III** Formation of the disemiquinone. **IV** Both electrons are transferred to the FMN to form the hydroquinone. **V** Full four-electron reduction to the dihydroquinone by a second molecule of NADPH. **VI** Transfer of reducing equivalents from the enzyme to terminal electron acceptors regenerates the fully oxidized enzyme. The presence/absence of the oxidized coenzyme is not absolutely known and depicted as parentheseses around $NADP^+$.

Early experiments with spinach FNR established a clear bipartite binding model for NADPH binding.[62,63] Bipartite binding is defined as the initial anchoring of the 2',5'-ADP moiety to the enzyme, followed by displacement of the conserved FAD-stacking aromatic residue by the nicotinamide mononucleotide (NMN) moiety of NADPH. This productive placement orients the *pro*-R-hydrogen on the C4 atom of the nicotinamide ring to the N5 atom of the FAD isoallaoxazine ring shown in Figure 1.20. Deng *et al.* determined that for FNR, the binding energy for the coenzyme is derived from polar interactions between the 2',5'-ADP moiety and that initial docking of this moiety ensures that the enzyme favours

binding of NADPH over NADH.[62] Evidence of this bipartite binding model has also been found in diflavin oxidoreductases, including CPR and MSR.[64,65]

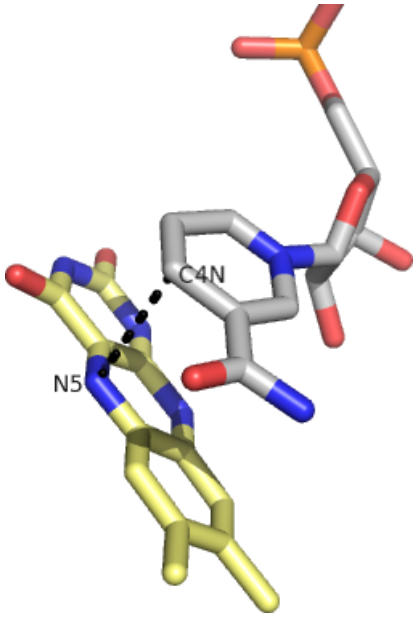

Figure 1.20: Stereospecific orientation of the NADPH nicotinamide ring over the FAD isoalloxazine ring. For clarity, only partial NADPH is shown in grey and the isoalloxazine ring is shown in yellow with standard atom colouring.

Following productive placement of the nicotinamide ring, a hydride ion is donated to the isoalloxazine ring to form the $FADH_2$ hydroquinone.[60] The midpoint potentials of the redox couples NADPH/$NADP^+$ (-320 mV) and $FAD_{ox/hq}$ (-333 mV) are similar, indicating that reaction is not spontaneous (see Figure 1.21 for redox potentials).[66] However, the highly electropositive $FMN_{ox/sq}$ couple (-66 mV) ensures that the next electron transfer step is thermodynamically favourable. Thus, the $FMN_{ox/sq}$ couple provides the driving force to favour the forward flow of electrons in CPR. Kinetic analysis has shown that the hydride and interflavin electron transfer steps (II and III) are tightly coupled.[66,67]

Following the first hydride transfer, the two-electron reduced CPR forms a quasi-equilibrium mixture of disemiquinone (FADH•-FMNH•) and FMN hydroquinone (FAD-$FMNH_2$) due to the near isopotential values between the $FAD_{ox/sq}$ and $FMN_{sq/hq}$ couples.[66–68] Since the FMNH• has extremely low reactivity towards cytochrome P450 reduction, $FMNH_2$ is envisioned to serve as the electron donor.[66,69] The final electron transfer from FMN to the heme center of cytochrome P450 ($\sim$ -300 mV) is a thermodynamically unfavourable step. However, recent studies have shown that, when bound with substrate, the heme center becomes +10-80 mV more electropositive than the $FMN_{sq/hq}$.[70,71] In addi-

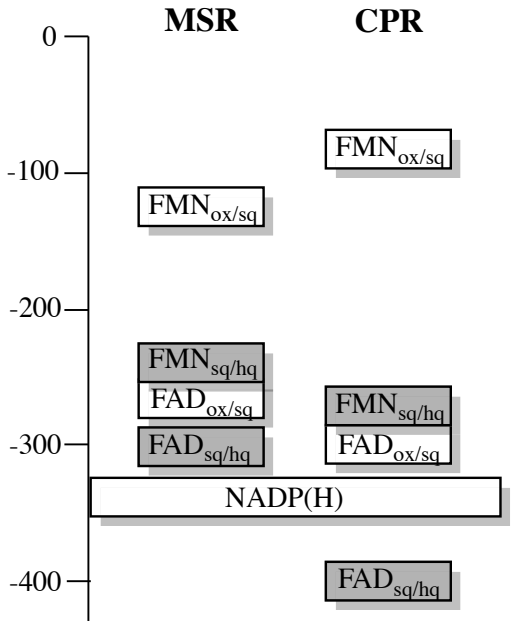

Figure 1.21: Flavin redox potentials for diflavin oxidoreductases human MSR and CPR. The oxidized/semiquinone redox couples are shown in white boxes, and the semiquinone/hydroquinone redox couples are in grey boxes.

tion, the redox potentials of membrane-embedded CPR may shift to a less electronegative value compared to soluble CPR.[72]

For intra- and intermolecular electron transfer, CPR undergoes large-scale conformational changes. Global domain motion in CPR has been extensively investigated through a number of techniques including small-angle X-ray scattering, small-angle neutron scattering, NMR and Forster fluorescence resonance energy transfer.[73–76] All solved crystal structures of native CPR are in a compact closed conformation where the interflavin distance is shortened to favour intramolecular electron transfer. However, since the FMN flavin is buried in the closed state, it does not allow for electron transfer to an external protein partner.[57] Therefore, the FMN domain must dissociate from the FAD/NADPH domain into an open conformation that exposes the FMN cofactor for contact with and electron transfer to the appropriate protein partner. Figure 1.22 shows the conformational dynamics of CPR with respect to cytochrome P450 using available crystal structures.

1.2.3 Physiological Role

CPR catalyzes electron transfers to numerous physiological acceptors, including cytochrome b_5, squalene monooxygenase, and heme oxygenase.[77–79] It also supplies electrons to all microsomal cytochrome P450s, a large heme monooxygenase superfamily.[67,80,81] In

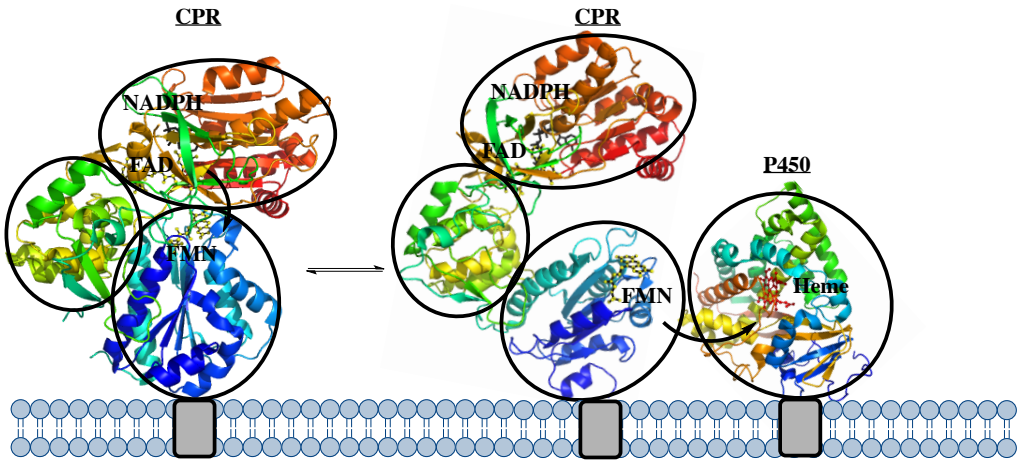

Figure 1.22: Conformational rearrangements adopted by cytochrome P450 reductase during catalysis with cytochrome P450. Crystal structures are in cartoon coloured from N-terminal (blue) to C-terminal (red) [PDB 3QE2, 3ES9 and 2CPP]. NOTE: the 'open' structure is of a CPR variant with 4 amino acids deleted from the hinge region and does not reflect the exact *in vivo* conformation.

humans, fifty seven cytochrome P450 genes have been identified.[82] These P450 enzymes catalyze reactions as diverse as hydroxylations, N-, O- and S-dealkylations, peroxidations, and epoxidations. Collectively, they act on a broad repertoire of substrates and are involved in the metabolism of lipids, steroids, and fat-soluble vitamins.[82,83] Additionally, P450s metabolize xenobiotics such as drugs, polycyclic biphenols and the carcinogenetic benzo[α]pyrene found in tobacco smoke.[81] In general, the P450-catalyzed hydroxylation of metabolites increases their solubility for downstream metabolism and excretion.

Microsomal P450 activity requires two consecutive electron transfers onto the P450 heme to catalyze oxygen activation and substrate hydroxylation as presented in Figure 1.23. The heme is an iron-protoporphyrin IX coordinated to a cysteine thiolate.[84–87] In the resting state, the ferric heme is bound to water. The incoming substrate displaces the water from the center and shifts the redox potential of the heme (from -330 mV to -173 mV) to favour electron transfer from CPR.[84] A single electron is shuttled from the FMN hydroquinone of CPR to the P450 heme. The reduced ferrous heme readily binds molecular oxygen to yield a ferrous-dioxygen complex, which rapidly converts to a ferric superoxide complex. It is reduced by a second electron and protonated to generate the ferric hydroperoxide complex. This unstable complex rapidly undergoes a second protonation and heterolytic cleavage of the O-O bond. Water is then released and the Fe^{IV}-oxo radical is formed.[84,88] It is a powerful oxidant and abstracts a substrate hydrogen to generate a short-lived carbon radical and ferryl hydroxo intermediates.[88] Finally, through a rebound mechanism the substrate is hydroxylated and released, and the heme returns to the resting state.

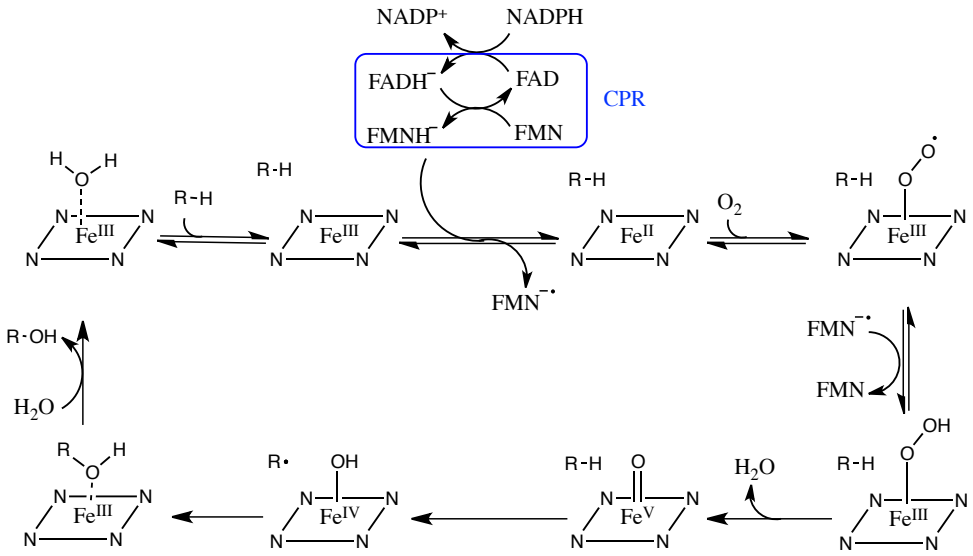

Figure 1.23: The mechanism of molecular oxygen activation and two-step rebound radical alkane hydroxylation by microsomal cytochrome P450 and reduction by cytochrome P450 reductase. The heme porphyrin ring is abbreviated to the pyrrole nitrogens coordinated to iron. *See text for details.*

All microsomal P450s share similar overall topology: the conserved motif around the heme-binding pocket, a proline-rich region, and an N-terminal hydrophobic transmembrane domain. The most structural variation is around the substrate binding site.[89,90] This structural variation accounts for the ability of the P450 family to utilize such a varied collection of substrates. Although only 57 genes were found in humans, many more can be found in flora. For example, 272 are identified in *Arabidopsis thaliana* and 457 in rice *Oryza sativa* genomes.[82,91,92] In plants, more P450s are required for the synthesis of pigments, growth regulators, and plant toxins.[93]

1.2.4 Health Implications

CPR acts to maintain the activity of all microsomal cytochrome P450s, therefore derangements in CPR function result in a broad spectrum of clinical phenotypes. These are dependent on the affected P450s and the degree of CPR impairment. There are over 40 naturally occurring mutations identified in the gene encoding for CPR, *POR*.[94,95] A polymorphic variation in one allele may not elicit any adverse effects, while eliciting subtle effects on the physiological activity of P450s. For example, three polymorphisms in *POR* have been identified that influence the P450-mediated metabolism of warfarin.[96] Warfarin is a potent anticoagulant with a very narrow therapeutic range, thus there is a potential for thrombolic complications and haemorrhage if the dosage is overestimated. A recent

method proposed to ensure safe dosage entails pharmacogenetic testing to determine the specific *POR* polymorphisms in the patient to predict that individual's ability to metabolize the drug.[96,97]

Severe CPR deficiency arises from missense mutations in functionally important structural regions. This deficiency is a rare autosomal recessive disease with clinical phenotypes such as congenital adrenal hyperplasia, disordered sexual development, and Antley-Bixler Syndrome (ABS).[95,98] ABS is a rare disease that causes craniofacial malformations and additional skeletal anomalies. A comprehensive study of patients with apparant ABS revealed two distinct diseases.[98] First, 'classic' ABS with normal steroidogenesis that is caused by mutations in the fibroblast growth factor receptor 2 gene. Second, an ABS-phenotype with steroid abnormalities and ambiguous genitalia that is caused by missense mutations in *POR*.[98,99] Clearly, normal CPR function is necessary for normal development. Interestingly, while complete *POR* gene knockout mice is embryonically lethal, liver-specific knockout mice develop normally with reproductive capabilities despite impaired bile acid production and steroid metabolism.[100–102] Therefore, hepatic CPR activity is not essential for survival and nonhepatic CPR dysfunction must be the origin of the dysmorphology seen in CPR deficiency.

1.3 Methionine Synthase Reductase

1.3.1 Structure

MSR and CPR share a diflavin topology with 42% amino acid sequence similarity. Figure 1.24 displays the superimposition of MSR and CPR crystal structures to illustrate their shared structural motifs. Unlike CPR, MSR is a 78 kDa monomeric soluble enzyme that is localized in the cytosol.[103,104] Although crystallization of full-length native human MSR has not yet been successful, the structure of the enzyme without the FMN domain has been solved.[65] Based on the sequence alignment with CPR, the FMN domain of MSR is expected to have the conserved FMN-binding fold, as described in Section 1.2.1. A notable structural difference is the 82 amino acid hinge region in MSR, which is 5 times longer than the corresponding region in CPR. The extended hinge is partially captured in the MSR crystal structure. However, since the hinge is located at the N-terminal end of the truncated protein, the observed extended position is likely nonphysiological.

Like CPR, the MSR FAD domain contains the 'catalytic triad', a trio of residues (Asp695, Cys650 and Ser454), and a conserved aromatic residue, Trp697, that lies planar to the *re*-face of the FAD isoalloxazine ring, shown in Figure 1.25.[65] Interestingly, the orientation of the indole side chain of Trp697 in MSR - both with and without $NADP^+$ bound to the active site - is similar to that found in $NADP^+$-free CPR where the entire

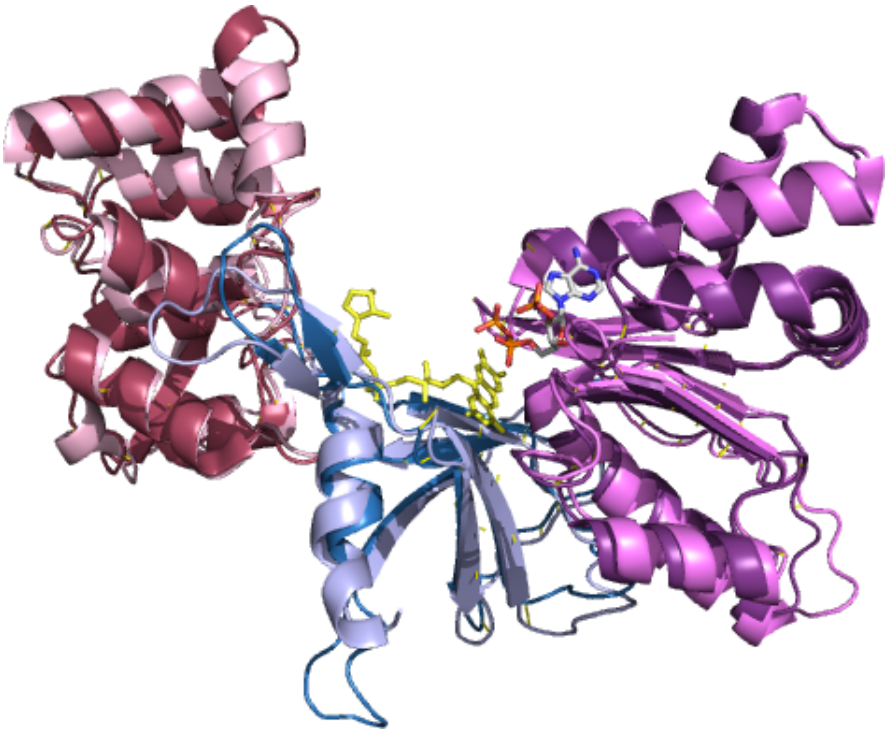

Figure 1.24: Superimposition of the crystal structure of human MSR and CPR (with the FMN domain of CPR removed) [PDB 3QE2 and 2QTZ]. Crystal structures are represented in cartoon model. The connecting domain of CPR is red and light pink for MSR, FAD-domain is in blue for CPR and light blue for MSR, NADPH-domain is in purple for CPR and light purple for MSR. FAD bound flavin and NADPH are represented stick model as yellow and grey, respectively.

indole side chain lies planar to the FAD. Moreover, the MSR aspartic acid residue (Asp652) which is in the adjacent loop, projects towards the pyrophosphate in both $NADP^+$-bound and $NADP^+$-free MSR. Again, while the position of the Asp652 carboxylate is similar to that observed in the substrate-free engineered rat CPR, it is in stark contrast with that of the substrate-bound human CPR.[57,65] Thus, it seems that the binding of $NADP^+$ to CPR can induce stable structural changes in the coenzyme-binding cleft. These changes include flipping of Trp676 and repositioning of the Asp loop which enables docking of the $NADP^+$ pyrophosphate closer to the N-terminal end of the helix.[57] In contrast, coenzyme binding to MSR is unable to induce the same stable structural changes. Inspection of the 2'-phosphate binding pocket, see Figure 1.26, reveals a similar network of polar residues that include Tyr624, Ser610, and Arg611. A notable difference is Lys623, which is shifted by one amino acid position in the primary sequence. This shift means that it is unable to form a direct hydrogen bond with the 2'-phosphate.[65] Figure 1.26 shows the coenzyme binding cleft of MSR around the NADP(H) pyrophosphate. Compared to CPR, the cleft is more negatively

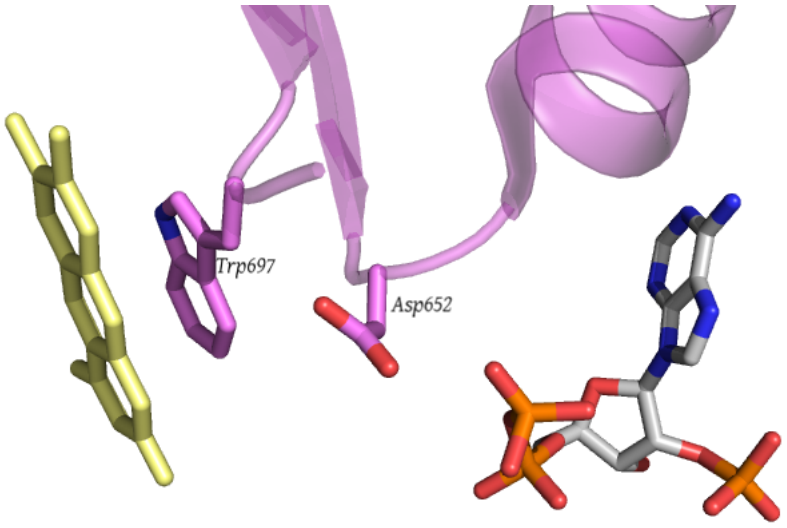

Figure 1.25: Key residues around the active site in MSR [PDB 2QTZ]. The FAD isoalloxazine ring is in yellow with the ribityl adenosine moiety removed for clarity. The ribose and nicotinamide ring moieties of NADPH are disordered in this crystal structure, the 2',5'-ADP moiety is in grey with the standard atom colouring.

charged, but the electrostatic interactions from Thr547 and Lys291 with the coenzyme are conserved.

1.3.2 Enzymology

The reductive half-reaction of MSR is expected to follow the same general reaction scheme offered earlier for CPR in Section 1.2.2. Previous isothermal titration experiments have also revealed the two-step binding mode of NADPH as discussed earlier for FNR and CPR.[65] Coenzyme binding in MSR is much weaker than in CPR, by >700-fold. Furthermore, while in CPR the dissociation constants (K_d) for $NADP^+$ and 2',5'-ADP are the same ($\sim$ 50 nM), in MSR they are not.[64,65] The K_d for $NADP^+$ is 37 μM and 2.4 μM for 2',5'-ADP, suggesting that the NMN moiety contributes unfavourably to the overall coenzyme binding energy, as has been described for FNR.[63,65]

Like in CPR, hydride transfer is dependent on the displacement of Trp697 (Step I in Figure 1.19). In contrast to CPR, hydride transfer is thermodynamically favourable, because the $FAD_{ox/hq}$ is more electropositive (-272 mV). Moreover, hydride transfer is not coupled to subsequent interflavin electron transfer (II and III).[105] Interflavin electron transfer is a much slower kinetic event in MSR. While the redox potentials of MSR are similar to CPR, they span a much narrower range as shown in Figure 1.21. More compressed redox

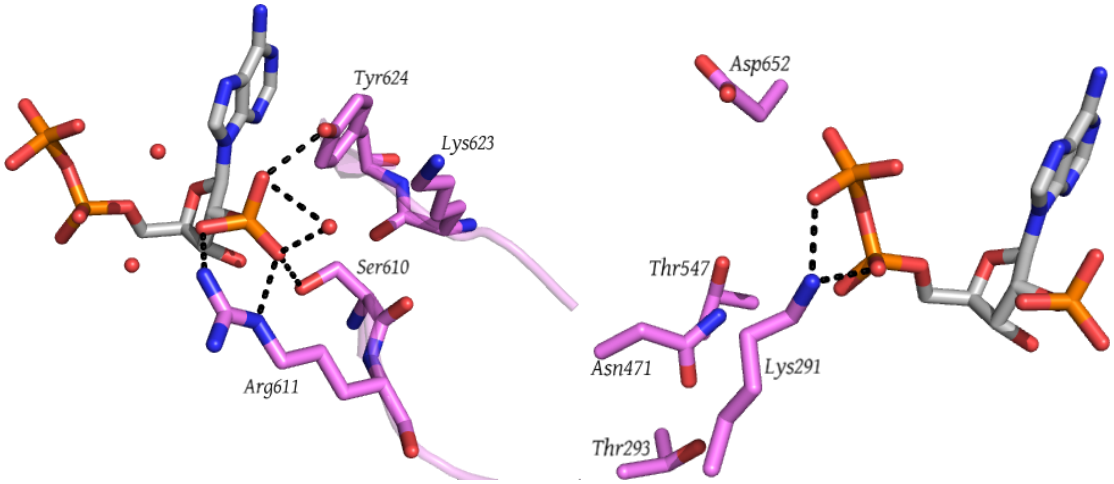

Figure 1.26: Stabilizing residues at the NADPH-binding cleft for MSR [PDB 2QTZ]. NADPH is shown in grey with the standard atom-coloured stick model. Potential hydrogen bonding interactions are shown in black dashes and water molecules are represented as red spheres.

potentials may be a factor in the limited and slower formation of the disemiquinone in MSR. In Step IV, the FMN hydroquinone is formed by a second electron transfer. Binding of another NADPH generates the four-electron reduced state in Step V. Final electron delivery to the physiological electron acceptor cobalamin-dependent methionine synthase is thermodynamically unfavourable. The midpoint potential of the $FMN_{sq/hq}$ couple is -260 mV, while that for the cob(I)alamin/cob(II)alamin couple is -490 mV.[106] However, this endergonic step is overcome by coupling electron transfer to the highly exogonic methylation of cob(I)alamin by S-adenosylmethionine.

1.3.3 Physiological Role

Methionine synthase reductase is critical in one-carbon and folate metabolism by maintaining the activity of methionine synthase (MS).[52,103,104] MS, a vitamin B_{12}(cobalamin)-dependent enzyme, is at the junction of two major metabolic pathways. It catalyzes the methyl group transfer from methyltetrahydrofolate (CH_3THF) to homocysteine to produce tetrahydrofolate (THF) and methionine.[52] In the catalytic cycle shown in Figure 1.27, the supernucleophilic cob(I)alamin (cobalt in 1^+ oxidation state) abstracts the methyl group from CH_3THF to yield methylcobalamin and THF. Methylcobalamin donates the methyl to the thiol group of homocysteine to generate methionine and regenerate cob(I)alamin. Approximately every 2000 catalytic turnovers, cob(I)alamin undergoes one electron oxidation, producing cob(II)alamin.[52] Cob(II)alamin is unable to carry on with catalysis, rendering MS inactive. To restore MS to its active state, the MSR FMN domain forms a complex with

the MS activation domain and transfers an electron to cob(II)alamin to yield cob(I)alamin. This reductive reaction is coupled with a methyl donation by S-adenosylmethionine.[106]

In addition, MSR is also a special molecular chaperone for the conversion of MS apoenzyme to holoenzyme. The presence of MSR not only stabilizes the apoenzyme but its reductase activity on aquacobalamin also produces cob(II)alamin. This is a cobalamin form that is more easily integrated into the apoenzyme.[107]

MS is important for cell homeostasis for several reasons.[108] First, CH_3THF is the circulating form of folic acid and MS is the only enzyme that can convert it to tetrahydrofolate. Tetrahydrofolate is an important biological cofactor for numerous pathways, including purine and pyrimidine biosynthesis. Second, ATP-dependent conversion of methionine yields S-adenosylmethionine (AdoMet), which is involved in all mammalian methylations including nucleic acid, amino acid, protein, lipid, and secondary metabolite methylations.[109] Enzymatic hydrolysis of the byproduct of AdoMet methylation, S-adenosylhomocysteine, generates homocysteine, which is toxic to vascular endothelial cells in high levels.[110] MS is vital for recycling homocysteine to methionine which, in turn, is needed in protein synthesis and reformation of AdoMet.

MS is a dynamic multidomain enzyme consisting of four distinct modules. The N-terminal module comprises two tightly packed α/β barrel domains that form respective substrate binding pockets for homocysteine and CH_3THF (PDB 2CCZ).[111] The central module binds to cobalamin, a cobalt-containing cofactor. In the crystal structure of *Escherichia coli* methionine synthase (MetH), the cobalamin lies at the interface of a Rossman-like fold ($\beta\alpha\beta\alpha\beta$ motif) and a four helix bundle cap.[112] The cap shields the cobalamin when substrates are not bound. Lastly, the C-terminal activation domain is a C-shaped mixed α and β domain with a central, bent antiparallel β-sheet with an AdoMet binding pocket.[113]

1.3.4 Health Implications

The importance of MSR in preserving the activity of MS is underscored by the clinical consequences of derangements in folate and homocysteine metabolism. Two highly prevalent polymorphisms have been identified in the MSR-encoding gene *MTRR* in humans: c.66A>G (p.Ile22Met) and c.524C>T (p.Ser175Leu).[103,114] Both polymorphisms result in MSR with a 4-fold reduced ability to reactivate MS.[115] Women that have the c.66A>G polymorphism on both alleles have an increased risk of bearing children with neural tube closure defects or trisomy 21 (Down's Syndrome).[116–119] Pregnant women with low plasma cobalamin levels exasperate this risk.[116,120]

Severe MSR dysfunction arises from the autosomal recessive inheritance of mutations in the *MTRR* gene.[103] Impaired MSR leads to a decrease in MS activity that results in hyperhomocysteinemia and hypomethioninemia.[103,121] These metabolic conditions can

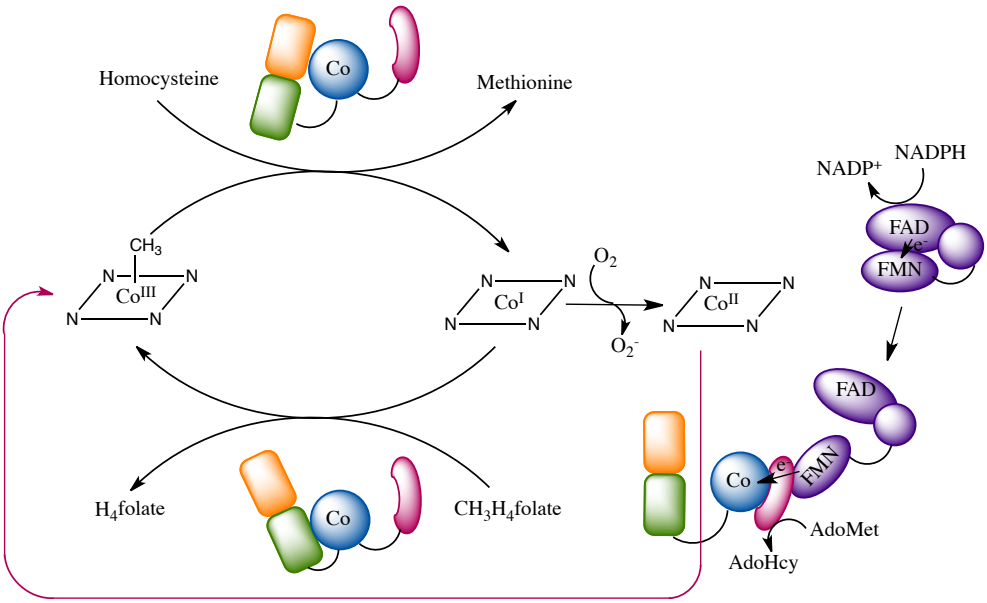

Figure 1.27: Catalytic cycle and reactivation mechanism of methionine synthase and methionine synthase reductase. For the modular methionine synthase, the homocysteine-, CH_3THF-, cobalamin-, and activation domain are shown in orange, green, blue, and purple, respectively. MSR is shown in purple.

lead to megaloblastic anemia, severe neurological deficits, developmental delay, and blindness.[122,123] Elevated plasma homocysteine levels are linked to an increase in risk for cardiovascular disease and Alzheimer's disease.[122,124–126] Neurological disorders may be caused by a depletion of folate pools, thereby disrupting protein and DNA synthesis and cellular division.[126] The absence of any MSR activity is embryonically lethal, as shown in *MTRR* gene knockout studies in mice.[123]

1.4 Research Aims

The aim of this research was to investigate the structural origins of the differential kinetics of electron transfer in two diflavin oxidoreductases, CPR and MSR. Superimposition of primary and tertiary structures of CPR and MSR allowed for the design of structural variants based on conserved and nonconserved amino acid residues at the FAD/NADPH-binding domain. First of all, I sought out the role of the conserved FAD-stacking tryptophan residue in the coenzyme binding and electron transfer properties in MSR. Through comparative mutagenesis studies with CPR, I aimed to determine if the homologous tryptophan retained the same functional role. Through each experiment, I strove to shed insight into the regulation of electron flux in these enzymes. Secondly, I targeted potential active site

residues involved in coenzyme binding and examined their influence on catalysis. Finally, for an additional perspective of diflavin oxidoreductase catalysis, I extended my research to CPR from *Artemisia annua*, a plant species.

In an effort to meet these research goals, conspicuous and subtle structural variants of CPR and MSR were expressed and isolated. The overall catalytic performance of these variants was assessed by the steady state reduction of an artificial terminal electron acceptor. Furthermore, the strength of coenzyme binding in enzyme variants was measured by product and dead-end inhibition studies. Rapid enzymatic reduction kinetics were characterized by stopped-flow spectrophotometry. A comprehensive analysis of various enzyme variants by these techniques revealed the functional role of specific structural elements in the catalytic mechanism of CPR and MSR.

Chapter 2

Probing the Regulatory Role of an Active Site Trp697 in Methionine Synthase Reductase

2.1 Summary

In this chapter, the role of the FAD isoalloxazine ring-shielding tryptophan residue (Trp697) in MSR is investigated through various strategic amino acid exchanges. Two mutations are made to the penultimate Trp697 to reduce and remove the π-π-stacking interaction with the isoalloxazine ring: W697H and W697S. The C-terminal residue Ser698 is also targeted for mutagenesis: S698A and S698Δ. Steady state and pre-steady state kinetic properties of each MSR variant are characterized through the use of aerobic spectrophotometry and anaerobic stopped-flow spectrophotometry. Through these experimental techniques, the large indole side chain of Trp697 is found to play an important regulatory role in coenzyme recognition and intramolecular electron flow in MSR. Interflavin electron transfer is enhanced by the presence of Trp697. Bipartite binding of the coenzyme is supported by shielding the FAD isoalloxazine ring, thereby ensuring substrate selectivity based on the 2'-phosphate group.

2.2 Background

FNR enzymes, including diflavin oxidoreductases, all have a conserved aromatic residue that stacks against the *re*-face of the FAD isoalloxazine ring. The conserved aromatic is a tyrosine in FNR, phenylalanine in nitric oxide synthase, and a tryptophan in cytochrome P450 reductase and methionine synthase reductase.[49,65,127] X-ray crystallography of plant FNRs show that the tyrosine lies coplanar to maximize π orbital overlap with the FAD isoalloxazine ring.[44] For direct hydride transfer, the nicotinamide ring must position the C4 *pro*-R hydrogen within 4Å of the N5 nitrogen of the isoalloxazine ring.[61,128] In this conformation (see Figure 2.1), the nicotinamide ring occupies the same space as the aromatic

residue, and therefore productive substrate binding requires a structural rearrangement that, at a minimun, involves residue displacement.[44]

Early X-ray crystallography and mutagenesis studies in FNR have provided insight into the role of the aromatic residue in coenzyme binding. Productively-bound nicotinamide has only been captured in FNR crystals upon deletion or mutation of the aromatic to a smaller side chain, suggesting that the residue does obstruct nicotinamide ring placement.[62] By mutating Tyr308 to a nonaromatic serine, the FNR variant has a much greater affinity for $NADP^+$ and NAD^+.[63] Thus, Tyr308 destabilizes the nicotinamide ring such that the energetic cost of residue displacement outweighs the energetic gain of nicotinamide ring binding.[62,63,129] Moreover, the Tyr308Ser variant also significantly reduced the preference for NADPH over NADH. Equivalent mutations in NOS and CPR were shown to produce similar effects on substrate binding.[61,130–132] By obstructing the nicotinamide ring of NADPH and NADH, the residue ensures the coenzyme binds according to the bipartite binding model first described for FNR.[44,62] Despite enhanced coenzyme binding, nonaromatic mutations to the FAD active site residue generate reduced catalytic activities in both FNR and CPR variants. The reduced catalytic activity is attributed to slow $NADP^+$ release.[61,63,132]

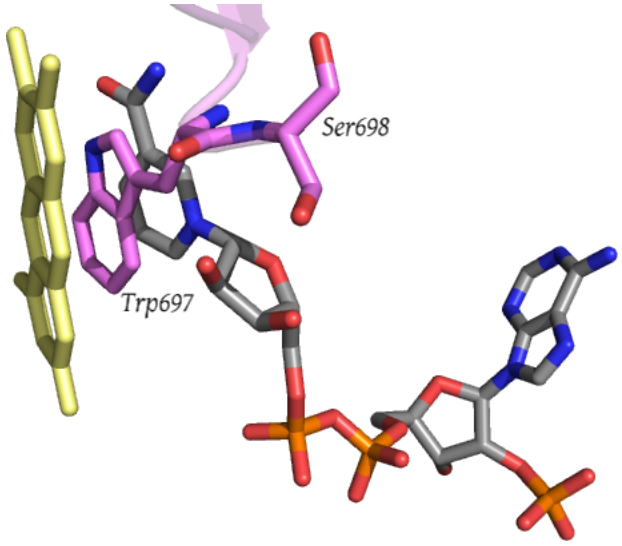

Figure 2.1: Crystal structure of MSR (PDB 2QTZ) superimposed with a NADPH-bound variant rat CPR W676XS677X (PDB 1JAO) to illustrate the inevitable steric clash between Trp and the nicotinamide ring. The flavin is shown in yellow with the ribityl adenosine tail removed for clarity. NADPH is in grey and the MSR C-terminal residues, Trp697 and Ser698, are shown in light purple with the standard elemental colouring.

For MSR, the *re*-face of the FAD isoalloxazine ring forms π-π interactions with the indole ring of a tryptophan residue (Trp697). X-ray crystallography shows that the entire indole ring of Trp697 overlaps with the isoalloxazine ring.[65] In $NADP^+$-bound MSR, only electron

density for the bound 2',5'-ADP moiety is observed, which indicates that the nicotinamide ring moiety is delocalized. Isothermal titration calorimetry revealed that 2',5'-ADP binds to MSR with a 14-fold stronger affinity than $NADP^+$.[65] As in FNR and other diflavin oxidoreductases, the coenzyme binds to MSR in a bipartite manner which promotes a strong preference for NADPH over NADH. Thus, the nicotinamide ring energetically disfavours coenzyme binding which, by analogy with FNR, is attributed to the energetic cost of aromatic residue displacement. To determine if the penultimate Trp697 has a differential role in coenzyme binding in MSR, the effects of mutations to this residue are examined. Furthermore, since coenzyme binding precedes hydride transfer and subsequent electron flow through the enzyme, the effects of mutations to Trp697 on the catalytic activities of human MSR are also investigated.

The functional role of C-terminal residues, Trp697 and Ser698, in regulating coenzyme binding and electron flux in MSR was determined by mutagenesis. Two mutations of Trp697 were made: W697H and W697S. The imidazole side chain of W697H reduces the π-π stacking interaction with the FAD isoalloxazine ring. This variant is designed to reduce the energetic cost of residue displacement by the coenzyme. The W697S variant abolishes any π orbital overlap with the isoalloxazine ring of FAD and is anticipated to significantly improve coenzyme binding by favouring the productive nicotinamide ring conformation. Structural rearrangement of Trp697 is expected to confer movement to the adjacent C-terminal Ser698, and therefore the S698Δ and S698A mutations were constructed. The S698Δ variant was designed to examine the effect of the additional conformational change of the C-terminal serine backbone on coenzyme binding, while the S698A variant assessed the potential contribution of the hydroxyl side chain. The steady state kinetic properties of each variant were measured by spectrophotometric analysis of cytochrome c reduction. Coenzyme binding was evaluated through product and dead-end inhibition studies with $NADP^+$ and 2',5'-ADP, respectively. Finally, stopped-flow spectrophotometry allowed for detection of the rapid reduction of each variant with saturating NADPH.

2.3 Results

2.3.1 Steady state kinetic data

MSR-catalyzed reduction of cytochrome c^{3+} was used to determine the steady state kinetic parameters for the four variants. The data are summarized in Table 2.1. Cytochrome c^{3+} is widely used as a nonphysiological terminal electron acceptor for the kinetic analysis of diflavin oxidoreductases, making it an ideal substrate for comparative purposes. It also only accepts an electron from the FMN cofactor, therefore catalytic turnover, k_{cat}, encompasses both the hydride transfer to FAD and the FAD to FMN electron transfer steps. For wild-

Table 2.1: Steady state kinetic parameters of wild-type and variant MSR with NADPH. Conditions: 1 mL reaction volume, 8 μM cytochrome c^{3+}, 2 *p*mole enzyme, varied [NADPH] and [inhibitor], 50 mM Tris-HCl pH 7.5 at 25 °C. Assays were done in triplicate and fit to the Michaelis-Menten equation. Inhibition data from four inhibitor concentrations were fit to a competitive inhibition equation.[a] Data acquired from Wolthers *et al.*[65]

MSR	Inhibitor	k_{cat} (s^{-1})	K_m ($M \times 10^{-6}$)	K_i ($M \times 10^{-6}$)	k_{cat}/K_m ($s^{-1}M^{-1} \times 10^{+6}$)
[a]MSR_{WT}	$NADP^+$	7.23 ± 0.14	2.37 ± 0.17	37 ± 3	3.1 ± 0.3
	2',5'-ADP	6.62 ± 0.13	1.95 ± 0.14	1.44 ± 0.11	3.4 ± 0.3
S698Δ	$NADP^+$	12.2 ± 0.4	1.95 ± 0.18	2.2 ± 0.3	6.2 ± 0.8
	2',5'-ADP	13.9 ± 0.5	2.7 ± 0.3	0.45 ± 0.05	5.2 ± 0.8
S698A	$NADP^+$	3.2 ± 0.2	4.7 ± 1.1	9 ± 2	0.7 ± 0.2
	2',5'-ADP	2.56 ± 0.13	5.6 ± 0.8	0.43 ± 0.06	0.45 ± 0.09
W697S	$NADP^+$	0.64 ± 0.02	0.25 ± 0.06	0.09 ± 0.02	2.6 ± 0.7
	2',5'-ADP	0.69 ± 0.01	0.44 ± 0.06	2.4 ± 0.5	1.6 ± 0.2
W697H	$NADP^+$	15.3 ± 0.6	4.0 ± 0.5	26 ± 5	3.8 ± 0.6
	2',5'-ADP	18.3 ± 0.5	3.8 ± 0.3	0.98 ± 0.08	4.8 ± 0.5

type MSR, the catalytic turnover, k_{cat}, for cytochrome c^{3+} reduction is 3-7 s^{-1}.[65] An enhanced k_{cat} of 15 s^{-1} and 12 s^{-1} is observed for W697H and S698Δ, respectively. The rate of reduction for W697S is reduced by 12-fold to 0.6 s^{-1} while that for S698A (3 s^{-1}) remains similar to wild-type. The catalytic efficiency (k_{cat}/K_m) with NADPH for all variants is also comparable to wild-type, with the exception of a 6-fold less efficient S698A.

Steady state inhibition studies were conducted to measure the affect of the amino acid variations on the binding of $NADP^+$ and 2',5'-ADP. The results are compiled in Table 2.1. Inhibition constants, K_i, for 2',5'-ADP binding in the variants range from 0.4 μM to 2.4 μM, similar to wild-type. Across all variants, the 2',5'-ADP moiety elicits a tighter binding affinity over $NADP^+$, as observed for wild-type MSR, with the exception of W697S. Stronger binding affinity for the oxidized coenzyme was measured in all variants, with the highest binding affinity observed for W697S (K_i = 0.09 μM). Notably, the W697S variant also elicited the slowest catalytic turnover. Next strongest is S698Δ with K_i of 2 μM, followed by S698A (K_i = 9 μM) and then W697H (K_i = 25 μM).

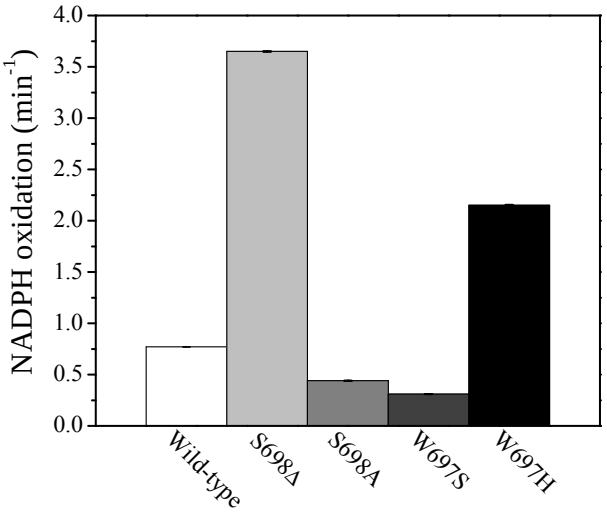

Figure 2.2: The NADPH oxidation activity of MSR variants. Conditions: 1 mL reaction volume, 2 *p*mole enzyme, 1 mM NADPH, 50 mM Tris-HCl pH 7.5 at 25 °C. The average of three replicates and the associated error are listed above for each variant.

2.3.2 Uncoupled NADPH oxidation

To dissect the individual steps of the catalytic mechanism that are affected by the active site substitutions, uncoupled NADPH oxidase activity was evaluated. The results are shown in Figure 2.2. Uncoupled NADPH oxidase activity is defined as flavin reduction by NADPH and the subsequent flavin re-oxidation by O_2. Therefore, the observed rates of NADPH oxidation are not dependent on interflavin electron transfer. W697H and S698Δ exhibited enhanced NADPH oxidase activity of 8- and 10-fold, respectively. S698A oxidase activity was modestly slower than wild-type, while that of W697S was reduced by approximately half. As the interflavin electron transfer step is excluded from these activity studies, the enhanced steady state turnover rates observed are accredited to improved hydride transfer and/or coenzyme binding/dissociation.

2.3.3 Coenzyme Preference

Wild-type MSR possesses a strong >19 000-fold preference for 2'-phosphorylated NADPH over NADH.[65] To test if this coenzyme specificity is preserved in the W697 variants, the kinetic properties using NADH as an electron donor were measured, and the results are summarized in Table 2.2. Coenzyme specificity is reported by the ratio of $[(k_{cat}/\mathrm{K}_{NADPH})/(k_{cat}/\mathrm{K}_{NADH})]$; W697H preference for NADPH dropped to 3473-fold, while W697S almost lost coenzyme discrimination with only a 20-fold preference for

Table 2.2: Steady state kinetic parameters of wild-type and W697 MSR variants with NADH. Conditions: 1 mL reaction volume, 2 *p*mole enzyme, 8 μM cytochrome c^{3+}, varied [NADH], 50 mM Tris-HCl pH 7.5 at 25 °C. Assays were done in triplicate and fit to Michaelis-Menten equation. [a] Data acquired from Wolthers *et al.*[65]

MSR	k_{cat} (s^{-1})	K_m (M $\times 10^{-3}$)	k_{cat}/K_m ($s^{-1}M^{-1}$ $\times 10^{+3}$)	$(k_{cat}/K_{NADPH})/(k_{cat}/K_{NADH})$
[a]MSR_{WT}	0.24 ± 0.03	3.5 ± 0.6	0.068 ± 0.014	19400
W697S	8.1 ± 0.4	0.06 ± 0.01	131 ± 30	20
W697H	4.7 ± 0.9	4.5 ± 0.4	1.1 ± 0.3	3473

NADPH. Aromatic stacking with the isoalloxazine ring clearly imparts regulatory control in the proclivity of NADPH use versus NADH.

2.3.4 Multiple wavelength pre-steady state kinetics

Pre-steady state reduction of MSR variants with saturating NADPH was followed by stopped-flow spectrophotometry in an oxygen-free environment. Photodiode array detection allowed for the recording of UV-visible spectra from 380 to 700 nm over a select time domain. Figure 2.3 shows the full spectra collected for S698A over 200 s by this method. These spectral data are then resolved by the singular value decomposition (SVD) algorithm to give an approximate number of spectral intermediates. This analysis aids in determining the best model for use in global analysis, see Figure 2.4 and Table 2.3. As for wild-type MSR, the S698 variants were best fit to a four species, triphasic irreversible model (a→b→c→d).[133] W697 variants fit best to a three species, biphasic model (a→b→c). The intermediate spectral profiles and their respective observed rate constants of formation/decay represent an equilibrium distribution of enzyme intermediates that form over the course of the reaction. As such, the spectral intermediates (a, b, c, d) do not represent distinct enzyme intermediates.

The first kinetic phase is assigned to the reduction of fully oxidized enzyme, spectral species a, to a partially reduced species b. Across all variants, this kinetic phase (k_{obs1}) shows only a partial loss of absorbance at the flavin maxima 454 nm. Based off of this absorbance change, the first kinetic phase represents hydride transfer to FAD to form $FADH_2$. The fastest observed rate constants for hydride transfer were observed for W697H and S698Δ (115 s^{-1} and 82 s^{-1}, respectively), which are 4- and 3-fold faster than wild-type MSR. The rate constant for S698A is comparable to native MSR. The W697S variant, however, is 8-fold slower (3 s^{-1}).

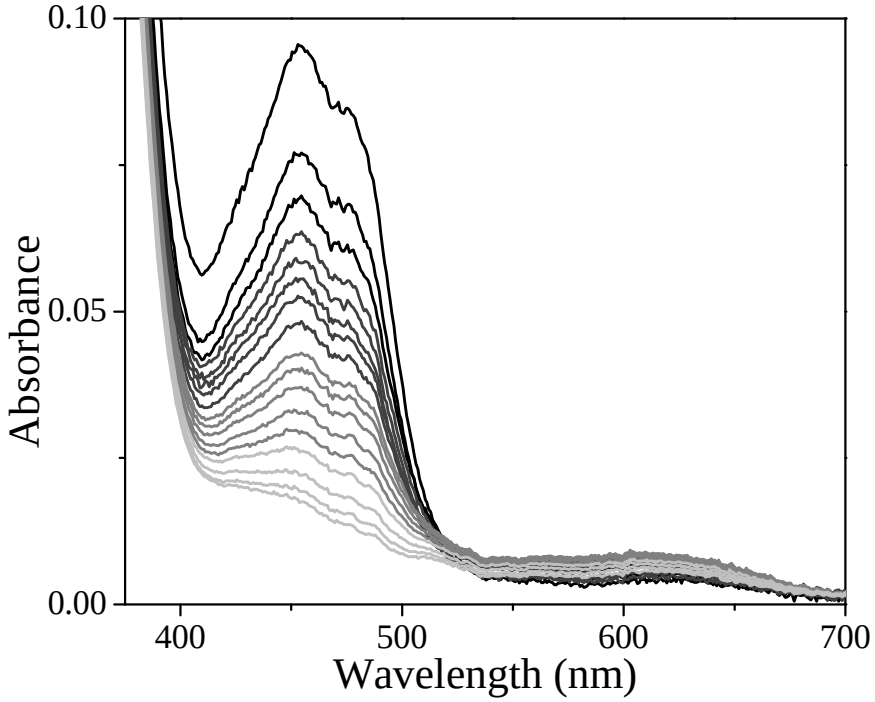

Figure 2.3: Anaerobic reduction of MSR variant S698A with saturating NADPH monitored with multiple wavelength stopped-flow spectrophotometry. Conditions: 10 μM enzyme, 100 μM NADPH, anaerobic 50 mM Tris-HCl pH 7.5 at 25 °C. Full spectral reduction of S698A, 300 scans over 200 s, is reduced to ∼20 traces for clarity.

Table 2.3: Observed rate constants of the pre-steady state reduction of MSR variants. Conditions: 10 μM enzyme, 100 μM NADPH, anaerobic 50 mM Tris-HCl pH 7.5 at 25 °C. S698 variant reduction was best fit to a three-step kinetic model while W697 variant reduction was best fit to a two-step kinetic model.[a] Data acquired from Wolthers *et al.*[65]

MSR	k_{obs1} (s^{-1})	k_{obs2} (s^{-1})	k_{obs3} (s^{-1})
[a]MSR_{WT}	24.9 ± 0.1	0.18 ± 0.01	0016 ± 0.003
S698Δ	82.1 ± 0.7	2.01 ± 0.04	0.019 ± 0.001
S698A	27.2 ± 0.3	2.33 ± 0.01	0.025 ± 0.001

MSR	k_{obs1} (s^{-1})	k_{obs2} (s^{-1})
W697S	3.4 ± 0.1	0.011 ± 0.001
W697H	115.3 ± 0.6	0.008 ± 0.001

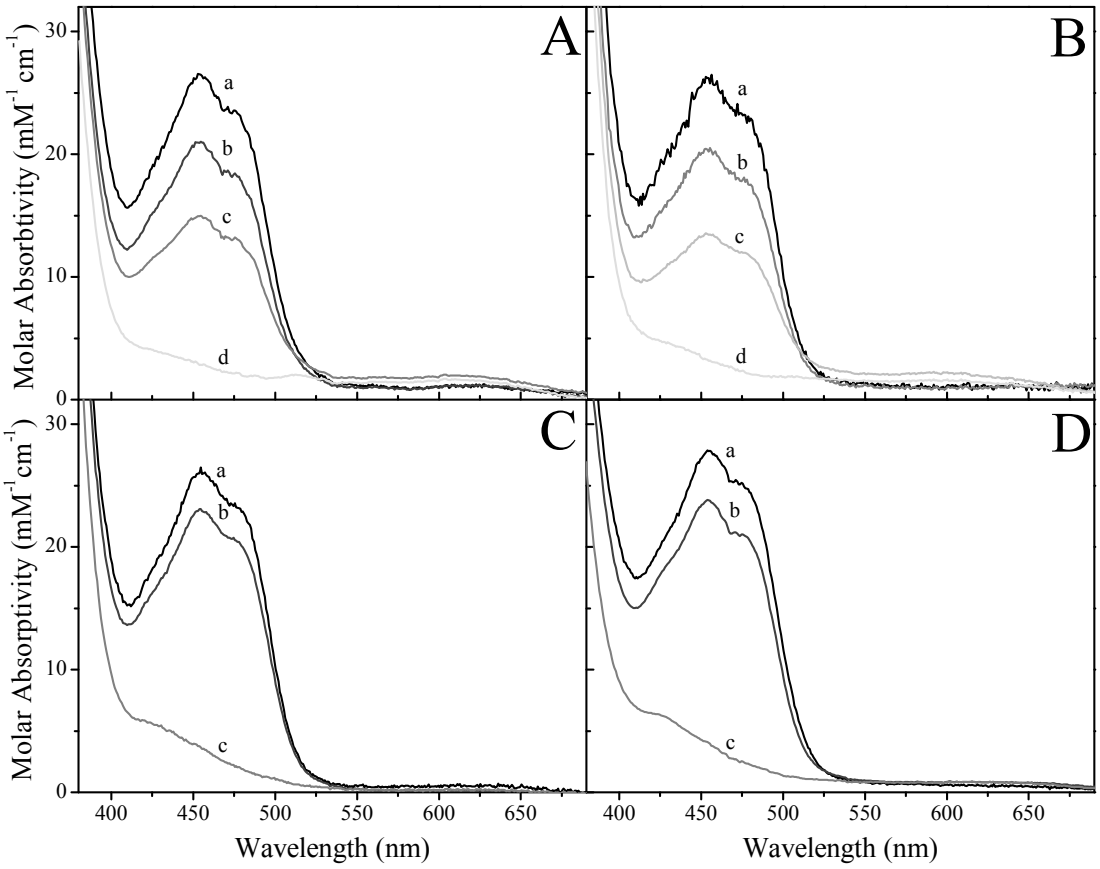

Figure 2.4: Spectral profiles for anaerobic reduction of MSR variants by saturating NADPH monitored with multiple wavelength stopped-flow spectrophotometry. Conditions: 10μM enzyme, 100 μM NADPH, anaerobic 50 mM Tris-HCl pH 7.5 at 25 °C. Time-resolved spectral intermediates for S698A (A), S698Δ (B), W697H (C), and W697S (D). S698 variants follow a three-step kinetic model with four discrete spectral species (a→b→c→d) and W697 variants follow a two-step kinetic model with three discrete spectral species (a→b→c), associated rate constants are summarized in Table 2.3.

The second kinetic phase (k_{obs2}) for the S698 variants is attributed to interflavin electron transfer, and this is represented by a further decrease in absorbance at 454 nm and an increase in absorbance at 600 nm. The latter absorbance change is indicative of the formation of the disemiquinone species E-FADH•-FMNH•. Both S698A and S698Δ elicit a k_{obs2} of ∼2 s^{-1} for the conversion of spectral species b to c. Over 100 s, the formation and decay of the disemiquinone is observed at 600 nm, see Figure 2.7. The third phase, conversion of species c to d, represents the binding of a second molecule of NADPH and reduction to the four-electron reduced state E-$FADH_2$-$FMNH_2$. This final phase, k_{obs3}, is equivalent to wild-type MSR for both S698 variants (∼0.02 s^{-1}).

The kinetic profile for the W697 variants are notably different. For these variants, reduction occurs in two kinetic phases without an observable disemiquinone intermediate. As stated above, the first kinetic phase occurs with the absorbance loss at 454 nm. For both variants, the associated amplitude change for the first kinetic phase is less than that observed in wild-type and S698 variants. Furthermore, unlike the native enzyme, the second kinetic phase is not accompanied by an increase in absorbance at 600 nm. Inspection of absorbance traces at 600 nm over 100 s (Figure 2.7) reveals a lack of any detectable disemiquinone. Thus, the second kinetic step encompasses the conversion of two-electron reduced species b to the full four-electron reduced species c by a second NADPH molecule. The k_{obs2} for this second kinetic phase is ∼0.01 s^{-1} for both W697 variants.

The fact that W697H and W697S are reduced to the full four-electron reduced state (evident by the final absorbance spectra), indicates that interflavin electron transfer occurs in these enzyme variants. This is further confirmed by the ability of the two variants to reduce cytochrome c^{3+}, which accepts electrons from the FMN cofactor. To further test that the W697 variants are capable of interflavin electron transfer and formation of the disemiquinone species, they were rapidly mixed with an equimolar concentration of NADPH to produce a two-electron reduced species. As predicted, a decrease in absorbance at 454 nm with an increase at 600 nm marked the slow interflavin exchange of electrons as equilibrium is established over 750 s (Figure 2.5). These results suggest that the lack of detectable disemiquinone is a consequence of attenuated interflavin electron transfer, rather than the inability of the enzymes to form the disemiquinone species.

2.3.5 Single wavelength pre-steady state kinetics

Enzymatic reduction was followed at the flavin and disemiquinone absorption maxima 454 nm and 600 nm, respectively, by anaerobic stopped-flow spectrophotometry. The collected traces are shown in Figure 2.6 and Figure 2.7. Data acquisition over a single wavelength generates stopped-flow traces which facilitate determination of individual, fast rate constants. Fitting traces at 454 nm to a double-exponential equation produced two

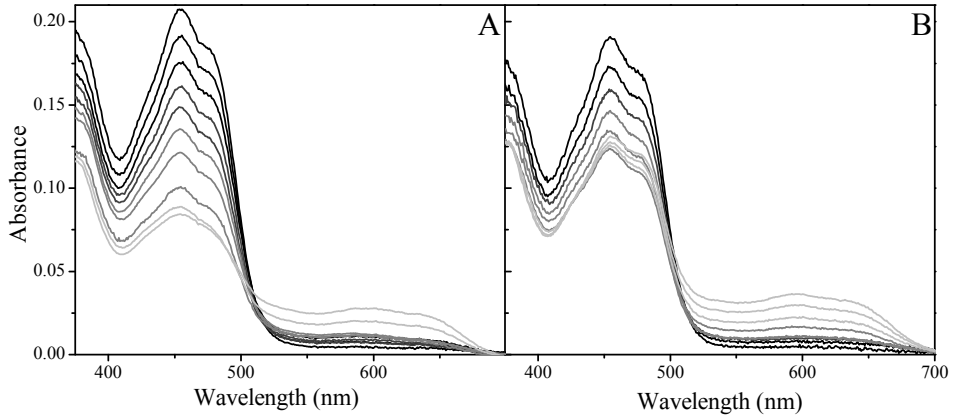

Figure 2.5: Anaerobic reduction of MSR variants by equimolar NADPH monitored with multiple wavelength stopped-flow spectrophotometry. Conditions: 10μM enzyme, 10 μM NADPH, anaerobic 50 mM Tris-HCl pH 7.5 at 25 °C. W697S (Panel *A*) and W697H (Panel *B*) were rapidly mixed with NADPH and monitored over 750 s.

observed rate constants for each variant over a 10 s time frame. As in the PDA data analyses, k_{obs1} is fastest for W697H (136 s^{-1}) followed by S698Δ (106 s^{-1}), S698A (23 s^{-1}) and W697S (3.5 s^{-1}). The second kinetic phase for S698Δ and S698A occurs with a rate constant k_{obs2} of 3.7 s^{-1} and 1.6 s^{-1}, respectively. An extended time frame of 500 s captures the complete reduction of W697S and W697H and yields a k_{obs2} of 0.005 s^{-1} for both which are comparable to the PDA acquired rate constants.

The dependence of k_{obs1} on the concentration of NADPH for each variant was also analyzed by single wavelength absorption studies at 454 nm. In wild-type MSR, the hyperbolic dependence of k_{obs1} on NADPH concentration allows for the extraction of a dissociation constant, K_d.[133] Figure 2.8 shows the independence of k_{obs1} on [NADPH] observed for all MSR variants, which suggests that the binding of NADPH is much tighter for these variants.

2.4 Discussion

2.4.1 Regulation of coenzyme preference by Trp697

Coenzyme preference is clearly established in native MSR with a strong 19 400-fold preference for NADPH over NADH.[65] The two coenzymes only differ by a 2'-phosphate group. At the coenzyme binding cleft, the 2'-phosphate group sits in a pocket of well-conserved polar residues. The strong affinity for the 2',5'-ADP moiety is attributed to

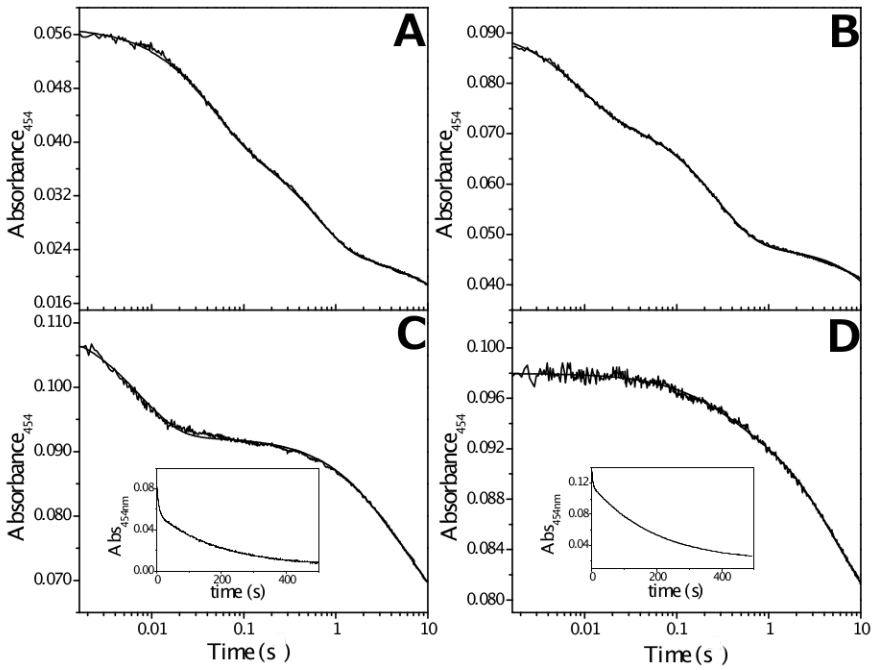

Figure 2.6: Anaerobic reduction of MSR variants by saturating NADPH monitored with single wavelength stopped-flow spectrophotometry at 454 nm. Conditions: 10 μM enzyme, 100 μM NADPH, anaerobic 50 mM Tris-HCl pH 7.5 at 25 °C. S698A (Panel *A*), S698Δ (Panel *B*), W697H (Panel*C*), and W697S (Panel *D*) were rapidly mixed with NADPH and monitored over 10 s at 454 nm. Insets for Panel *C* and *D* are the linear absorbance traces at 454 nm over 500 s to show completion.

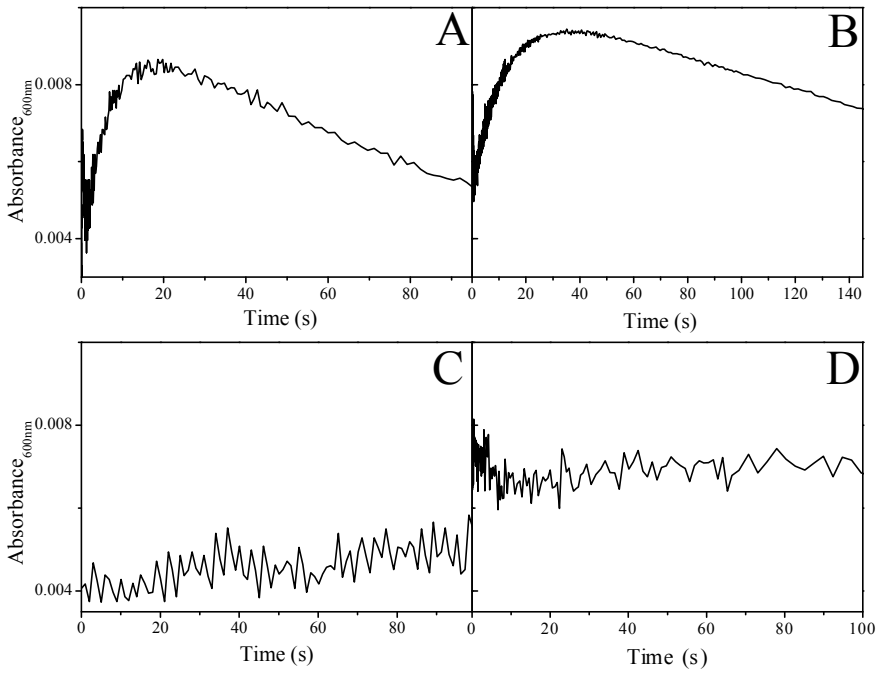

Figure 2.7: Anaerobic reduction of MSR variants by saturating NADPH monitored with single wavelength stopped-flow spectrophotometry at 600 nm. Conditions: 10 μM enzyme, 100 μM NADPH, anaerobic 50 mM Tris-HCl pH 7.5 at 25 °C. S698A (Panel *A*), S698Δ (Panel *B*), W697S (Panel*C*), and W697H (Panel *D*) were rapidly mixed with NADPH and monitored over 100 - 150 s at 600 nm.

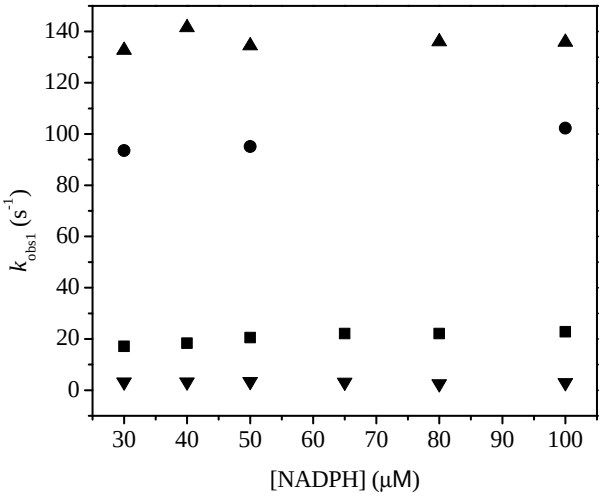

Figure 2.8: Dependence of k_{obs1} on NADPH concentration. S698A (■), S698Δ(●), W697H (▲) and W697S (▼).

polar interactions with these residues. While the 2',5'-ADP moiety binds tightly, the binding of full-length $NADP^+$ is 15-fold weaker, indicating that the nicotinamide mononucleotide (NMN) moiety does not contribute favourably to the coenzyme binding energy.

By exchanging the bulky indole side chain of Trp697 for a smaller side chain, a loss in NADPH specificity over NADH was observed. The mutations did not affect the 2',5'-ADP binding site, as the inhibition constants (K_i) for 2',5'-ADP remained similar to wild-type. However, the resulting K_i for $NADP^+$ revealed a more pronounced effect on the binding of the NMN moiety among the variants. In W697H, the affinity for $NADP^+$ is only 1.5-fold stronger, indicating that the aromatic imidazole can partially substitute for the indole in disrupting NMN binding. For this variant and both S698 variants, the two-step binding of NADPH is still preserved where the 2',5'-ADP first binds tightly and then the NMN moiety moves into the FAD active site. The tighter binding of $NADP^+$ reflects the reduced energetic cost of productive nicotinamide binding in these variants. In contrast, bipartite binding is not maintained in W697S since $NADP^+$ binds with a greater affinity than 2',5'-ADP. The energetic cost of NMN binding is substantially reduced as removal of the aromatic residue likely exposes the *re*-face isoalloxazine ring to solvent, which would favour binding of the nicotinamide ring. Therefore, both binding sites are immediately accessible. As a consequence, the initial selection for the 2'-phosphorylated substrate by the polar pocket is lost, hence the weak 64-fold preference for NADPH over NADH in W697S. Thus, the presence of Trp697 controls substrate preference for NADPH over NADH.

2.4.2 Regulation of hydride transfer by Trp697

Hydride ion transfer to the isoalloxazine ring occurs directly from the nicotinamide ring, therefore variants that reduce the energetic barrier for nicotinamide stacking against the flavin are expected to accelerate this first chemical step. The first observed rate constant, k_{obs1}, is assigned to hydride transfer. For both W697H and S698Δ, the rate constant is indeed accelerated by 5- and 6-fold respectively, while the rate constant was unchanged for S698A. The accelerated rate constant for W697H is likely attributed to the reduced π-π stacking between the FAD isoalloxazine ring and the imidazole side chain, which presumably lowers the thermodynamic barrier for residue displacement. Likewise, the increase in k_{obs1} for S698Δ suggests that the C-terminal residue may also contribute to the thermodynamic barrier to Trp697 conformational change, possibly through steric constraint. Thus, removal of S698 would alleviate some conformational restriction on Trp697 displacement. Since the equivalent rate constant for S698A is the same as wild-type, the steric constraint likely originates from the C-terminal residue backbone rather than the Cβ-hydroxyl side chain.

Although W697S is expected to ameliorate productive NADPH binding by removing the thermodynamic barrier for residue displacement, the variant elicited a 8-fold slower k_{obs1}.

Since it exhibits strong coenzyme affinity, the W697S variant may be limited by $NADP^+$ release. However, no evidence of a charge-transfer complex between the nicotinamide ring and the FAD cofactor was observed in the stopped-flow data. The bipartite binding mode of NADPH is impaired in W697S and may be the origin of the slower k_{obs1}. Without the initial docking of the 2',5'-ADP moiety, the nicotinamide ring may adopt a number of nonproductive binding states before attaining a catalytically relevant orientation. Moreover, while the FAD active site is more accessible to the nicotinamide ring in W697S, as serine occupies less space than the bulky tryptophan, the distance between the nicotinamide and isoalloxazine rings may not be optimal for hydride transfer.

2.4.3 Regulation of interflavin electron transfer by Trp697

During the MSR reductive half-reaction, the disemiquinone species forms as an intermediate. This is evident by the appearance and subsequent disappearance of an absorbance band centered at 600 nm. For the W697 variants, the disemiquinone intermediate does not accumulate to a detectable amount. However, interflavin electron transmission does still take place, as both W697 variants are able to catalyze cytochrome c^{3+} reduction, fully reduce to the four-electron level under saturating NADPH conditions, and achieve the disemiquinone state upon equilibration with equimolar NADPH. Therefore, while electron transfer between the flavins is still possible in the W697 variants, the presence of Trp697 in wild-type and the S698 variants accelerates this step and allows for buildup of the disemiquinone.

The mechanism by which Trp697 accelerates interflavin electron transfer is still unclear, however given that the Trp697 is positioned at the FAD/FMN domain interface, it is conceivable that the residue influences the conformational equilibria of the enzyme. The enzyme is envisioned to alternate between a closed conformation for intramolecular electron transfer and an open conformation for intermolecular electron transfer. The open state increases the distance between flavins, thereby disfavouring interflavin electron transfer. The closed state, captured in the crystal structure of rat CPR, brings the flavins less than 4 Å together in an arrangement that is anticipated to allow for rapid electron exchange.[49] Since Trp697 lies at the FAD/FMN domain interface, it is proposed that the residue stabilizes the interdomain contact to favour the closed state in which the interflavin distance is minimized and interflavin electron transfer is favoured. Thus, mutation of this residue may shift the conformational equilbiria to the open state which would attenuate interflavin electron transfer.

Despite the enhanced rate constants associated with hydride transfer and uncoupled NADPH oxidation in W697H and S698Δ, the variants only modestly increased the rate of steady state cytochrome c^{3+} reduction. Cytochrome c^{3+} receives a single electron from the

FMN cofactor, thus reduction of cytochrome c^{3+} reflects the sum of all the forward and reverse rate constants of the catalytic mechanism, including NADP(H) binding and release, hydride transfer, and interflavin electron transfer. For W697H, the faster rate constant for hydride transfer is offset by slower disemiquinone formation, so turnover is only modestly affected. S698Δ elicited a faster rate constant for hydride transfer, interflavin electron transfer, and a strong NADPH binding affinity. However, the turnover for this variant may be limited by the slower dissociation of the tightly bound oxidized coenzyme for the next round of catalysis.

2.4.4 Extension of regulatory role of tryptophan to CPR

Wild-type human CPR evokes an over 4 300-fold preference for NADPH over NADH. Previous studies have shown that by exchanging the Trp676 residue (CPR equivalent of Trp697) for a histidine or alanine, the substrate affinity is greater and the preference for NADPH drops. A dramatic decrease was measured for W676A whose preference for NADPH over NADH is only 4-fold. The shift in coenzyme selectivity is attributed to the loss of bipartite binding due to a lack of steric control by the active site Trp676.[132]

For full-length CPR, hydride transfer is tightly coupled to interflavin electron transfer, and this is observed in one kinetic phase with a k_{obs1} of 20 s^{-1}.[67] For CPR W676H, this rate constant decreases to 3 s^{-1} and the enzyme only reduces to the two-electron level. Interestingly, the k_{obs1} for W676H reduction is the same as that measured for the wild-type FAD domain. In full-length native CPR, the hydride transfer step is not thermodynamically favourable since the midpoint potential of the hydride-receiving $FAD_{ox/hq}$ redox couple (-340 mV) is more electronegative than that of NADP(H) (-320 mV).[66,67] However, the presence of the very electropositive $FMN_{ox/sq}$ couple (-66 mV) shifts the equilibria towards reduced FMN. In the isolated FAD domain, the $\sim$ 7-fold slower k_{obs1} is a consequence of the lost thermodynamic pull by FMN, and this is reflected by an attenuated rate constant. Although the FMN domain is still present in W676H, the lack of reduction past the two-electron level, along with the reduced k_{obs1} and slow overall catalytic turnover, indicates that interflavin electron transfer is impeded in this variant.

If the role proposed for Trp697 in accelerating interflavin electron transfer in MSR is applied to CPR, then the histidine variant would be expected to slow down the k_{obs1} in CPR but not in MSR. In W697H of MSR, the k_{obs1} for hydride transfer is not negatively affected by the reduced interflavin electron transfer because the two events are kinetically distinct. In contrast, the two kinetic events are coupled in CPR. As such, the slow k_{obs1} of CPR W676H is due to disruption of electron transfer from FAD to the more electropositive FMN, thereby adversely affecting the thermodynamic drive of electron flux through the

enzyme. Thus, the role of the conserved active site tryptophan in accelerating interflavin electron transfer is conserved in CPR and MSR.

2.5 Experimental Procedures

2.5.1 Materials

Unless otherwise stated, all chemical reagents were purchased from Fisher. The reagents NADPH, NADH, $NADP^+$, 2',5'-ADP, and cytochrome c^{3+} were obtained from Sigma Aldrich (Oakville, ON, Canada). *Pfu* Turbo DNA polymerase, *Taq* DNA polymerase and Xl1 Blue cell lines were purchased from Agilent Technologies (Mississauga, ON, Canada). Rosetta(DE3)pLysS competent cells were obtained from EMD Biosciences. Protein purification supplies, Resource Q column and glutathionine sepharose 4B resin, were purchased from GE Biosciences.

2.5.2 Generation and expression of MSR tryptophan variants

The W697S, W697H, S698Δ and S698A MSR variants were generated from the wild-type MSR plasmid template pGEX-4T1-MSR using the QuikChange Site-Directed Mutagenesis Kit (Agilent Technologies). Oligonucleotide primers were designed based on the published sequence (Accession number AF121214) and purchased from Integrated DNA Technologies (Coralville, Iowa, USA). The primers used are tabulated in Table 2.4. The NAPS DNA Sequencing Laboratory of the University of British Columbia (Vancouver, Canada), confirmed the desired amino acid mutations and the absence of additional PCR-induced errors. Successfully designed mutant plasmids were transformed into the *Escherichia coli* strain Rosetta2(DE3)pLysS using the heat shock method. Recombinant GST-fusion proteins were grown in 200 mL cultures of Luria-Bertani medium, containing 100 μg mL^{-1} of ampicillin and 34 μg mL^{-1} chloramphenicol, overnight at 37 °C and 225 rpm using a Innova44 incubator shaker. With 10 mL of the 200 mL cultures, 0.5 L cultures of Terrific Broth containing 100 μg mL^{-1} ampicillin and 34 μg mL^{-1} chloramphenicol were inoculated and grown at 30 °C to an Abs_{600} of 0.8. Cultures were then induced with 0.1 mM IPTG and the temperature was lowered to 25 °C overnight. The cells were harvested at 6,360 × g for 10 min and stored at −80 °C.

2.5.3 Purification of MSR variants

All purification steps were performed on ice or at 4 °C. Cells overexpressing the recombinant enzyme were resuspended in 200 mL of 1×GST bind/wash buffer (10×GST = 43 mM Na_2HPO_4, 14.7 mM KH_2PO_4, 1.37 M NaCl, 27 mM KCl, pH 7.3 with 1 mM EDTA,

Table 2.4: The forward (F) and reverse (R) oligonucleotide primers designed for each MSR C-terminal variant. Mutation is in bold.

MSR Variant	Oligonucleotide Sequence
S698Δ	F 5' CTTCAGGATATTTGGΔTAGCGGCCGCATCGTGAC 3' R 5' GTCACGATGCGGCCGCTAΔCCAAATATCCTGAAG 3'
S698A	F 5' CTTCAGGATATTTGG**GCA**TAGCGGCCGCATCGTGAC 3' R 5' GTCACGATGCGGCCGCTA**TGC**CCAAATATCCTGAAG 3'
W697H	F 5' CTTCAGGATATT**CAT**TCATAGCGGCCGCATCGTGAC 3' R 5' GTCACGATGCGGCCGCTATGA**ATG**AATATCCTGAAG 3'
W697S	F 5' CTTCAGGATATT**TCG**TCATAGCGGCCGCATCGTGAC 3' R 5' GTCACGATGCGGCCGCTATGA**CGA**AATATCCTGAAG 3'

1 mM DTT) and protease inhibitors benzamidine (2 mM) and PMSF (1 mM). The cell mixture was sonicated with the Sonicator S-4000 (Misonix Inc.) at 22% power amplitude with alternating 8 s pulses and 1 min pauses for a total of 45 min. Cell lysate was then centrifuged at 39,120 × g for 45 minutes to separate the soluble protein from cellular debris. The supernatant was collected and loaded onto a Glutathione-Sepharose 4B (GE Healthcare) column equilibrated with 1×GST bind/wash buffer and was washed with 5 column volumes of 1×GST bind/wash buffer. The GST-tagged protein was eluted with the elution buffer (50 mM Tris-HCl, 1 mM EDTA and DTT, and 10 mM glutathione). The eluate was then dialyzed overnight with 20 U/mg thrombin (GE Healthcare) at 4 °C in dialysis buffer (4 L of 1×GST bind/wash buffer, 1 mM EDTA and 1 mM DTT). The dialyzed sample was again applied to a 1×GST-equilibrated column and the cleaved protein was collected from the flow-through. The sample was further purified by anion exchange chromatography on a 1 mL Resource Q column (GE Healthcare) using an AKTApurifier system (GE Healthcare) with a linear gradient from 50 to 500 mM NaCl in 50 mM Tris-HCl pH 7.5 at a flow rate of 2 mL/min. The desired fractions were collected based on the absorbance readings at 280 nm and the yellow colour that is characteristic of oxidized flavoproteins. The final concentration of purified MSR was determined by the absorption at 454 nm and the Beer-Lambert Law, Equation 3.1.

$$Abs = \varepsilon lc \tag{2.1}$$

where c is the concentration of sample, Abs is the absorbance at 454 nm, ε is the molar extinction coefficient of MSR (25.6 $mM^{-1}cm^{-1}$), and l is the light path length (1 cm).

The purified MSR mutants were flash-frozen in liquid nitrogen and stored in 20% glycerol at −80 °C for later steady-state assays and pre-steady state stopped-flow analysis.

2.5.4 Steady state turnover analysis

The rate of cytochrome c^{3+} reduction was assessed for each variant at 25 °C by the change in absorbance at 550 nm ($\Delta\ \varepsilon = 21.1\ \mathrm{mM^{-1}cm^{-1}}$) on a Lambda 25 UV/Vis Spectrometer (Perkin Elmer). The 1 mL reaction mixture contained 50 mM Tris-HCl buffer, pH 7.5, 8 μM cytochrome c^{3+}, and varied NADPH concentrations from 0.25 μM - 50 μM, and the reaction was initiated by 2 *p*moles of the MSR variant. Reaction velocites for each NADPH concentration were collected in triplicate and the data were fit to the Michaelis-Menten equation by non-linear least-squares regression analysis using Origin 8.5 software (OriginLab Co.). For the inhibition assays, the reaction mixtures contained 50 mM Tris-HCl, pH 7.5, 8 μM cytochrome c^{3+}, and varying concentrations of substrate, NADPH, and inhibitor ($NADP^+$, 2',5'-ADP); the inhibition reactions were initiated by 2.0×10^{-12} mole of MSR. Product and dead-end inhibition assays were triplicated and fit with non-linear least-squares regression analysis to the competitive inhibition equation, Equation 2.2 in the Origin 8.5 software (OriginLab Co.)

$$\nu_i = \frac{VA}{K_m(1 + \frac{I}{K_i}) + A} \tag{2.2}$$

where ν_i is the initial velocity, V is the maximal velocity, A is the varied substrate concentration, K_m is the apparent Michaelis constant, I is the inhibitor concentration, and K_i is the inhibition constant.

Uncoupled NADPH oxidation 1 mL reactions were carried out at 25 °C in 50 mM Tris-HCl, pH 7.5 with saturating 1 mM NADPH. Consumption of NADPH was monitered spectrally at 340 nm over 90 s. The assays were performed in triplicate. Initial velocity ($\mathrm{M/min^{-1}}$) was calculated from the slope at 340 nm using the extinction coefficient of 6.22 $\mathrm{mM^{-1}cm^{-1}}$.

2.5.5 Pre-steady state kinetic analysis

Stopped-flow studies were performed under anaerobic conditions using the SF-61DX2 Stopped-flow apparatus from TgK Scientific in a Belle Technology glove box. Kinetic experiments were conducted in 50 mM Tris-HCl pH 7.5 that was degassed by extensive bubbling with nitrogen gas and allowed to equilibriate in the glove box overnight. Protein samples were brought into the glove box and oxygen was removed via gel filtration over Bio-Rad Econo-Pac 10 DG column equilibrated with anaerobic 50 mM Tris-HCl pH 7.5. Substrate was dissolved in anaerobic 50 mM Tris-HCl pH 7.5 buffer. A diluted sample was taken out

of the glove box to determine the concentration spectrally at 340 nm ($\epsilon = 6.22$ mM^{-1}cm^{-1}). For single and multiple wavelength studies, pseudo-first order conditions were established with a 10-fold saturating concentration of substrate. Two syringes were filled with an initial concentration of 20 μM enzyme and 200 μM substrate, respectively.

Multiple wavelength absorption changes over substrate-mediated reduction were monitored with a photodiode array detector (PDA) (TgK Scientific). Substrate and MSR variant samples were both diluted 2-fold after mixing. The spectra were measured over 200 s with the monochromator auto-shutter on to reduce the likelihood of photoreduction. Spectral species were resolved by applying the singular value decomposition (SVD) algorithm to the spectral data in ReactLab Kinetics (Jplus Consulting Pty Ltd., Karawara, Australia). SVD is an unbiased algorithm that decomposes the original data matrix into a reduced set of output data that is defined in terms of the linearly independent components and their weighted significance. This allows for the determination of the number of spectral species in a reaction model. Global analysis of the reduced SVD data were best fitted to a three-step (a→b→c→d) or two-step (a→b→c) model with four or three discrete spectral species.

For single wavelength studies, the reduction of NADPH was followed at 454 nm with a photomultiplier detector at 25 °C with varying NADPH concentrations. The substrate and MSR sample were both diluted 2-fold after mixing. An average of 3 traces of the single-wavelength data were fitted to a double-exponential equation (Equation 2.3)

$$A = C_1 e^{-k_{obs1}t} + C_2 e^{-k_{obs2}t} + b \tag{2.3}$$

where k_{obs1} and k_{obs2} are the observed rate constants for the fast and slow phases, respectively. C_1 and C_2 are their relative amplitudes, and b is the final absorbance. The data were extracted from an Excel file generated from ReactLab and imported into Origin for graphical representation.

Chapter 3

Comparative investigation into the role of coenzyme-coordinating residues and the FAD-shielding tryptophan in coenzyme binding and electron flux in MSR and CPR

3.1 Summary

In this chapter, the functional role of the FAD isoalloxazine ring-stacking tryptophan is further investigated in MSR with a comparative study in CPR. In addition, the influence of stabilizing interactions between active site residues and the coenzyme on MSR and CPR catalytic properties is examined. First, conservative amino acid mutagenesis of the active site tryptophan to phenylalanine and tyrosine assessed the effect of residue side chain size and polarity on catalytic properties in MSR (W697F and W697Y) and in CPR (W676F and W676Y). Second, strategic mutations were made to coenzyme-coordinating residues to strengthen or weaken the interaction with NADPH in MSR (K291R and A622K) and in CPR (R298A and K602AV603K). Aerobic and anaerobic spectrophotometric techniques were employed to characterize the steady state and pre-steady state kinetics of each variant. Through these studies, I determined a differential regulatory role for the FAD-shielding tryptophan in electron flux in MSR and CPR. The hydride transfer step in MSR is gated by tryptophan displacement, as the free energy cost of disrupting the FAD-Trp interaction outweighs the gain of nicotinamide placement. In contrast, electron flow through CPR is not gated by tryptophan displacement but rather by displacement of the oxidized nicotinamide ring by the bulky residue following hydride transfer. Alterations at the coenzyme-binding sites of MSR and CPR also elicited differential results. As anticipated, the removal or addition of potential hydrogen bonding interactions with the coenzyme resulted in weakened or strengthened coenzyme binding affinity, respectively. The accelerated flavin reduction

in CPR variants with weaker coenzyme binding affinity was attributed to faster release of oxidized coenzyme. In contrast, the accelerated flavin reduction in MSR variants with stronger coenzyme binding affinity was ascribed to improved coenzyme binding.

3.2 Background

Of the diflavin oxidoreductase family members, MSR and CPR are the most structurally related with 41 % amino acid sequence similarity. Despite the high level of sequence similarity, the human forms of MSR and CPR elicit different rates of electron transfer and coenzyme binding affinity. Both 2',5'-ADP and $NADP^+$ bind tightly to CPR with a dissociation constant (K_d) of ~50 nM.[64] The nearly equal binding affinities indicates that the nicotinamide ring moiety does not contribute to the coenzyme binding energy of $NADP^+$. In contrast, for MSR and also for FNR, the K_d values for $NADP^+$ and 2',5'-ADP are not equivalent with values of 37 μM and 2μM for MSR and 14 μM and 2μM for FNR.[65,134] Thus, the nicotinamide ring moiety contributes unfavourably (7 kJ/mol MSR and 5 kJ/mol FNR) to the $NADP^+$ binding energy of these enzymes.[63,65] The K_d values also reveal that the binding of 2',5'-ADP and $NADP^+$ is 40- and 700-fold weaker in MSR compared to CPR.

For the electron transfer kinetics, the differences between these two enzymes are evident in their overall turnover rates for the non-physiological electron acceptor cytochrome *c in vitro*. The reductase activity of CPR is >7-fold faster than that of MSR (in varied buffer conditions).[65,132] Cytochrome *c* reduction by CPR was performed in 300 mM phosphate buffer, while 50 mM Tris was used for MSR assays. This distinction is made since inorganic phosphate competitively inhibits NADPH at the 2'-phosphate-binding site and may influence the measured rate of cytochrome *c* reduction at high concentrations.[135] Analogous mutagenesis studies on the FAD-shielding tryptophan residue in MSR and CPR emphasize their differing kinetic properties. While in the W676H variant of CPR the rates of FAD reduction and cytochrome *c* turnover are attenuated, the W697H variant of MSR elicits an enhancement of both kinetic events.[132,136,137] In light of these differences, the specific role of the FAD-isoalloxazine ring-shielding tryptophan in MSR and CPR was further scrutinized by generating more conservative substitutions. In addition to providing insight into the functional role of this active site tryptophan, these substitutions also enabled evaluation of the clear preference for the bulky tryptophan over smaller aromatic residues in diflavin oxidoreductases.

Furthermore, the structural origin of the contrasting coenzyme binding affinities in MSR and CPR are investigated. Inspection of the available crystal structures for MSR and CPR shows that the coenzyme binds to the NADPH/FAD-binding domain primarily through a number of polar interactions and hydrophobic contacts with the 2',5'-ADP moiety of

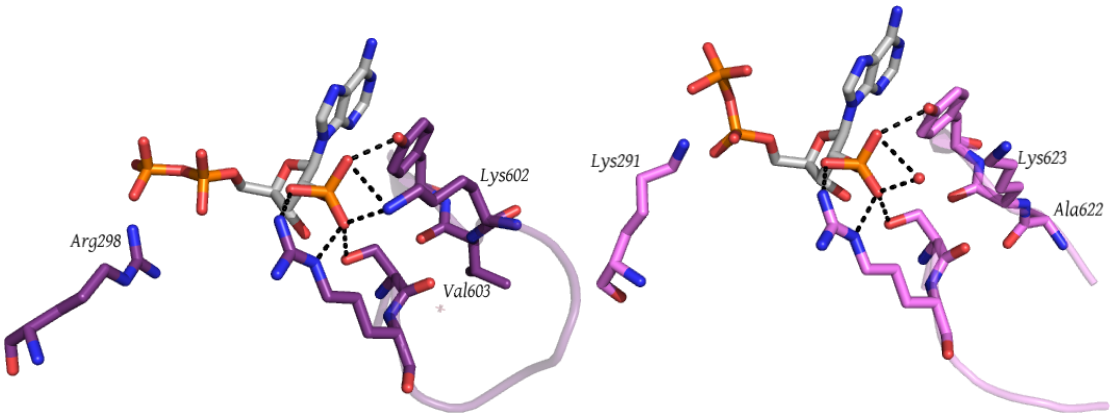

Figure 3.1: NADPH-coordinating residues at the coenzyme-binding pocket for CPR (PDB 3QE2) *Right* and MSR (2QTZ) *Left*. NADPH is shown in grey with the standard atom-coloured stick model. Potential hydrogen bonding interactions are shown in black dashes.

the substrate. Most of these residues are conserved between MSR and CPR, however two notable differences are highlighted in Figure 3.1. At the pocket lined with polar residues that coordinate to the 2'-phosphate group of the substrate, a lysine residue (Lys602) of CPR is clearly within hydrogen bonding distance to the 2'-phosphate group. In MSR, a water molecule instead hydrogen bonds with the 2'-phosphate as the equivalent residue is an alanine (Ala622). A lysine residue (Lys623) is present in the polar pocket, however it is not in a position for direct hydrogen bonding to the phosphate group. At the NADPH pyrophosphate-coordinating site, CPR has an additional interaction with the substrate through an arginine (Arg298) as opposed to a lysine (Lys291) in MSR. Thus, amino acid substitutions to these designated active site residues are made in an effort to identify the origin of the respective coenzyme binding affinities of MSR and CPR, and also to examine how substrate binding influences intramolecular electron flux.

The specific nature of the functional role of the penultimate C-terminal residue, Trp697 and Trp676, in regulating coenzyme binding and electron flux in MSR and CPR was determined through mutagenesis. The FAD isoalloxazine ring-shielding tryptophan was mutated to a tyrosine and a phenylalanine: W697Y and W697F (MSR) and W676Y and W676F (CPR). These conservative residues were chosen to preserve residue aromaticity and π-π interactions with the FAD isoalloxazine ring, while testing the effect of residue side chain size and polarity. To study the potential benefit of a bidentate over a monodentate interaction with the substrate pyrophosphate group, CPR Arg298 was mutated to an alanine and MSR Lys291 was mutated to an arginine. In an effort to mirror the polar pocket active site of CPR, the Ala622 of MSR was exchanged for a lysine. The active site of CPR was made more MSR-like by a double mutation of Lys602Ala Val603Lys. Steady state kinetic properties of each variant were measured by spectrophotometric analysis of cytochrome *c* reduction.

Table 3.1: Steady state kinetic parameters of MSR W697 and CPR W676 variants. Conditions: 1 mL reaction volume, 8 μM cytochrome c^{3+}, 0.2-2 *p*mole enzyme, varied [NADPH] and [inhibitor] at 25 °C. Assay buffer for MSR is 50 mM Tris-HCl pH 7.5 and 50 mM KPi pH 7.5 for CPR. Assays were done in triplicate and fit to the Michaelis-Menten equation. Inhibition data from four inhibitor concentrations were fit to a competitive inhibition equation.[a] Data acquired from Wolthers *et al.*[65]

Enzyme	k_{cat} (s^{-1})	K_m ($M \times 10^{-6}$)	K_i ($M \times 10^{-6}$)		k_{cat}/K_m ($s^{-1}M^{-1} \times 10^{+6}$)
			$NADP^+$	2',5'-ADP	
Wild-type$_{MSR}$[a]	7.2 ± 0.1	2.4 ± 0.2	37 ± 3	1.4 ± 0.1	3.1 ± 0.3
W697F$_{MSR}$	17.0 ± 0.3	1.2 ± 0.1	3.0 ± 0.3	0.10 ± 0.01	15 ± 2
W697Y$_{MSR}$	24.3 ± 0.4	1.2 ± 0.1	4.2 ± 0.5	0.7 ± 0.1	21 ± 2
Wild-type$_{CPR}$	20.0 ± 0.2	0.7 ± 0.1	1.0 ± 0.1	0.6 ± 0.1	28 ± 2
W676F$_{CPR}$	3.8 ± 0.1	0.3 ± 0.1	0.4 ± 0.1	1.9 ± 0.3	12 ± 1
W676Y$_{CPR}$	13.1 ± 0.2	0.6 ± 0.1	0.7 ± 0.1	1.2 ± 0.1	24 ± 2

Product and dead-end inhibition studies with $NADP^+$ and 2',5'-ADP, respectively, were performed to assess coenzyme binding. The pre-steady state kinetics of flavin reduction were measured by stopped-flow spectrophotometry. Lastly, to determine if the amino acid substitutions affected the redox potentials of the flavin centers, redox potentiometry was performed for the CPR W676F and W676Y variants.

3.3 Results

3.3.1 Steady state kinetic data

The steady state kinetic parameters for cytochrome c^{3+} reduction by MSR and CPR variants are summarized in Table 3.1. For the MSR variants, a 2.4- and 3.4-fold faster k_{cat} was measured for W697F and W697Y. They were also more catalytically efficient with k_{cat}/K_m values 4.8- and 6.7-fold greater than wild-type. In contrast, the same mutations in CPR resulted in slower and less efficient catalytic turnover. The k_{cat} decreased by 6.4- and 1.5-fold for W676F and W676Y, with a 2.4- and 1.2-fold reduced catalytic efficiency.

The effect of amino acid substitutions on substrate binding was examined by steady state inhibition studies with $NADP^+$ and 2',5'-ADP; the results are summarized in Table 3.1. Previous isothermal titration calorimetry (ITC) experiments with MSR revealed a K_d of 34.5 μM for $NADP^+$ which is in agreement with the inhibition constant of 37 μM determined from steady state inhibition assays.[65] For CPR, a K_d of 50 nM was determined from ITC

experiments in phosphate-free buffer.[64] This K_d represents an over 700-fold tighter $NADP^+$ binding affinity in CPR compared to MSR. In the present studies, the $NADP^+$ K_i in CPR is only ∼40-fold tighter. The discrepancy is accredited to the buffer conditions used. A phosphate-free buffer is used for MSR assays, while a potassium phosphate (KPi) buffer is used for CPR assays. Binding studies in housefly CPR reveal that the free inorganic orthophosphate anion in the KPi buffer will competitively bind to the NADPH binding site. This competitive inhibition leads to an increase in the observed K_i for $NADP^+$ and 2',5'-ADP and in the apparant K_m for NADPH.[135] Indeed, ITC experiments conducted in phosphate buffer demonstrated a 15-fold increase in the K_i for $NADP^+$ binding in CPR.[64] Presumably, due to competition of the phosphate anion with the substrate at the 2',5'-ADP binding site. Here, the CPR assays are in 50 mM KPi buffer because the true K_m is too low for the detection limits of a 1 cm path length cuvette. In the analyses to follow, I assume that the orthophosphate anion binds to each of the CPR variants with the same affinity and, thus, perturbs the apparant K_i and K_m values to the same extent.

In MSR, a 12.3- and 8.8-fold tighter binding affinity for $NADP^+$ was observed for W697F and W697Y, respectively. Slightly tighter binding of the substrate analogue 2',5'-ADP was also observed in W697Y (K_i = 0.1 μM) and W697F (K_i = 0.7 μM). A modest increase in $NADP^+$ binding affinity was measured for CPR W676Y (K_i = 0.4 μM) and W676F (K_i = 0.7 μM) compared to the native enzyme (K_i = 1.0 μM). In addition, a slight decrease is observed for 2',5'-ADP.

3.3.2 Multiple wavelength pre-steady state kinetics of CPR variants

Pre-steady state reduction of the CPR variants by saturating NADPH was monitored by stopped-flow spectrophotometry in an anaerobic environment. The spectral changes upon reduction with NADPH, shown in Figure 3.2, were resolved by SVD and fitted globally to a best fit model. The observed rate constants are tabulated in Table 3.2. For wild-type CPR, reduction occurs in two kinetic phases. The first kinetic phase involves the reduction of oxidized enzyme to a two-electron reduced species ($a \rightarrow b$). This relatively fast phase has a rate constant of 19 s^{-1}. The spectral changes show flavin bleaching at 454 nm accompanied with the appearance of a broad absorbance band centered at 600 nm. These spectral features indicate that the hydride anion transfer from NADPH to FAD is kinetically coupled to interflavin electron transfer. The second kinetic phase entails further reduction of the enzyme population by another molecule of NADPH to spectral species c with an observed rate constant of 2.7 s^{-1}. The spectral changes associated with this kinetic phase include additional bleaching of absorbance at 454 and 600 nm. Unlike wild type CPR, the reduction of W676 variants occurs in only a single kinetic phase. Conversion of oxidized spectral species a to spectral species b shows loss of absorbance at 454 nm concomitant

Table 3.2: Observed rate constants of the pre-steady state reduction of CPR W676 variants. Conditions: 22 μM wild-type CPR, 16 μM W676F, 36 μM W676Y, 10-fold excess NADPH, anaerobic 50 mM Tris-HCl pH 7.5 at 25 °C. Wild-type CPR was best fit to a two-step model with three spectral intermediates (a $\rightarrow$ b $\rightarrow$ c). W676 variant spectral data were best fit to a single-step model with two spectral intermediates (a $\rightarrow$ b).

CPR	k_{obs1} (s^{-1})	k_{obs2} (s^{-1})
Wild-type	19.00 ± 0.01	2.72 ± 0.01
W676F	0.64 ± 0.01	–
W676Y	6.12 ± 0.03	–

with the emergence of a flat absorbance band in the longer wavelengths (550-700 nm). The rate constant for this kinetic step is 0.64 s^{-1} for W676F and 6.12 s^{-1} for W676Y.

In addition, unique spectral features are observed for these variants. In wild-type CPR, the absorbance maxima is at 454 nm with a shoulder at 474 nm, Figure 3.2A,D. The absorbance maxima at 454 nm is attributed to both flavins, while the shoulder at 474 nm originates from the FMN cofactor. For native CPR, the shoulder at 474 nm becomes less prominent in the conversion of spectral species *a* to *b*, which indicates that the FMN is reduced over this kinetic phase. The spectra of W676Y is similar to that of wild-type CPR (Figure 3.2 E,F). On the other hand, the flavin absorbance maxima of W676F shifts to 474 nm with a 456 nm shoulder. Upon NADPH reduction of both CPR variants, the absorbance maxima decreases and shifts to reveal a pronounced 474 nm shoulder (more so for W676F). Given that the 474 nm shoulder is a diagnostic of the oxidized FMN flavin, the stopped-flow data suggests that the FMN is not significantly reduced to the semiquinone in the first kinetic phase. Instead, this phase involves the reduction of FAD by a hydride ion transfer from NADPH, followed by formation of the $FADH_2$-$NADP^+$ charge-transfer complex. Evidence of the charge-transfer complex is provided by the broad, flat absorbance band over the longer wavelengths (>550 nm). The lack of appreciable disemiquinone absorbance maxima centered at 600 nm supports the formation of the charge-transfer complex rather than the disemiquinone species. Lastly, the greater amplitude change at 454 nm observed for W676Y over W676F, indicates that W676Y is further shifted from the oxidized state to the two-electron reduced form (E-$FADH_2$-FMN).

3.3.3 Primary kinetic isotope effect with (R)-[4-^{2}H]-NADPH on CPR reduction

Rapid reduction of the CPR variants with NADPH and (R)-[4-^{2}H] NADPH was followed at 454 and 600 nm by stopped-flow spectrophotometry. The absorbance traces collected

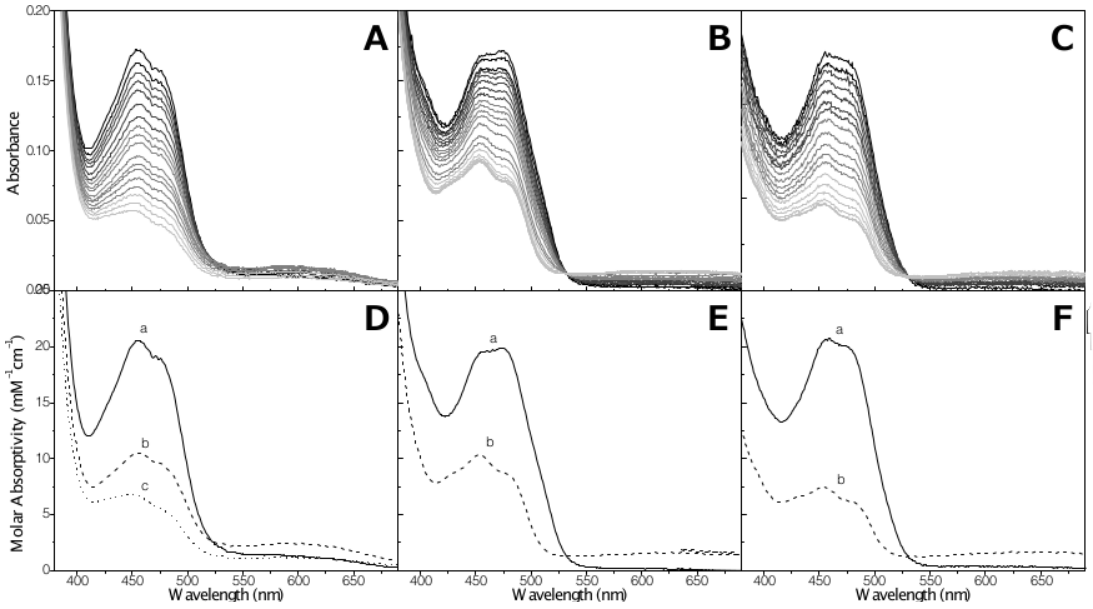

Figure 3.2: Spectral changes upon NADPH reduction of CPR W676 variants monitored by multiple-wavelength stopped-flow spectrophotometry. Conditions: 22 μM wild-type CPR, 16 μM W676F, 36 μM W676Y, 10-fold excess NADPH, anaerobic 50 mM Tris-HCl pH 7.5 at 25 °C. Time-dependent spectral changes over a 200 s time frame are shown for wild-type CPR (A), W676F (B) and W676Y (C). Global analysis of SVD-resolved spectra generated deconvoluted spectral intermediates for wild-type CPR (D), W676F (E) and W676Y (F). Wild-type CPR was best fit to a two-step model with three spectral intermediates (a $\rightarrow$ b $\rightarrow$ c). W676 variant spectral data were best fit to a single-step model with two spectral intermediates (a $\rightarrow$ b).

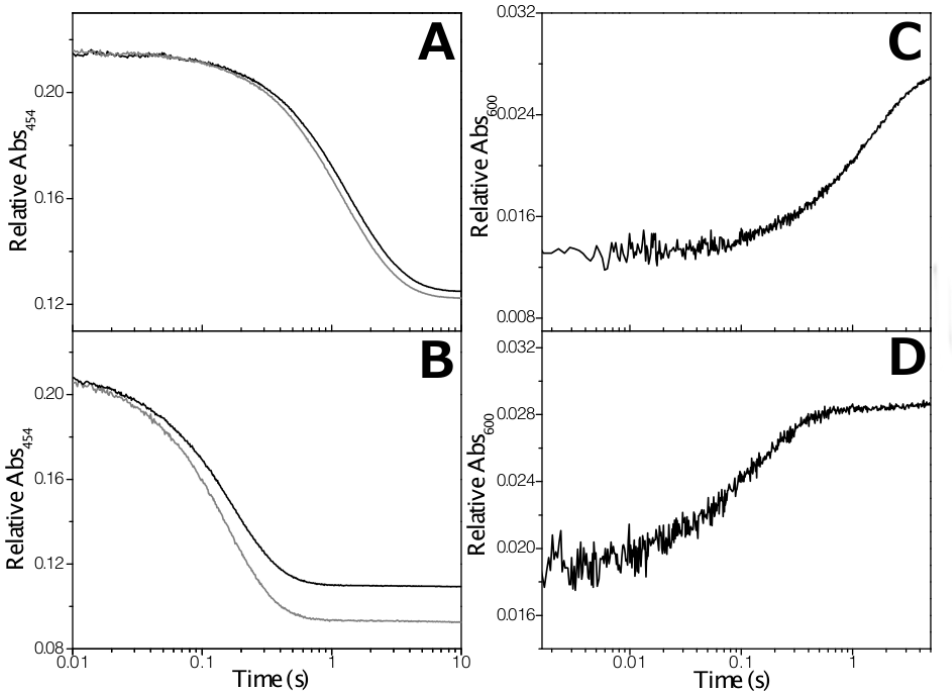

Figure 3.3: Anaerobic reduction of CPR variants by saturating substrate monitored at 454 and 600 nm by single-wavelength stopped-flow spectrophotometry. Conditions: 10 μM enzyme, 100 μM NADPH, 100 μM (R)-[4-^{2}H] NADPH, anaerobic 50 mM Tris-HCl pH 7.5 at 25 °C. Absorbance traces at 454 nm over 10 s for W676F (A) and W676Y (B) reduction with NADPH (black line) and (R)-[4-^{2}H]-NADPH (grey line). Absorbance traces at 600 nm over 10 s for NADPH-mediated reduction of W676F (C) and W676Y (D).

at 454 and at 600 nm over 10 s are shown in Figure 3.3 and were best fit to a single exponential equation. The equivalent rate constants for the monophasic spectral changes at 454 and 600 nm represent the same kinetic phase and are assigned to substrate binding, hydride transfer, and charge-transfer formation. The resulting observed rate constants are summarized in Table 3.3. In W676F and W676Y, reduction with (R)-[4-^{2}H]-NADPH yields a slight increase in the observed rate constant for flavin reduction, and the primary kinetic isotope effect is lost with KIE of 0.90 for W676F and 0.94 for W676Y. In these variants there is more of a commitment to the reverse reaction (e.g. hydride transfer from $FADH_2$ to $NADP^+$) than there is in native enzyme.

3.3.4 Thermodynamic analysis of CPR variants

Anaerobic redox potentiometry was performed with each CPR variant to determine if the kinetic behavior observed is a consequence of altered flavin redox potentials. Spectral data were collected during gradual titration of the fully oxidized enzyme with 0.25

Table 3.3: Observed rate constants and kinetic isotope effects for the pre-steady state reduction of CPR W676 variants monitored at 454 and 600 nm by single-wavelength stopped-flow spectrophotometry over 10 s. Conditions: 10 μM enzyme, 100 μM NADPH, 100 μM (R)-[4-^{2}H] NADPH, anaerobic 50 mM Tris-HCl pH 7.5 at 25 °C. Absorbance traces were averaged (3-5) then fit to a single exponential equation.

Wavelength	CPR	Substrate	k_{obs1} (s^{-1})	k_{obs2} (s^{-1})	isotope effect $k_{obs1}{}^H/k_{obs1}{}^D$
454 nm	Wild-type	NADPH	15.8 ± 0.2	4.12 ± 0.06	1.08 ± 0.02
		NADPD	14.63 ± 0.07	3.29 ± 0.05	
	W676F	NADPH	0.66 ± 0.01	–	0.90 ± 0.03
		NADPD	0.73 ± 0.01	–	
	W676Y	NADPH	5.60 ± 0.04	–	0.94 ± 0.02
		NADPD	6.0 ± 0.1	–	
600 nm	W676F	NADPH	0.70 ± 0.01		
	W676Y	NADPH	7.5 ± 0.1		

μL aliquots of sodium dithionite until full reduction was reached. With each addition of dithionite, the potential value and the absorbance spectrum were recorded. A plot of the summed absorbance values from 590 to 605 nm (the semiquinone absorbance maxima) versus the reduction potential (normalized to the standard hydrogen electrode) allowed for the extraction of midpoint potentials. For W676F, the midpoint potentials of the $FMN_{ox/sq}$ (-99 mV) and $FMN_{sq/hq}$ (-215 mV) couples are comparable to those of wild-type enzyme. On the other hand, the $FAD_{ox/sq}$ (-252 mV) and $FAD_{sq/hq}$ (-275 mV) couples are ∼30 and 110 mV more electropositive. However, this shift in potential would be anticipated to favour hydride transfer from NADPH, which is not reflected in the first rate constant. For W676Y, the redox potentials of $FAD_{ox/sq}$ (-263 mV) and $FAD_{sq/hq}$ (-260 mV) are also more electropositive than native enzyme and similar to those values determined for W676F albeit with greater error. Surprisingly, the tyrosine substitution has a more pronounced effect on the FMN redox couples with midpoint potentials of -166 mV and -198 mV for $FMN_{ox/sq}$ and $FMN_{sq/hq}$, respectively. It is unclear as to why W676Y elicits such an effect on the FMN redox center, however it may be due to an altered electronic environment surrounding W676Y since tyrosine is a polar residue and the isoalloxazine rings are highly polarizable. Although the midpoint potentials are more compressed in these variants compared to native CPR, the electron flow is still thermodynamically favoured through NADPH to FAD to FMN. Therefore, the dampened rates of flavin reduction observed are not a product of less favourable thermodynamics.

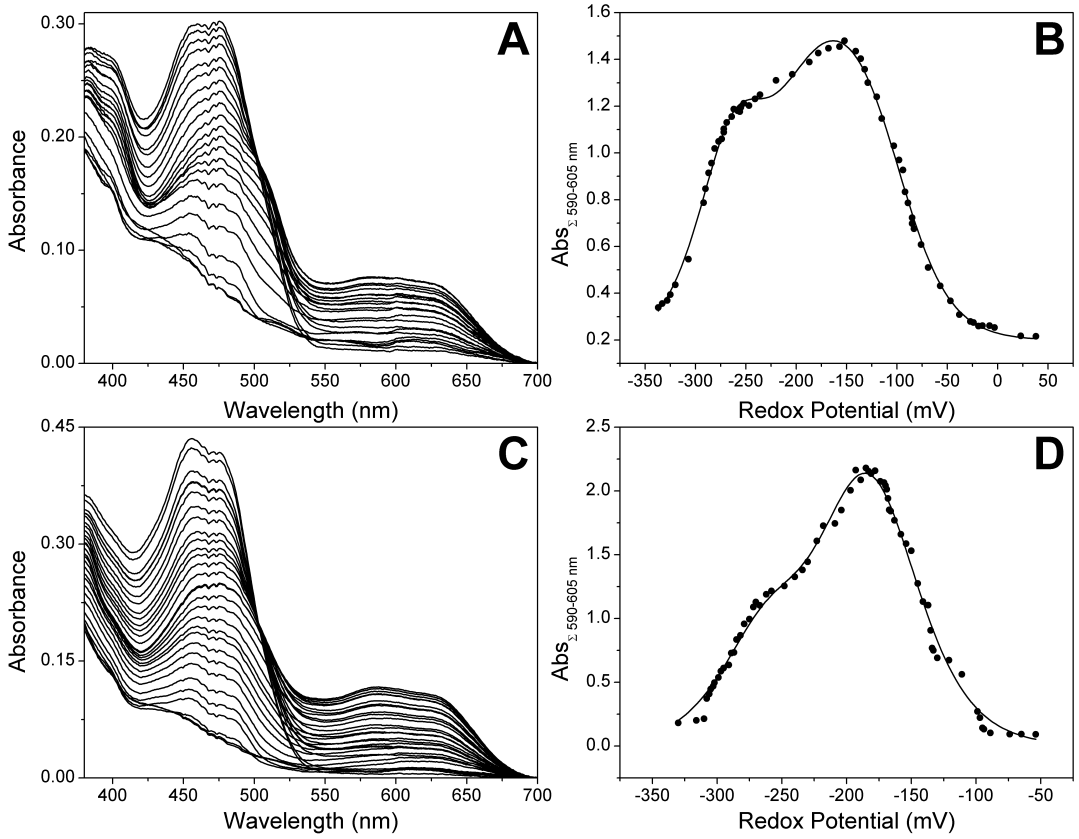

Figure 3.4: Redox potentiometric data of human CPR W676Y and W676F variants. Spectral properties of W676F (A) and W676Y (C) during redox titration. Spectra were recorded after each addition of the reductant dithionite. Plots of the summed absorbance values between 590 and 605 nm versus the normalized reduction potential for W676F (B) and W676Y (D). Fits of both data sets were made with the four-electron Nernst equation, as described in Experimental Procedures, and results are summarized in Table 3.4.

Table 3.4: Reduction potentials of the flavin couples of W676Y and W676F CPR variants.[a] Data acquired from Munro *et al.*[66]

	reduction potential (mV) vs standard hydrogen electrode					
	FAD cofactor			FMN cofactor		
Enzyme	Ox/Sq	Sq/Hq	Ox/Hq	Ox/Sq	Sq/Hq	Ox/Hq
Wild-type CPR[a]	-283 ± 5	-382 ± 8	-333 ± 7	-66 ± 8	-269 ± 10	-168 ± 9
W676F	-252 ± 10	-275 ± 8	-263 ± 9	-99 ± 1	-215 ± 5	-157 ± 5
W676Y	-263 ± 56	-260 ± 25	-262 ± 40	-166 ± 3	-198 ± 4	-182 ± 4

Table 3.5: Observed rate constants of the pre-steady state reduction of MSR W697 variants. Conditions: 10 μM enzyme, 100 μM NADPH, anaerobic 50 mM Tris pH 7.5 at 25 °C. W697 variant reduction was best fit to a three-step kinetic model.[a] Data acquired from Wolthers *et al.*[65].

MSR	k_{obs1} (s^{-1})	k_{obs2} (s^{-1})	k_{obs3} (s^{-1})
Wild type[a]	24.9 ± 0.1	0.18 ± 0.01	0.016 ± 0.003
W697F	215.1 ± 0.1	1.15 ± 0.01	0.016 ± 0.001
W697Y	214.5 ± 0.1	1.32 ± 0.01	0.015 ± 0.001

3.3.5 Multiple wavelength pre-steady state kinetics of MSR variants

The anaerobic NADPH-mediated reduction of MSR variants was followed by stopped-flow photodiode array detection. The spectral changes over the course of the reductive half-reaction are shown in Figure 3.5. Bleaching at the flavin absorbance maxima 454 nm is not accompanied by significant formation of an absorbance band at 600 nm. Inspection of the single absorbance trace at 454 nm reveals three resolvable kinetic phases, shown in Figure 3.6. The first extracted rate constant (k_{obs1}) is 215 s^{-1} and 213 s^{-1} for W697F and W697Y, respectively. Since this first kinetic phase occurs in less than 6 ms and photodiode array detector scans every 1.5 ms, this initial rate constant could not be extracted from the PDA data. However, the time-resolved spectral data were globally fit to a three-step kinetic model with the first rate constant fixed at the value determined from single wavelength analysis, refer to Section 3.2.6.

Similar rate constants were extracted for k_{obs2} (1.2 - 1.3 s^{-1}) and k_{obs3} (0.015 s^{-1}) for both MSR variants. The second rate constant is 5-fold higher than native MSR but similar to S698A and S698Δ. Full reduction of the enzyme by a second equivalent of NADPH is comparable in W697F, W697F and native enzyme. Neither variant shows accumulation of the semiquinone absorbance band at 600 nm from data acquired from single or multi-wavelength mode. The stopped-flow data reveal that reduction in the size of the aromatic side chain significantly increases the rate of FAD reduction in MSR, while suppressing electron transfer from FAD to FMN.

3.3.6 Primary kinetic isotope effect with (R)-[4-^{2}H]-NADPH on MSR reduction

Reduction of MSR variants using NADPH and (R)-[4-^{2}H] NADPH was monitored at 454 nm using stopped-flow spectrophotometry. The absorbance traces were biphasic over 5 s with a third slow phase observed over 200 s. The absorbance traces were fit from 0.001

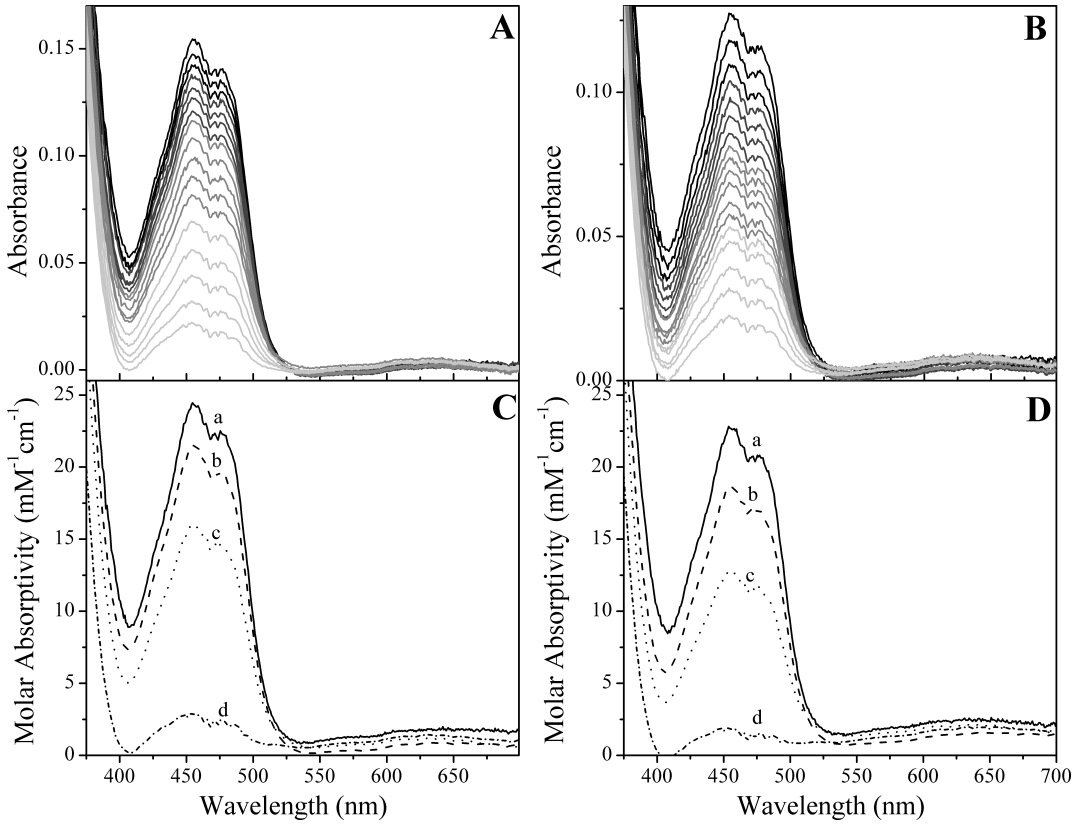

Figure 3.5: Anaerobic reduction of MSR W697 variants by saturating NADPH monitored by multiple-wavelength stopped-flow spectrophotometry. Conditions: 10 μM enzyme, 100 μM NADPH, anaerobic 50 mM Tris-HCl pH 7.5 at 25 °C. Full spectra of W697F (A) and W697Y (B) NADPH-mediated reduction over 200 s with $\sim$ 20 traces shown for clarity. Time-resolved spectral intermediates for W697F (C) and W697Y (D) variants follow a three-step kinetic model with four discrete spectral species (a→b→c→d), associated rate constants are summarized in Table 3.5.

Table 3.6: Observed rate constants and kinetic isotope effects for the pre-steady state reduction of MSR W697Y and W697F variants monitored at 454 and 600 nm by single-wavelength stopped-flow spectrophotometry.

Wavelength	MSR	Substrate	k_{obs1} (s^{-1})	k_{obs2} (s^{-1})	isotope effect ${k_{obs1}}^H/{k_{obs1}}^D$
454 nm	W697F	NADPH	215 ± 13	0.91 ± 0.12	2.02 ± 0.12
		NADPD	106 ± 10	1.36 ± 0.03	
	W697Y	NADPH	213 ± 12	1.11 ± 0.01	2.05 ± 0.14
		NADPD	104 ± 1	1.3 ± 0.2	
600 nm	W697F	NADPH	0.20 ± 0.01	–	
	W697Y	NADPH	0.207 ± 0.006	–	

to 5 s to a double exponential generating an initial rate constant k_{obs1} of 215 and 213 s^{-1} and a k_{obs2} of 0.91 and 1.1 s^{-1} for W697F and W697Y, respectively. The k_{obs1} is 10-fold faster than the corresponding rate in native MSR, indicating that the indole side chain of tryptophan greatly attenuates step(s) in the mechanism leading to the first hydride transfer event. When the same experiments were performed with deuterated substrate, the k_{obs1} decreased to 108 and 106 s^{-1} for W697F and W697Y. As a result, these variants both elicit a primary kinetic isotope effect of 2.0. Compared to wild-type MSR (KIE = 1.7), the KIE is slightly greater which indicates that hydride transfer becomes less rate-determining in these variants.

Unlike the W697H and W697S variants described in Chapter 2, W697F and, to a greater degree, W697Y exhibited a very small signal for the disemiquinone at 600 nm. The amplitude change of the formation and decay of the signal is very minor but shows that the W697Y can partially preserve the role of the Trp697 in facilitating disemiquinone formation.

3.3.7 Steady state kinetic data of the coenzyme-binding variants of MSR and CPR

MSR and CPR variant-catalyzed reduction of cytochrome c^{3+} was monitored by spectrophotometric methods. The determined steady state kinetic parameters are summarized in Table 3.7. In CPR, substituting the coenzyme pyrophosphate-coordinating Arg298 to an alanine only moderately affected the overall catalytic turnover, with a slower k_{cat} of 12 s^{-1} for cytochrome c reduction and a moderate decrease in catalytic efficiency compared to native CPR. The binding affinity for $NADP^+$, as measured by the inhibition constant K_i, was 2-fold weaker for R298A. Likewise, a reduced k_{cat} of 13 s^{-1} was determined for the double variant at the coenzyme 2'-phosphate-binding site, K602AV603K. A significant 39-fold reduction in the catalytic efficiency was also measured. K602AV603K elicited a much

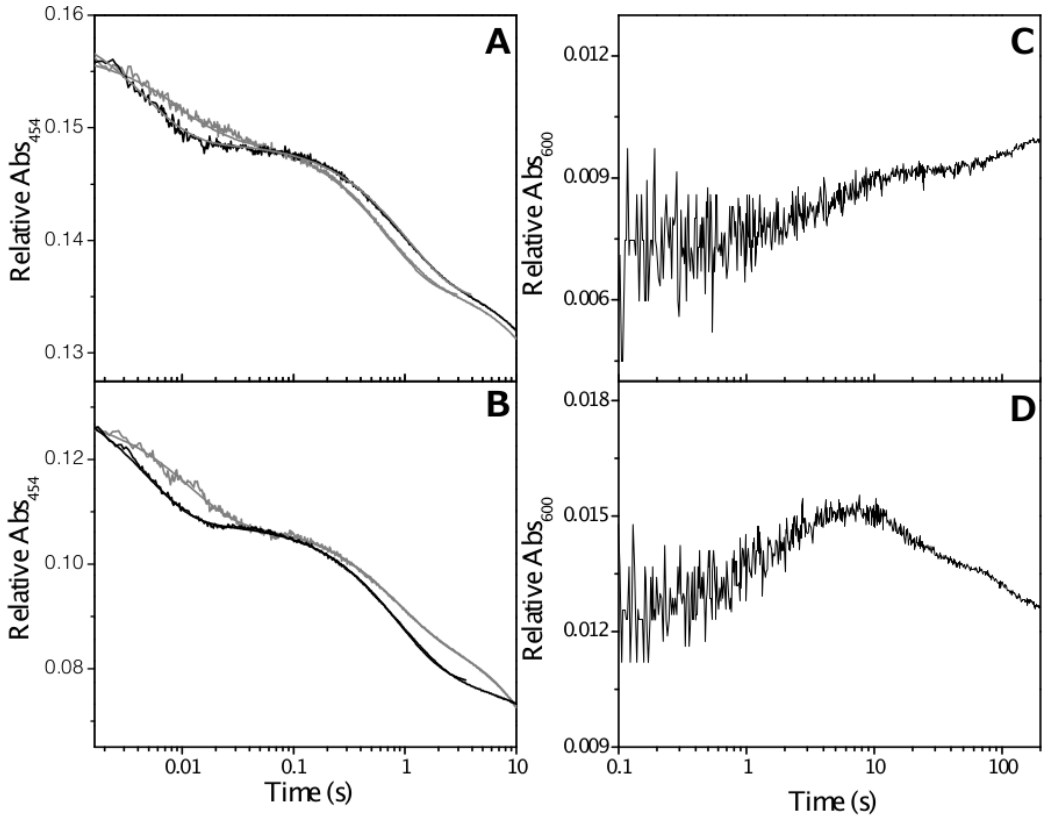

Figure 3.6: Anaerobic reduction of MSR W697 variants by saturating substrate monitored with single-wavelength stopped-flow spectrophotometry at 454 and 600 nm. Conditions: 12.5 μM enzyme, 250 μM NADPH, 250 μM (R)-[4-^{2}-H] NADPH, anaerobic 50 mM Tris-HCl pH 7.5 at 25 °C. W697F (Panel *A* and *C*) and W697Y (Panel *B* and *D*) were rapidly mixed with NADPH (black line) and (R)-[4-^{2}-H] NADPH (grey line) and monitored over 10 and 200 s at 454 nm and 600 nm, respectively.

Table 3.7: Steady state kinetic parameters of coenzyme-binding residue variants of CPR and MSR. Conditions: 1 mL reaction volume, 8 μM cytochrome c^{3+}, 2-12 pmole enzyme, varied [NADPH] and [inhibitor], 50 mM KPi pH 7.5(CPR), 50 mM Tris-HCl pH 7.5(MSR) at 25 °C. Assays were done in triplicate and fit to the Michaelis-Menten equation. Inhibition data from four inhibitor concentrations were fit to a competitive inhibition equation. [a] Assays were conducted in 50 mM Tris pH 7.5 to compare this CPR variant with wild-type MSR.[b] Data acquired from Wolthers *et al.*[65]

Enzyme	k_{cat} (s^{-1})	K_m ($M \times 10^{-6}$)	K_i ($M \times 10^{-6}$)	k_{cat}/K_m ($s^{-1}M^{-1} \times 10^{+6}$)
CPR_{WT}	20.0 ± 0.2	0.7 ± 0.1	1.0 ± 0.1	28.2 ± 1.8
R298A	12.4 ± 0.1	0.64 ± 0.02	2.0 ± 0.1	19.5 ± 0.9
K602AV603K[a]	13.1 ± 0.1	18.1 ± 1.1	46.4 ± 6.5	0.72 ± 0.05
MSR_{WT}[b]	7.23 ± 0.14	2.37 ± 0.17	36.89 ± 2.70	3.05 ± 0.28
K291R	3.73 ± 0.08	2.92 ± 0.29	16.08 ± 1.05	1.28 ± 0.15
A622K	1.90 ± 0.02	0.84 ± 0.07	13.07 ± 1.88	2.26 ± 0.20

greater effect on coenzyme binding, with a 46-fold weaker binding affinity for $NADP^+$ (K_i = 46 μM).

For MSR, exchanging the coenzyme pyrophosphate-coordinating Lys291 for an arginine, produced no notable effect on the catalytic turnover with only an approximate 2-fold decrease in catalytic efficiency. However, the $NADP^+$ binding affinity was 2.3-fold stronger for K291R. Mutation at the 2'-phosphate-coordinating polar pocket in the A622K variant elicited a moderately slower reduction of cytochrome *c* with slightly reduced catalytic efficiency. As with K291R, A622K exhibited a stronger binding affinity for $NADP^+$ compared to native MSR, by 2.8-fold.

3.3.8 Multiple and single wavelength pre-steady state kinetics of coenzyme-binding variants of MSR and CPR

The pre-steady state kinetics of flavin reduction in the coenzyme-binding variants of MSR and CPR were measured by stopped-flow spectrophotometry. The spectral changes occurring over the reductive half-reaction were resolved and fit to the appropriate kinetic model. CPR variant spectra are featured in Figure 3.7 and the observed rate constants are in Table 3.8. Both R298A and K602AV603K elicited biphasic reduction and were best fit to a two-step kinetic model with three discrete spectral species, as described for wild-type CPR in Section 3.3.2. The observed rate constants for the first (k_{obs1}) and second (k_{obs2}) kinetic phases are 14 s^{-1} and 3 s^{-1} for R298A, which are comparable to those determined for wild-type CPR reduction. See Table 3.9 and Figure 3.8 for rate constants derived from double

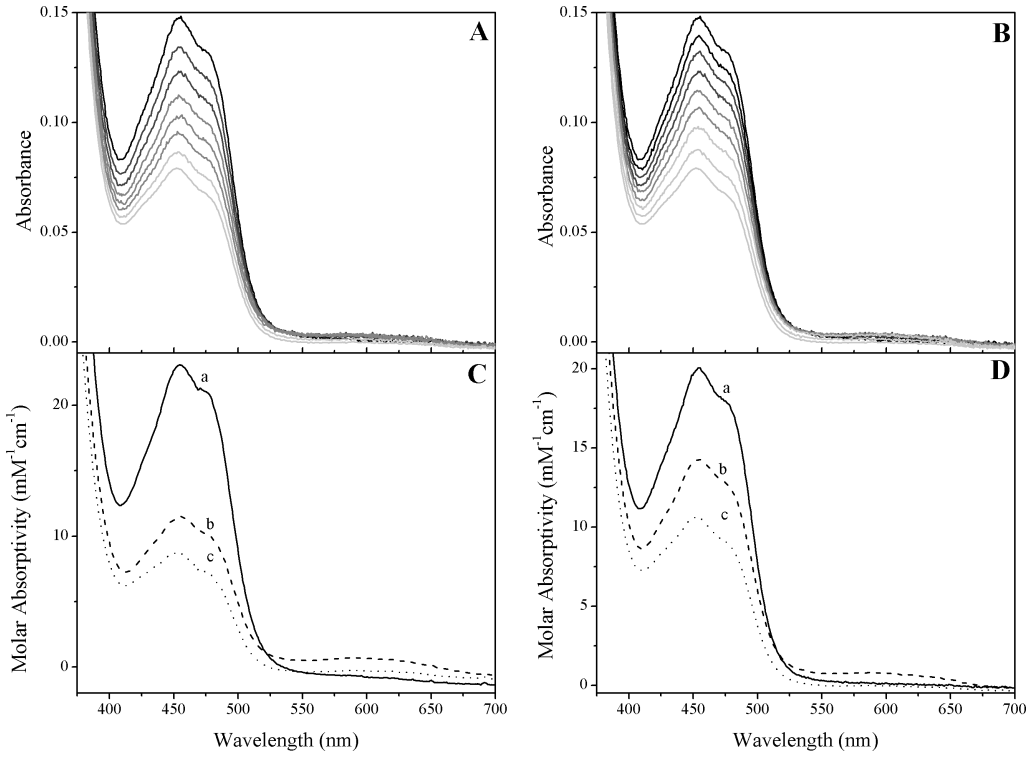

Figure 3.7: Spectral changes upon NADPH reduction of CPR coenzyme-binding variants monitored by multi-wavelength stopped-flow spectrophotometry. Conditions: 10 μM enzyme, 100 μM NADPH, anaerobic 50 mM Tris-HCl pH 7.5 at 25 °C. Full spectra of R298A (A) and K602AV603K (B) NADPH-mediated reduction over 100 s with $\sim$ 20 traces shown for clarity. Time-resolved spectral intermediates for R298A (C) and K602AV603K (D) variants follow a two-step kinetic model with three discrete spectral species (a→b→c), associated rate constants are summarized in Table 3.8.

exponential fits of single wavelength absorbance data at 454 nm. These are in agreement with the multiple wavelength data. No significant differences were observed in the single and multiple wavelength spectra of R298A. In contrast, K602AV603K elicited observed rate constants that were both accelerated with a k_{obs1} of 57 s^{-1} and a k_{obs2} of 17 s^{-1}. These rates are moderately faster than those measured from single wavelength absorbance traces. Spectral data from single wavelength traces show considerable differences in the amplitude change at 454 nm and particularly at 600 nm. The small amplitude change at 600 nm suggests that the disemiquinone does not accumulate in this variant to the same extent as in wild-type. Furthermore, variant reduction by (R)-[4-^{2}H] NADPH yielded a k_{obs1} of 34.76 $\pm$ 0.18 s^{-1}, resulting in a KIE of 1.2 that suggests the hydride transfer step is less rate-determining.

Table 3.8: Observed rate constants for flavin reduction in CPR and MSR coenzyme-binding residue variants acquired from multi-wavelength stopped-flow data. Conditions: 10 μM enzyme, 100 μM NADPH, anaerobic 50 mM Tris-HCl pH 7.5 at 25 °C. CPR variants were best fit to a biphasic kinetic model while MSR variants were best fit to a triphasic kinetic model.[a] Data acquired from Wolthers *et al.*[65]

Enzyme	k_{obs1} (s^{-1})	k_{obs2} (s^{-1})	k_{obs3} (s^{-1})
Wild-type$_{CPR}$	19.00 ± 0.01	2.72 ± 0.01	–
R298A	13.58 ± 0.03	3.37 ± 0.01	–
K602AV603K	57.34 ± 0.01	17.44 ± 0.06	–
Wild-type$_{MSR}$[a]	24.9 ± 0.1	0.18 ± 0.01	0.016 ± 0.003
K291R	28.64 ± 0.01	3.12 ± 0.01	0.033 ± 0.001
A622K	35.00 ± 0.01	0.372 ± 0.002	0.017 ± 0.001

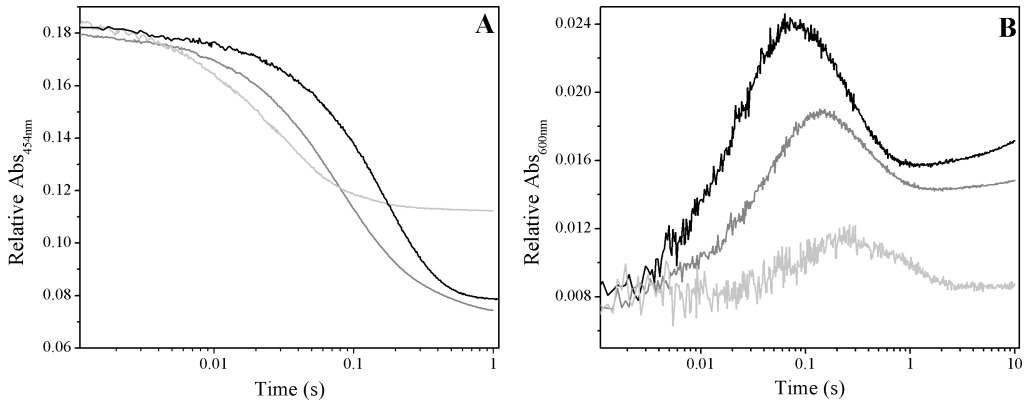

Figure 3.8: Anaerobic reduction of CPR coenzyme-binding variants by saturating NADPH monitored at 454 and 600 nm with single wavelength stopped-flow spectrophotometry. Conditions: 10 μM enzyme, 100 μM NADPH, anaerobic 50 mM Tris-HCl pH 7.5 at 25 °C. Panel *A* shows the absorbance traces over 1 s at 454 nm of native CPR (black line), R298A (gray line) and K602AV603K (light gray line). Panel *B* shows the absorbance traces over 10 s at 600 nm of the CPR variants in the same colours detailed for Panel *A*.

Table 3.9: Observed rate constants for flavin reduction in CPR and MSR coenzyme-binding residue variants acquired from single wavelength 454 nm stopped-flow data. Conditions: 10 μM enzyme, 100 μM NADPH, anaerobic 50 mM Tris pH 7.5 at 25 °C. CPR variants were best fit to a biphasic kinetic model while MSR variants were best fit to a triphasic kinetic model.[a] Data acquired from Wolthers *et al.*[65]

Enzyme	k_{obs1} (s^{-1})	k_{obs2} (s^{-1})
R298A	12.52 ± 0.05	1.95 ± 0.09
K602AV603K	40.9 ± 0.4	10.9 ± 0.4
K291R	25 ± 2	2.00 ± 0.01
A622K	26.9 ± 0.4	1.76 ± 0.14

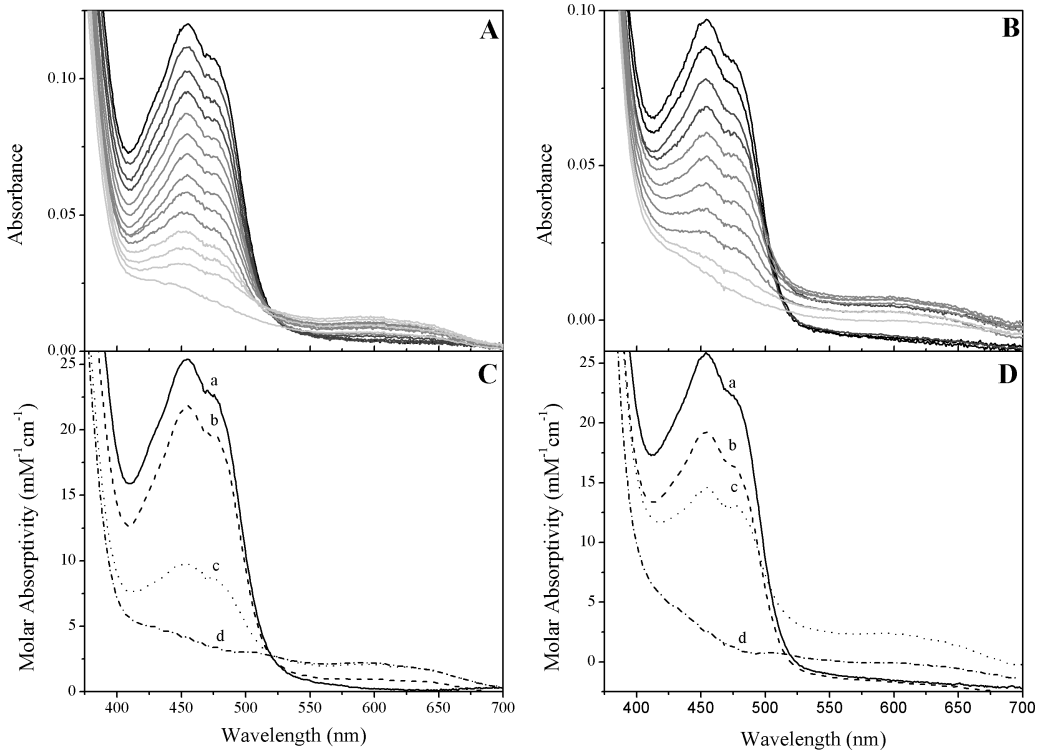

Figure 3.9: Spectral changes upon NADPH reduction of MSR coenzyme-binding variants monitored by multiple wavelength stopped-flow spectrophotometry. Conditions: 10 μM enzyme, 100 μM NADPH, anaerobic 50 mM Tris-HCl pH 7.5 at 25 °C. Full spectra of K291R (*A*) and A622K (*B*) NADPH-mediated reduction over 150 s with ∼ 20 traces shown for clarity. Time-resolved spectral intermediates for K291R (*C*) and A622K (*D*) variants follow a three-step kinetic model with four discrete spectral species (a→b→c→d), associated rate constants are summarized in Table 3.8.

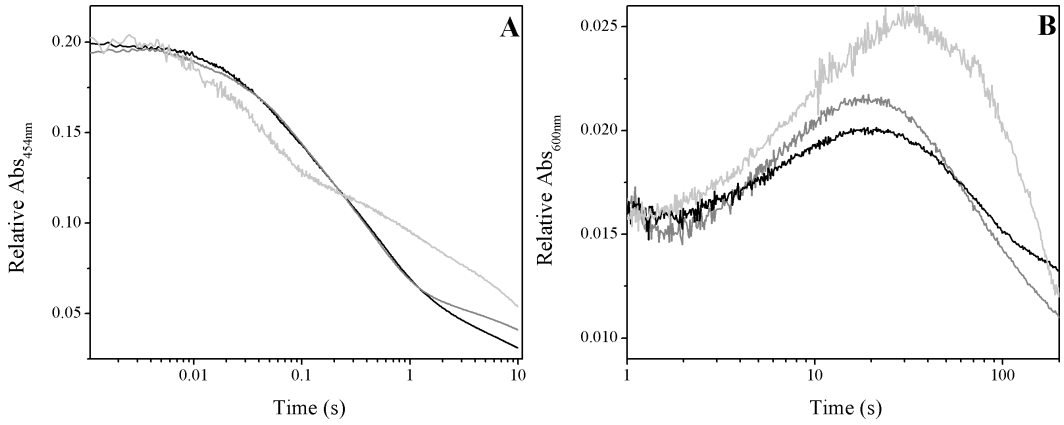

Figure 3.10: Anaerobic reduction of MSR coenzyme-binding variants by saturating NADPH monitored at 454 and 600 nm with single wavelength stopped-flow spectrophotometry. Conditions: 10 μM enzyme, 100 μM NADPH, anaerobic 50 mM Tris-HCl pH 7.5 at 25 °C. Panel *A* shows the absorbance traces over 10 s at 454 nm of native MSR (black line), K291R (gray line) and A622K (light gray line). Panel *B* shows the absorbance traces over 200 s at 600 nm of the MSR variants in the same colours detailed for Panel *A*.

For NADPH-mediated reduction of MSR variants, the spectral changes occurring over the course of the reaction are similar to native MSR. Figure 3.9 shows the progressive loss of absorbance at the flavin maxima at 454 nm along with the appearance and partial disappearance of the semiquinone absorbance signal centered at 600 nm. Global analysis of the photodiode array-derived data revealed a k_{obs1} of 29 s^{-1} for K291R, which is only slightly improved from wild-type, and a k_{obs1} of 35 s^{-1} for A622K. Similar rate constants were extracted for k_{obs2} (3.7 and 0.1 s^{-1}) and k_{obs3} (0.03 and 0.02 s^{-1}) of K291R and A622K, respectively. Rate constants determined from global analysis are consistent with those obtained from double-exponential fits of 454 nm absorbance traces (Table 3.9). Figure 3.10 shows the absorbance changes occurring over the course of the flavin reduction in K291R and A622K. At both 454 and 600 nm, K291R exhibits similar absorbance changes as wild-type MSR. However, for A622K at 454 nm, a faster kinetic phase is clearly observed followed by a slower multiphasic reduction from 0.1 - 10 s. Furthermore, a greater amplitude change at 600 nm is observed for A622K, indicating that a greater fraction of the enzyme population is forming the disemiquinone compared to wild-type.

3.4 Discussion

3.4.1 Hydride transfer is gated by Trp697 in MSR but not in CPR

Substitution of the FAD isoalloxazine ring-stacked Trp residue had opposite effects on MSR and CPR catalysis. In MSR, mutation of Trp697 to a smaller aromatic residue re-

sulted in variants with an enhanced rate of cytochrome *c* reduction with greater catalytic efficiency. These catalytic improvements originate from the 10-fold more rapid initial rate constant, k_{obs1}, for flavin reduction measured for both variants. In MSR, k_{obs1} is assigned to the hydride transfer step and also all the physical preceding steps including coenzyme binding and displacement of Trp697. Since hydride transfer is expected to be rapid once the nicotinamide ring is correctly positioned over the FAD isoalloxazine ring, the rate enhancement is likely due to a reduction in the energy barriers for the physical steps that lead to productive NADPH binding. As Trp697 forms extensive π-π stacking interactions with the FAD isoalloxazine ring, disruption of these dispersion forces presents an energetic barrier for productive nicotinamide ring placement and subsequent hydride transfer[136]. Thus, substitution of Trp697 with a smaller aromatic is expected to reduce the energy barrier. Moreover, the slight increase in the kinetic isotope effect of W697Y and W697F for k_{obs1} suggests that the isotopically insensitive steps (e.g. structural rearrangement of the aromatic residue) are less rate-determining in these variants and the intrinsic isotope effect associated with breakage of a C-H bond is partially unmasked. As an additional note, the polarity of the residue does not affect the rate of displacement since both variants have, within error, similar values for k_{obs1} and KIE.

Swapping Trp676 for a tyrosine or phenylalanine in CPR did not result in as dramatic effects as in MSR. Instead of enhancing flavin reduction, the same variants elicited slightly slower rates of flavin reduction. The size of the aromatic residue does not influence productive substrate binding in the same way as in MSR, as the CPR variants only elicited moderately tighter $NADP^+$ binding affinity. Subtle conformational changes at the active site upon coenzyme binding may account for these results.

As previously proposed for CPR, two separate conformational rearrangements of the active site tryptophan are envisioned to take place in MSR prior to hydride transfer.[57] In substrate-free and $NADP^+$-bound forms of MSR, the indole ring is orientated over the *re*-side of the FAD isoalloxazine ring to maximize π orbital overlap with the FAD. In CPR, however, substrate binding may induce structural rearrangements in the active site that lead to a flip and rotation of the indole where only partial π-π interaction is maintained. This may be the stable position of Trp676, as it is consistently captured in all wild-type crystal structures of substrate-bound CPR. This second conformation may weaken the residue-FAD interaction such that the energetic cost of tryptophan displacement is overcome by the energetic gain of nicotinamide ring placement. Since CPR appears to adopt this conformation more readily than MSR, it may be the origin of the differential coenzyme binding properties between these two enzymes. Thus, the weaker interaction of the smaller aromatic residues with the FAD isoalloxazine in MSR would be expected to lower the energetic cost of the required conformational changes and may account for the dramatic increase in k_{obs1} for

the MSR variants. For the CPR variants, a similar shift to the second conformation as in native CPR is expected. Thus, the weakened interaction between the isoalloxazine ring and residue is potentially very similar among the variants and wild-type CPR, thereby having little effect on the overall rate of flavin reduction.

3.4.2 Interflavin ET influenced by residue polarity in MSR and CPR

MSR and CPR adopt closed and open conformational states over the course of catalysis. In the closed state, the interflavin distance is shortened to facilitate electron transfer. According to Dutton's electron transfer rate ruler and the 4 $\AA$ interflavin distance (obtained from CPR crystal structure), the internal electron transfer rate should be approximately 3 x 10^{10} s^{-1}.[138] However, the measured rates in wild-type MSR and CPR are substantially lower.[133,138] In MSR, although the rate of electron transfer from FAD to FMN is relatively slow, we have previously shown that the active site Trp697 accelerates this step.[136] By exchanging Trp697 for histidine or serine, the transient absorbance signal at 600 nm is lost indicating a lack of any detectable semiquinone buildup. However, interflavin electron transfer does still take place (at an attenuated rate) since these variants achieve full four-electron reduction by two NADPH molecules and reduce cytochrome *c*, which receives electrons directly from FMN. In the W697Y variant there remained an absorbance signal at 600 nm albeit with a smaller amplitude than in wild type MSR. This indicates that, to a certain degree, tyrosine can act as trytophan in accelerating FAD to FMN electron transfer. The modest increase in internal electron transfer in W697Y may be the origin of the slightly faster cytochrome *c* turnover compared to W697F. This may also be the case for the CPR variants since the W676Y variant has a greater rate of flavin reduction with a large amplitude change compared to W676F as well as faster cytochrome *c* turnover. The precise mechanism of how Trp, and to a lesser extent Tyr, enhance internal electron transfer is still unclear. However, it may arise from the role of the bulky tryptophan residue in displacing the oxidized nicotinamide ring which is discussed further in the following section.

3.4.3 Trp676 displaces the oxidized nicotinamide ring and as such controls electron flow

The hydride transfer and interflavin electron transfer steps are tightly coupled in one kinetic phase in CPR. Let us consider the reduction potentials of the CPR flavins. Based off of the -320 mV midpoint potential of NADP(H) and -333 mV of $FAD_{ox/hq}$, the transfer of a hydride ion from NADPH to the FAD isoalloxazine ring is not thermodynamically favoured. However, the $FMN_{ox/sq}$ couple is much more electropositive (-66 mV) and provides the thermodynamic driving force for the forward electron flow through the enzyme.

By exchanging Trp676 for a smaller aromatic the transfer of an electron from $FADH_2$ to FMN is hindered, as evident by the lack of a disemiquinone absorbance signal at 600 nm that typically accompanies the loss of absorbance at 454 nm. Instead, the first phase of flavin reduction by NADPH results in the formation of a broad charge-transfer band that is assigned to a distribution of the NADPH-FAD-FMN and $NADP^+$-$FADH_2$-FMN complexes. Since the electrons remain on the FAD cofactor and the nicotinamide ring remains associated in the active site, there is a shift in favour of the reverse reaction (hydride transfer back to $NADP^+$). Moreover, the charge-transfer complex is not observed in wild-type CPR, indicating that $NADP^+$ dissociation is faster than in the variants. Thus, following hydride transfer to FAD, the bulky tryptophan is required for displacement of the oxidized nicotinamide ring.

Moreover, early stopped-flow studies on rabbit CPR first hypothesized that $NADP^+$ release was rate-limiting in the rapid flavin reduction kinetics.[68] Through mutagenesis and X-ray crystallographic methods, Hubbard *et al.* identified residues that form a hydrogen bond network around the FAD isoalloxazine ring, and the involvement of these residues in proton release and FAD semiquinone stabilization. They proposed that $NADP^+$ release was required prior to interflavin electron transfer.[61] Therefore, the impeded rate of flavin reduction observed in the W676 variants may be a consequence of a $NADP^+$ release becoming more rate-determining.

3.4.4 Differential influence of coenzyme binding affinity on CPR and MSR flavin reduction kinetics

Additional electrostatic interactions with the coenzyme improves substrate binding affinity, however tighter coenzyme binding has differential effects on flavin reduction in CPR and MSR. In CPR, removal of the Arg298 bidentate interaction with the coenzyme pyrophosphate group did not generate dramatic changes to CPR catalytic turnover. As expected, binding of $NADP^+$ was weakened by this mutation but only by 2-fold. The relatively small change in K_i may be due to the presence of other stabilizing active site residues, including a second arginine (Arg567) that coordinates to the pyrophosphate group (also present in MSR - Arg581). A much greater effect on coenzyme binding and flavin reduction was measured for K602AV603K. Removing the direct hydrogen bonding interaction of Lys602 with the 2'-phosphate group of NADPH resulted in a 46-fold weaker binding affinity for $NADP^+$. Since the binding energy for the coenzyme is largely derived from hydrogen bond interactions between the 2',5'-ADP moiety and polar residues at the coenzyme binding cleft, the significantly weaker binding affinity for $NADP^+$ in K602AV603K was anticipated.[64]

Weakening the interaction between the enzyme and substrate in K602AV603K produced a 3- and 6-fold enhancement in the k_{obs1} and k_{obs2} of flavin reduction, respectively. These

accelerated rate constants are attributed to faster dissociation of the oxidized coenzyme as $NADP^+$ release becomes less rate-determining. Indeed, a slight increase in the KIE to 1.2 from that of wild-type (KIE = 1.1), indicates that hydride transfer becomes slightly more rate-determining in K602AV603K.

As anticipated for MSR, coenzyme binding is improved by additional electrostatic interactions at the coenzyme-binding site. Replacing a monodentate with a bidentate interaction with the coenzyme pyrophosphate group, the K291R variant elicited tighter binding affinity for $NADP^+$ with modestly improved flavin reduction. Furthermore, an additional hydrogen bond interaction with the coenzyme 2'-phosphate group also increased the enzyme's affinity for $NADP^+$, as evident by the 2.8-fold lower K_i for A622K. This variant also elicited faster rates of flavin reduction with a k_{obs1} of 35 s^{-1}. As k_{obs1} encompasses hydride transfer as well as the preceding physical steps such as coenzyme binding, the accelerated k_{obs1} for these MSR variants is attributed to improved coenzyme binding affinity.

Despite the accelerated rates of flavin reduction in the K602AV603K and A622K variants, the overall k_{cat} of cytochrome *c* reduction was modestly slower than the wild-type counterparts. Although the origin of this effect is not immediately clear, it may be due to alterations in the active residues that confer subtle structural changes upon coenzyme binding. Previous studies with CPR have shown that binding of the coenzyme and the 2',5'-ADP moiety alone enhance the interflavin electron transfer rate in CPR.[73,75] This rate enhancement was attributed to a shift in the conformational equilibria to a closed state that brings the flavin cofactors together to facilitate interflavin electron communication. For CPR, and by extension for MSR, it is possible that the mutations introduced at the 2-phosphate-binding site may influence the residues involved in this conformational equilibrium. These variants may adopt the closed conformation more readily than the open conformation, which would disfavour electron transfer from $FMNH_2$ to the external electron acceptor.

3.5 Experimental Procedures

3.5.1 Materials

Reagents NADPH, NADH, $NADP^+$, 2',5'-ADP, and cytochrome c^{3+}, ethanol-d_6 and alcohol dehydrogenase were obtained from Sigma Aldrich (Oakville, ON, Canada). *Pfu* Turbo DNA polymerase, *Taq* DNA polymerase and Xl1 Blue cell lines were from Agilent Technologies (Mississauga, ON, Canada). Rosetta(DE3)pLysS and BL21(DE3)pLysS competent cells and yeast alcohol dehydrogenase were purchased from EMD Biosciences. Protein purification supplies, Resource Q column and glutathionine sepharose 4B resin, were obtained from GE Biosciences. All other chemical reagents were purchased from Fisher.

3.5.2 (R)-[4-^{2}H]-NADPH synthesis and purification

(R)-[4-^{2}H]-NADPH was synthesized enzymatically using a procedure adapted from Viola and colleagues.[139] In a 30 mL beaker wrapped in foil, a 20 mL reaction mixture was made of 20 mM TAPS buffer pH 9, 330 mg $NADP^+$, 33 units of alcohol dehydrogenase, 100 units aldehyde dehydrogenase and 0.343 mL of ethanol d_6. At room temperature, the reaction is stirred and the pH was monitored continuously to maintain a pH of 9. Throughout the day, small samples were analyzed at 340 nm using a Lambda 25 UV/Vis Spectrometer (Perkin Elmer). At a concentration of 5.37 mM, 100 μL of chloroform was added and the solution was mixed thoroughly. It was then spun at 27,170 $\times$ g for 30 minutes. The supernatant was lyophilized overnight.

The first purification method was by ethanol precipitation. In the morning, the NADPD preparation was resuspended in 2 mL of 20 mM TAPS pH 9 then 24 mL of $-20\,^\circ$C ethanol was added. The solution was spun at 27 170 $\times$ g for 30 minutes. The supernatant was discarded and the resuspension was repeated. After a second round of centrifugation, the supernatant was discarded and the pellet was resuspended in 2 mL 20 mM TAPS then transferred to a round bottom flask. Contents were lyophilized overnight.

A further purification step was performed with a Q-Sepharose column. The column was equilibrated with 10 mM ammonium hydrogen carbonate pH 9 (buffer A) and a 2 mL solution of the previously dried NADPD sample was applied to the column. The column was washed with two column volumes of buffer A then a gradient was applied with 400 mM ammonium hydrogen carbonate pH 9 over 3 column volumes (buffer B). Two additional column volumes were run at 100 % buffer B. The resulting peaks were collected and analyzed spectrophotoscopically to determine the 260/340 nm ratio. Fractions with a ratio of 2.5 or less were pooled together and lyophilized until completely dry. Samples were wrapped in foil and stored at $-80\,^\circ$C.

3.5.3 Generation and expression of CPR and MSR tryptophan variants

The CPR W676F and W676Y variants and the MSR W697F and W697Y variants were generated from soluble (transmembrane domain cleaved) wild-type CPR plasmid pET-15b and wild-type MSR plasmid pGEX-4T1 using the QuikChange Site-Directed Mutagenesis Kit (Agilent Technologies). Oligonucleotide primers were designed based on the published sequence (Accession number: NM000941 CPR and AF121214 MSR) and purchased from Integrated DNA Technologies (Coralville, Iowa, USA). The primers are tabulated in Table 3.10. Successful mutagenesis was confirmed by the NAPS DNA Sequencing Laboratory of the University of British Columbia (Vancouver, Canada). Mutant plasmids were then transformed into the *Escherichia coli* strain Rosetta2(DE3)pLysS for MSR and BL21(DE3)pLysS

Table 3.10: The forward (F) and reverse (R) oligonucleotide primers designed for each specified MSR and CPR variant. Mutation is in bold.

Enzyme Variant	Oligonucleotide Sequence
MSR	
W697F	F 5' CTTCAGGATATT**TTT**TCATAGCGGCCGCATCG 3'
	R 5' CGATGCGGCCGCTATGA**AAA**AATATCCTGAAG 3'
W697Y	F 5' CTTCAGGATATT**TAC**TCATAGCGGCCGCATCG 3'
	R 5' CGATGCGGCCGCTATGA**GTA**AATATCCTGAAG 3'
K291R	F 5' CGAATGATGCCATA**AGA**ACCACTCTGCTG 3'
	R 5' CAGCAGAGTGGT**TCT**TATGGCATCATTCG 3'
A622K	F 5' GAGGAGGAAGCCCCA**AAA**AAGTATGTACAAGAC 3'
	R 5' GTCTTGTACATACTT**TTT**TGGGGCTTCCTCCTC 3'
CPR	
W676F	F 5' GCCTACTCCTGGACGTG**TTT**AGCTAGGATCCGAATTCGG 3'
	R 5' CCGAATTCGGATCCTAGCT**AAA**CACGTCCAGGAGTAGC 3'
W676Y	F 5' GCTACTCCTGGACGTG**TAC**AGCTAGGATCCGAATTCGG 3'
	R 5' CCGAATTCGGATCCTAGCT**GTA**CACGTCCAGGAGTAGC 3'
R298K	F 5' CCAGGGAACCGAGC**GCC**CACCTCATGCACCTGG 3'
	R 5' CCAGGTGCATGAGGTG**GGC**GCTCGGTTCCCTGG 3'
K602AV603K	F 5' CGGGAGCAGTCCCAC**GCTAAG**TACGTCCAGCAC 3'
	R 5' GTGCTGGACGTA**CTTAGC**GTGGGACTGCTCCCG 3'

for CPR using the heat shock method. The MSR recombinant GST-fusion proteins were expressed and harvested as previously described in Section 2.5.2. The CPR recombinant His-tagged proteins were grown in 200 mL cultures of Luria-Bertani medium, containing 100 μg mL^{-1} of ampicillin and 34 μg mL^{-1} chloramphenicol, overnight at 37 °C and 225 rpm. 0.5 L cultures of Terrific Broth containing 100 μg mL^{-1} ampicillin and 34 μg mL^{-1} chloramphenicol were inoculated with 10 mL of the 200 mL cultures and grown at 30 °C to an Abs_{600} of 0.8. Cultures were then induced with 0.1 mM IPTG and the temperature was lowered to 20 °C to grow overnight. In the morning, cells were harvested at 6,360 × g for 10 min and stored at −80 °C.

3.5.4 Purification of MSR variants

Purification of MSR variants followed the procedure previously described in Section 2.5.4.

3.5.5 Purification of CPR variants

All purification steps were performed on ice or at 4 °C. Cells overexpressing the recombinant His-tagged enzyme were resuspended in 300 mL of 50 mM Tris/HCl pH 7.5 with protease inhibitors benzamidine (2 mM) and PMSF (1 mM). The resuspension was soni-

cated with the Sonicator S-4000 (Misonix Inc.) at 22% power amplitude with alternating 8 s pulses and 1 min pauses for a total of 45 min. Cell lysate was then centrifuged at 39 120 × g for 45 minutes to separate the soluble protein from cellular debris. 0.5 M NaCl and 20 mM imidazole was added to the collected supernatant. The crude extract was then loaded onto a HisTrap FF crude 5 mL affinity column (GE Healthcare) equilibrated with 10 column volumes of 50 mM Tris/HCl pH 7.5, 0.5 M NaCl and 20 mM imidazole. Followed by a 5 column volume wash, the column was attached to the AKTApurifier system (GE Healthcare). Buffer A: 50 mM Tris/HCl pH 7.5 and 0.5 M NaCl; Buffer B: 50 mM Tris/HCl pH 7.5, 0.5 M NaCl and 0.3 M imidazole. Nonspecifically bound protein was eluted with 10 % buffer B for 2 column volumes. His-tagged enzyme was eluted by a linear gradient from 10% to 100% buffer B over 8 column volumes. Fractions were pooled together and dialyzed overnight in 4 L 50 mM Tris/HCl pH 7.5, 1 mM EDTA and 1.7 mL β-mercaptoethanol at 4 °C to remove excess salt. Dialysate is concentrated down to 20 mL, loaded onto the AKTApurifier system and applied to an equilibrated 55 mL Q Sepharose anion exchange column. Buffer A: 50 mM Tris/HCl pH 7.5; Buffer B: 50 mM Tris/HCl pH 7.5 and 0.5 M NaCl. The enzyme was eluted with a linear gradiant from 0 % to 100 % buffer B over eight column volumes at a flow rate of 2 mL/min. The desired fractions were collected based on the absorbance readings at 280 nm and the yellow colour that is characteristic of oxidized CPR. The final concentration of purified CPR ($\Delta\varepsilon$ = 21.6 $mM^{-1}cm^{-1}$) was determined by the absorption at 454 nm and the Beer-Lambert Law, Equation 3.1.

$$Abs = \varepsilon lc \tag{3.1}$$

where c is the concentration of sample, Abs is the absorbance at 454 nm, ε is the molar extinction coefficient of CPR, and l is the light path length (1 cm).

3.5.6 Steady state turnover analysis

Steady state turnover assays for MSR variants were conducted as previously described in Section 2.5.5. CPR variant assays followed the same protocol but were performed in 50 mM KPi pH 7.5 buffer.

3.5.7 Pre-steady state kinetic analysis

Pre-steady state kinetic assays for MSR and CPR variants were conducted as previously described in Section 2.5.6.

3.5.8 Redox potentiometry

All potentiometric titrations were performed in an anaerobic nitrogen environment at room temperature in 50 mM Hepes/KOH pH 7.0 buffer. Through extensive bubbling with nitrogen, the buffer was made anaerobic and left to equilibrate in the glove box for over 16 hours. Enzyme samples W676Y and W676F were fully oxidized with potassium ferricyanide, brought into the glove box then gel-filtered over a 50 mM Hepes/KOH pH 7.0 equilibrated 10 mL size-exclusion column (Bio-Rad Econo-Pac 10 DG column, Mississauga, ON, Canada). Small fractions of the eluted protein were removed from the glove box for spectrophotometric determination of the sample concentration. In the anaerobic environment, the enzyme was diluted to 14-28 μM in a total volume of 3 mL. Redox mediators benzyl viologen (1 μM), methyl viologen (0.2 μM), 2-hydroxy-1,4-napththoquinone (5 μM) and phenazine methosulfate (2 μM) were added to the glass cuvette with the enzyme solution. A specially designed cuvette holder held the fiber optic cables of the stopped-flow to allow for sample illumination by the xenon lamp and the spectra were recorded by the photodiode array detector. Absorbance spectra (280-703 nm) were recorded on a SF-61DX2 Stopped-flow apparatus from TgK Scientific and the electrochemical potential was monitored using a Mettler Toledo FiveEasy voltmeter coupled to a platinum-Ag/AgCl electrode. The enzyme solutions were titrated electrochemically with small aliquot volumes of sodium dithionite as described by Dutton *et al.*[140] After each addition, the sample was mixed thoroughly, allowed to equilibrate, and the spectrum was recorded when the potential stabilized. This step was repeated until the enzyme was fully reduced. The observed potentials were normalized to the standard hydrogen electrode by adding 197 mV. The spectral data were adjusted to the same absorbance baseline at 703 nm to account for drift observed during the redox titration.

Data manipulation and analysis was performed using Origin 8.5 software (OriginLab Co.). Absorbance values from 590 to 605 nm, the semiquinone absorbance maxima, were summed and plotted against the normalized potential to determine the midpoint potentials. Data were fitted to Equation 3.1, which represents a sum of two two-electron redox processes derived by the Beer-Lambert Law and the Nernst equation.

$$A = \frac{a10^{(E-E_1')/59} + b + c10^{(E_2'-E)/59}}{1 + 10^{(E-E_1')/59} + 10^{(E_2'-E)/59)}} + \frac{d10^{(E-E_3')/59} + e + f10^{(E_4'-E)/59}}{1 + 10^{(E-E_3')/59} + 10^{(E_4'-E)/59)}} \tag{3.2}$$

In this equation, E is the observed potential, E_1' and E_2' are the oxidized/semiquinone and semiquinone/hydroquinone midpoint potentials of one flavin. E_3' and E_4' are the corresponding midpoint potentials for the second flavin. A is the total absorbance, a, b and c are the component absorbance values contributed by one flavin in the oxidized, semiquinone, and reduced states, respectively. The d, e and f are the corresponding absorbance com-

ponents for the second flavin. The absorbance contribution of oxidized and reduced forms of FAD and FMN are assumed to be equal ($a = d$ and $c = f$). The initial values for E_n' (where n = 1, 2, 3, 4) were based on the previously determined midpoint potentials for wild-type CPR.[66] With only one variable fixed and all others floating, data fitting resulted in decent flavin absorbance values (a-f). Several iterations of data fitting with varied combinations of absorbance values fixed (a and d, b and e, and c and f) with the potentials floating generated reasonable estimates of the individual midpoint potentials. This fitting was followed by a final iteration where the potential values and absorbance values a, c, d and f were allowed to vary. To prevent overparameterization, b and e were fixed in the final iteration.

Chapter 4

Role of histidine residue at the FAD active site in regulating intramolecular electron flow in CPR and MSR

4.1 Summary

In this chapter the functional role of a proximal FAD histidine residue in interflavin electron transfer is investigated in human CPR and MSR. Hydride transfer and interflavin electron transfer in CPR are tightly coupled in one kinetic step, while the two catalytic events are two kinetically distinct phases in MSR. The FAD proximal catalytic triad is well-conserved in CPR and MSR with an established role in stabilizing steps of the catalytic mechanisms. In CPR, Asp674 of the triad forms a hydrogen bond with His322. The equivalent residue in MSR is Ala312. Consequently, the potential role of this residue in regulating electron flux in CPR and MSR is evaluated by generating reciprocal substitutions: H322A and A312H. The steady state and pre-steady state kinetic properties of these variants were determined through aerobic and anaerobic spectrophotometric techniques. Through these studies, the hydride and interflavin electron transfer steps in MSR were successfully coupled in one kinetic phase. In CPR, I proposed that His322 weakens coenzyme binding affinity by competing with the nicotinamide ring for interaction with Asp674. By weakening the coenzyme-enzyme interaction, coenzyme release is promoted which, in turn, accelerates electron flow through CPR.

4.2 Background

MSR and CPR are envisioned to switch from a closed to an extended conformation during the transmission of electrons from NADPH to external electron accepting proteins.[73,74,113,141] The compact, closed conformation brings FAD and FMN flavins together, such that they are poised for rapid interflavin electron transfer. In this conformation, the

FMN cofactor is buried and cannot interact with and transfer an electron to the terminal electron acceptor. To accomplish this half of the reaction, the FMN domain undergoes large-scale conformational motion to adopt an extended state that leads to solvent exposure of the FMN.[73,74,113] Several studies using different methodologies including NMR and small-angle X-ray crystallography in CPR have provided strong evidence that these conformational transitions take place during catalysis.[73–76,142] The 12-amino acid hinge that tethers the FMN domain to the connecting domain of CPR has been shown to be critical to the conformational dynamics.[57] Interestingly, the corresponding hinge in MSR is an extra 82 amino acids longer suggesting an increased mobility of the FMN domain.

Spectroscopic studies of the rapid, single turnover kinetics of CPR and MSR reduction with NADPH reveal differential kinetic behaviors. Scheme 4.1 shows the mechanistic steps involved in MSR and CPR catalysis. In CPR, the initial event of hydride transfer from NADPH to FAD (II) and electron transfer from FAD to FMN (III) are tightly coupled such that there is no accumulation of the FAD hydroquinone intermediate. In MSR, however, these two catalytic events are represented by two discrete kinetic phases such that there is transient accumulation of E-$FADH_2$-FMN. This species accumulates due to the slow rate of interflavin electron transfer. To further investigate the origin of these different kinetic behaviors, the amino acids surrounding the FAD isoalloxazine ring were compared for CPR and MSR.

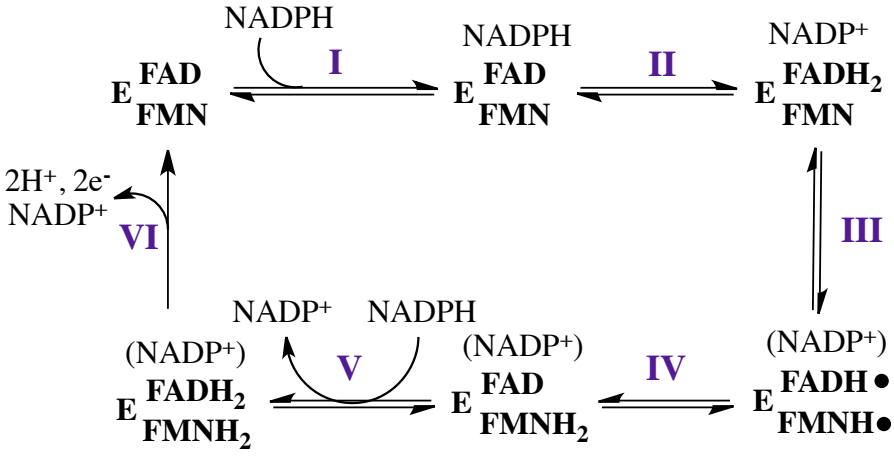

Figure 4.1: Proposed mechanism for NADPH-mediated reduction of CPR and MSR. **I** NADPH binds. **II** Donation of hydride ion from NADPH to FAD. **III** Formation of the disemiquinone. **IV** Both electrons are transferred to the FMN to form the hydroquinone. **V** Full four-electron reduction to the dihydroquinone by a second molecule of NADPH. **VI** Transfer of reducing equivalents from the enzyme to terminal electron acceptors regenerates the fully oxidized enzyme. The presence/absence of the oxidized coenzyme is not absolutely known and depicted as parentheseses around $NADP^+$.

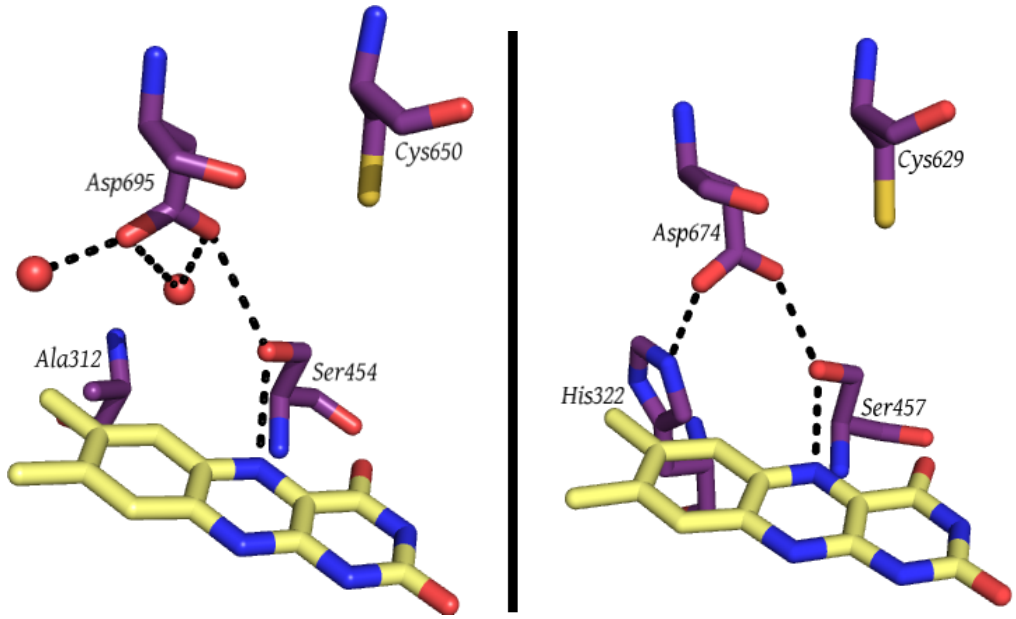

Figure 4.2: Proximal FAD isoalloxazine ring residues in wild-type MSR (*Right*) and CPR (*Left*). PDB 2QTZ and 3Q2E

Three well-conserved residues referred to as the catalytic triad, Asp674, Ser457 and Cys629 (CPR numbering), are positioned in close proximity to the FAD isoalloxazine ring active site, see Figure 4.2. Ser457 is positioned within hydrogen bonding distance to the catalytically important N5 atom of FAD. Asp674 forms a hydrogen bond interaction with Ser457; however, this interaction is disrupted upon coenzyme binding as Asp674 forms new contacts with the C4 atom of the nicotinamide ring. Cys629, lying above the isoalloxazine ring, is orientated to also interact with the incoming nicotinamide ring. These residues stabilize the transition state for hydride transfer from the C4 atom of the nicotinamide ring to the N5 atom of the FAD isoalloxazine ring. Upon nicotinamide ring release, the Ser457 and Asp674 residues reform a hydrogen bond network to the N5 atom of the reduced FAD and stabilize the semiquinone state.[44,60,61]

The catalytic triad is conserved in plant-type ferredoxin $NADP^+$-reductases, although the aspartate residue is replaced for a glutamate.[129] Recall that FNR operates in the reverse direction from MSR and CPR, by transferring reducing equivalents from reduced ferredoxin onto $NADP^+$. Theoretical studies on FNR by Dumit *et al.* have proposed that, during catalysis, the glutamate residue functions as a proton donor to the N5 nitrogen of the FAD isoalloxazine ring through the serine side chain.[143] Catalysis of MSR and CPR functions in the reverse of that of FNR, and the aspartate residue has been suggested to play a similar role in catalysis but as a proton acceptor. Notably, the FAD active site of CPR depicts a histidine residue (His322 - numbering based off of ratCPR crystal structure and not human

CPR sequence (His319)) that lies within hydrogen bond distance of Asp674 as shown in Figure 4.2. This histidine residue is conserved among CPR homologues and those of nitric oxide synthase, which also couple hydride and interflavin electron transfer. However, as shown in Figure 4.2, the equivalent residue in MSR is an alanine (Ala312). The presence of histidine in CPR and NOS but not in MSR may influence the ability of Asp to act as a general base and may be the origin of the differences in kinetic behaviors in CPR and MSR.

In an effort to determine the structural basis for the differential kinetic behavior of CPR and MSR, mutations were made to His322 in CPR and the equivalent residue Ala312 in MSR. Reciprocal mutations H322A and A312H were made in an attempt to replicate the local amino acid environment of MSR in CPR and vice versa. Both residues were also mutated to a glutamine, which can still participate in hydrogen bonding to aspartate but not in acid/base chemistry. The steady state kinetic properties of each variant were measured by spectrophotometric analysis of cytochrome *c* or ferricyanide ($Fe(CN)_6{}^{3-}$, abbreviated FeCN) reduction. Uncoupled NADPH oxidase activity was also determined for each variant. Product inhibition assays with $NADP^+$ reported on the relative coenzyme binding affinities of each variant. Lastly, stopped-flow spectrophotometric studies of flavin reduction under pseudo-first order conditions were utilized to evaluate the effect of the mutation on the rapid turnover kinetics for these two enzyme variants.

In addition, the effect of the hinge length on the kinetic properties of MSR was examined. The much longer hinge of MSR compared to CPR may impart greater conformational freedom to the FMN domain, which could limit electron transfer between FAD and FMN. Therefore, the MSR hinge was truncated to 12 amino acids (the equivalent length in CPR) to determine the potential consequence of a longer, more flexible hinge on electron flux in MSR.

4.3 Results

4.3.1 Flavin characteristics of variants

The visible absorption spectrum of each variant was measured under aerobic conditions using a UV-Vis spectrophotometer. Figure 4.3 shows the reduction of the enzyme variants by equimolar and saturating concentrations of NADPH. Under equimolar conditions, a loss of absorbance at the flavin absorbance maxima 454 nm was observed with the appearance of a large disemiquinone absorbance signal centered around 585-605 nm. In the presence of saturating amounts of NADPH, the absorbance peaks at both 454 nm and 600 nm were reduced. These spectral properties are similar to those observed for wild-type CPR and MSR, indicating that mutation at the His322 (CPR) and Ala312 (MSR) do not affect NADPH-mediated flavin disemiquinone formation in an aerobic environment.

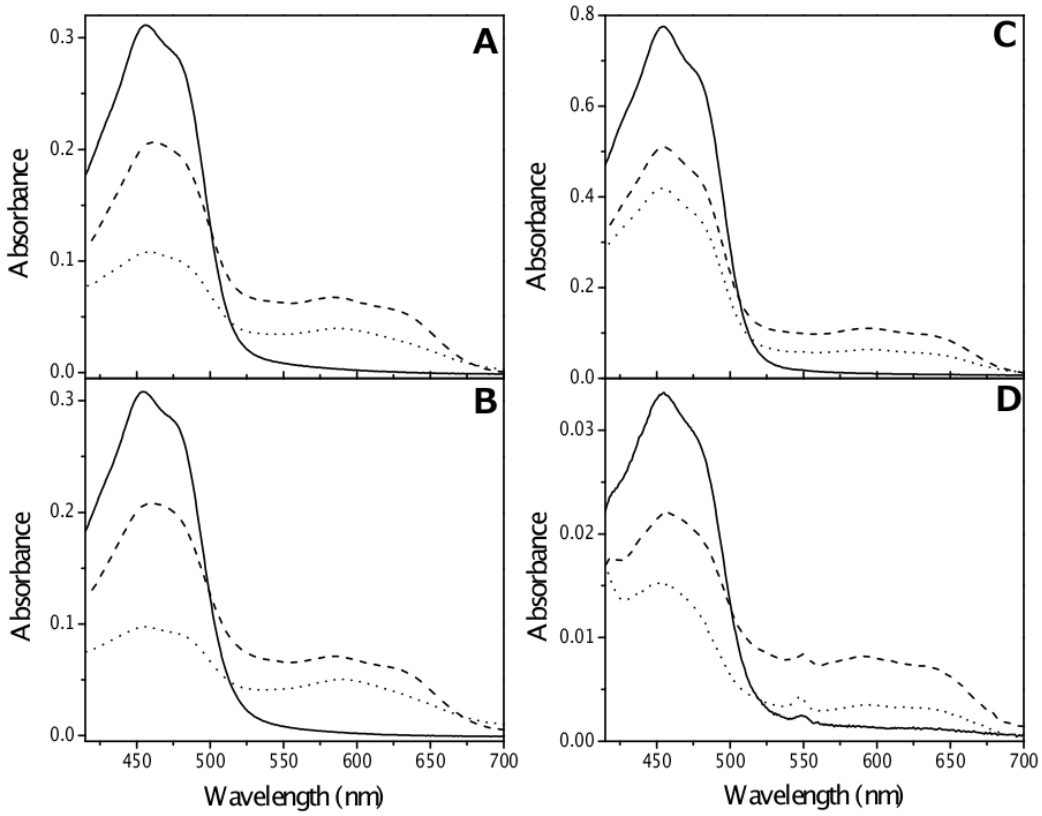

Figure 4.3: Visible absorption spectra of CPR and MSR variants H322Q (A), H322A (B), A312Q (C), and A312H (D) under aerobic conditions. The recorded spectral properties of fully oxidized enzyme (solid black line), after a 5 min incubation with an equimolar concentration of NADPH (dashed line), and after 10 min incubation with a saturating concentration of NADPH (dotted line).

Table 4.1: Steady state kinetic parameters of wild-type, A312 and H322 variants of MSR and CPR. Conditions: 1 mL reaction volume, 8 μM cytochrome c^{3+}, 0.5 mM FeCN, 2-10 pmole enzyme, varied [NADPH] and [$NADP^+$] at 25 °C. Assay buffer for MSR is 50 mM Tris-HCl pH 7.5 and 50 mM KPi pH 7.5 for CPR. Assays were done in triplicate and fit to the Michaelis-Menten equation. Inhibition data from four inhibitor concentrations were fit to a competitive inhibition equation.[a] Data acquired from Wolthers *et al.*

Enzyme	$k_{cat}{}^{cytc}$ (s^{-1})	K_m NADPH ($M \times 10^{-6}$)	K_i $NADP^+$ ($M \times 10^{-6}$)	k_{cat}/K_m ($s^{-1}M^{-1} \times 10^{+6}$)	$k_{cat}{}^{FeCN}$ (s^{-1})
WT_{MSR}[a]	7.2 ± 0.1	2.4 ± 0.1	36.9 ± 2.7	3.1 ± 0.3	7.9 ± 0.1
A312Q	7.8 ± 0.1	6.2 ± 0.2	29.1 ± 1.9	1.3 ± 0.1	7.1 ± 0.1
A312H	3.6 ± 0.1	15.0 ± 0.7	72.9 ± 7.8	0.24 ± 0.01	7.1 ± 0.1
WT_{CPR}	20.0 ± 0.2	0.71 ± 0.04	0.95 ± 0.05	28.3 ± 1.8	43.5 ± 0.1
H322Q	11.3 ± 0.2	0.58 ± 0.04	0.65 ± 0.05	19.4 ± 1.7	26.1 ± 0.1
H322A	5.4 ± 0.1	0.31 ± 0.04	0.30 ± 0.04	17.4 ± 2.5	18.1 ± 0.1

4.3.2 Steady state kinetic data

Steady state kinetics of each variant were analyzed using two different artificial electron acceptors, ferricyanide (FeCN) and cytochrome c^{3+}. FeCN receives an electron from either FAD or FMN cofactors, while cytochrome c only receives an electron directly from the FMN cofactor. The data collected from all steady state assays are summarized in Table 4.1. The H322A CPR variant elicited a 4-fold decrease in cytochrome c^{+3} reduction and a 1.5-fold decrease in FeCN reduction. H322Q showed an approximate 50% reduction in the steady state turnover of cytochrome c^{+3} and FeCN. Both variants had moderately tighter binding affinity for $NADP^+$ and a loss of catalytic efficiency attributed to the reduced rate of catalytic turnover with cytochrome c^{+3}. As shown in Figure 4.4, uncoupled NADPH oxidation assays revealed a modest decrease in k_{cat} (1.5-fold slower) for H322A, while k_{cat} was unchanged for H322Q compared to wild-type.

Exchanging alanine for histidine in MSR (A312H) weakened the binding of NADP(H), evident by the increase in the apparent K_m and K_i for the binding of NADP(H). This variant also elicited slower rates of FeCN and cytochrome c^{+3} turnover and, together with weaker substrate binding, has 13-fold lower catalytic efficiency. A312Q elicited a similar k_{cat} for cytochrome c^{+3} and FeCN reduction, with a modest increase in substrate binding affinity. Catalytic efficiency of this variant decreased by about half due to a higher apparent K_m value. The uncoupled NADPH oxidase activity of the MSR variants did not change significantly from that of the native enzyme.

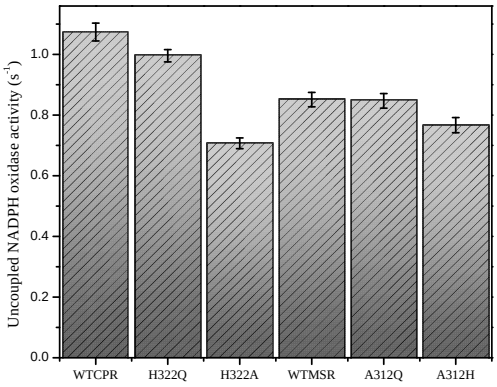

Figure 4.4: Uncoupled NADPH oxidation activity of CPR H322 and MSR A312 variants. Conditions: 1 mL reaction volume, 2 pmole enzyme, 1 mM NADPH, 50 mM Tris pH 7.5 at 25 °C. For wild-type CPR, H322Q and H322A, the rate constant of uncoupled NADPH oxidase activity generated from linear fits of triplicated data is 1.1 ± 0.1 s^{-1}, 1.0 ± 0.1 s^{-1} and 0.71 ± 0.02 s^{-1}, respectively. The rate constants measured for wild-type MSR, A312Q and A312H are 0.85 ± 0.02 s^{-1}, 0.85 ± 0.03 s^{-1} and 0.77 ± 0.003 s^{-1}.

4.3.3 Multiple and single wavelength pre-steady state kinetics of CPR variants

The pre-steady state rates of NADPH-dependent reduction of CPR variants were monitored by anaerobic stopped-flow spectrophotometry. Spectral changes upon reduction with NADPH were collected over 1 s and resolved by SVD. Spectral data are shown in Figure 4.5. Resolved data were then fitted to a two-step biphasic kinetic model for H322Q and a one-step monophasic kinetic model for H322A; the generated observed rate constants are summarized in Table 4.2. The kinetic profile of H322Q reduction was comparable to that of wild-type CPR. The initial fast rate constant (k_{obs1} = 17 s^{-1}) occurred with a 77% absorbance loss at 454 nm with a simultaneous appearance of a broad absorbance band at 600 nm representing formation of the disemiquinone. The second phase was slower (k_{obs2} = 5 s^{-1}) with only a 23% amplitude change at 454 nm and a slight loss of absorbance in the longer wavelengths. This second phase is assigned to a small portion of the two-electron reduced enzyme population being further reduced to the four-electron level by a second equivalent of NADPH.

The H322A variant exhibited monophasic reduction to the two-electron reduced state. This phase change occurred with a slower rate constant of 8 s^{-1}, 2.5-fold less than k_{obs1} of wild-type CPR. Unlike H322Q and wild-type CPR, the absorbance loss at 454 nm was not accompanied by the formation of an absorbance signal at 600 nm, see Figure 4.5. Indeed,

Table 4.2: Observed rate constants of the pre-steady state reduction of CPR H322 variants. For details see Figure 4.5

CPR	k_{obs1} (s^{-1})	k_{obs2} (s^{-1})
Wild-type	19.00 ± 0.01	2.72 ± 0.01
H322Q	16.6 ± 0.1	5.2 ± 0.1
H322A	8.0 ± 0.1	-

single wavelength traces for H322A at 600 nm do not show an absorbance change, confirming the absence of the disemiquinone species or charge-transfer (CT) complex (Figure 4.6) during the reductive half-reaction. These stopped-flow data indicate that the two-electron reduced enzyme population is either in the FAD hydroquinone (E-$FADH_2$-FMN), the FMN hydroquinone (E-FAD-$FMNH_2$), or perhaps a mixture of the two redox states. Over a longer time frame of 150 s with the autoshutter on to avoid light-induced flavin bleaching, there is a small, gradual buildup of the broad absorbance band at 600 nm indicative of the disemiquinone species(Figure 4.6). This signal is only a fraction of the equivalent signal in wild-type CPR and H322Q when allowed to reach equilibrium, suggesting that interflavin electron transfer is not as well supported in the H322A variant. Spectral data for the equimolar reduction of this variant over a longer time frame, in Figure 4.7, also show only a minor disemiquinone signal. As H322A does not reduce beyond the two-electron level during single turnover assays, the enzyme likely populates the FAD hydroquinone state (E-$FADH_2$-FMN) rather than the FMN hydroquinone (E-FAD-$FMNH_2$), as the latter would presumably allow for reduction by a second equivalent of NADPH, which is not observed in the stopped-flow data.

4.3.4 Multiple and single wavelength of isolated FAD domain of wild-type and H322A CPR

NADPH-mediated flavin reduction of the isolated FAD domain of wild-type (WT_{FAD}) and H322A ($H322A_{FAD}$) CPR were analyzed by stopped-flow spectrophotometry. Absorbance changes over multiple wavelengths (375-700 nm) over 10 s were collected and subjected to SVD analysis, show in Figure 4.8. Both WT_{FAD} and $H322A_{FAD}$ elicited biphasic reduction and were best fitted to a two-step kinetic model. The resulting rate constants were comparable for the two enzymes with a k_{obs1} of $\sim$ 32 s^{-1} and a k_{obs2} of 1 s^{-1}. These rates are also comparable to those obtained from single wavelength traces obtained at 454 nm, see Figure 4.9. Spectral changes associated with k_{obs1} include the loss of absorbance at 454 nm coupled with an appearance of a small flat absorbance band in the long wavelengths (>550 nm). This flat absorbance band represents the formation of a

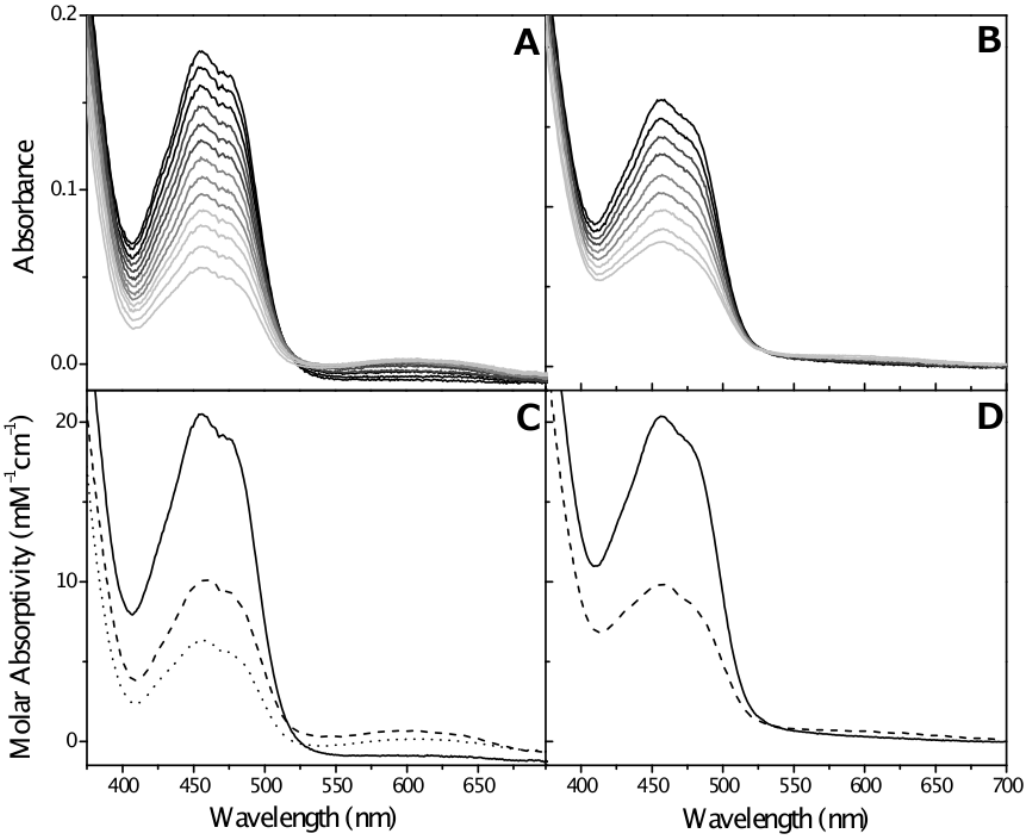

Figure 4.5: Spectral changes upon NADPH reduction of CPR H322 variants monitored by multi-wavelength stopped-flow spectrophotometry. Conditions: 20 μM enzyme, 10-fold excess NADPH, anaerobic 50 mM Tris-HCl pH 7.5 at 25 °C. Time-dependent spectral changes over a 1 s time frame are shown for H322Q (A) and H322A (B). Global analysis of SVD-resolved spectra generated deconvoluted spectral intermediates for H322Q (C) and H322A (D). H322Q spectral data were best fit to a two-step model with three spectral intermediates (a $\rightarrow$ b $\rightarrow$ c). H322A spectral data were best fit to a single-step model with two spectral intermediates (a $\rightarrow$ b).

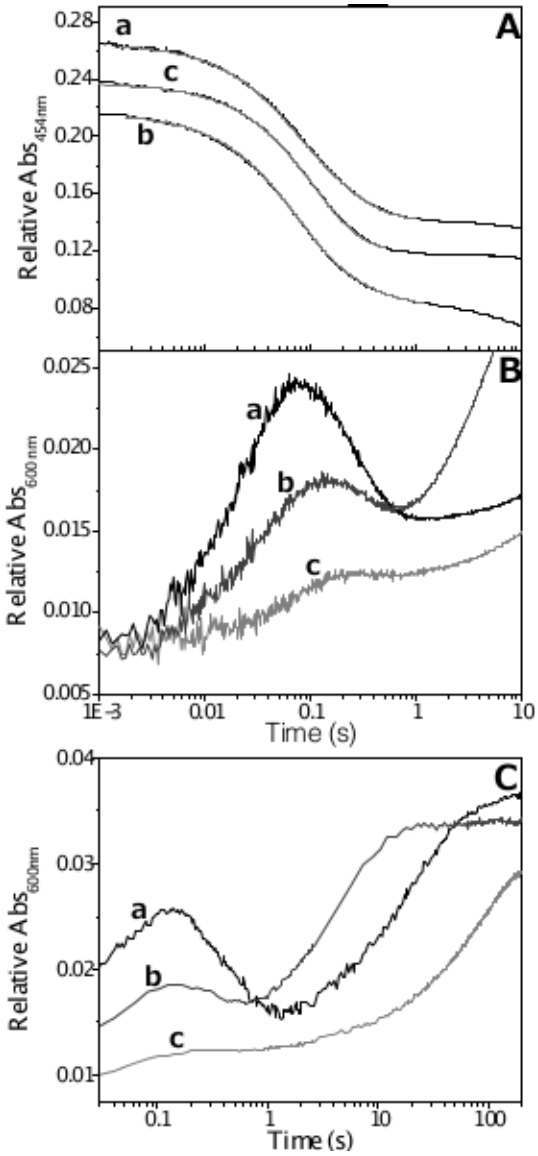

Figure 4.6: Anaerobic reduction of H322Q and H322A by saturating [NADPH] monitored by single wavelength stopped-flow spectrophotometry at 454 and 600 nm. Conditions: 20 μM enzyme, 200 μM NADPH, anaerobic 50 mM Tris-HCl pH 7.5 at 25 °C. Wild-type CPR (*a*), H322Q (*b*) and H322A (*c*). Rapid absorbance changes over 10 s at 454 nm (Panel *A*) and 600 nm (Panel *B*). Panel *C* shows the absorbance changes occuring at 600 nm over 150 s.

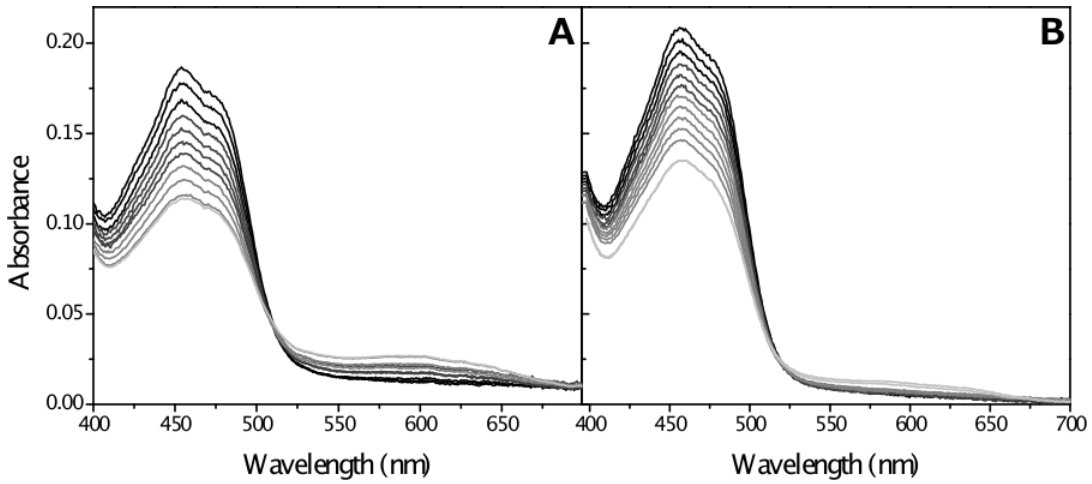

Figure 4.7: Spectral changes upon equimolar NADPH reduction of H322Q and H322A monitored by multi-wavelength stopped-flow spectrophotometry. Conditions: 20 μM enzyme, 20 μM NADPH, anaerobic 50 mM Tris-HCl pH 7.5 at 25 °C.

charge-transfer complex between the FAD isoalloxazine ring and $NADP^+$. Figure 4.9 shows the 454 nm single wavelength traces and double exponential fits of these spectra revealed that the first rate constant of flavin reduction at 454 nm is equal to that of the rate constant for the 'up' phase at 600 nm, while decay of the CT complex occurs with the same rate constant as the k_{obs2} for flavin reduction.

In full-length CPR, the flat absorbance band is not observed, instead the absorbance peak at 600 nm is attributed to the appearance and decay of the disemiquinone species. The lack of the CT signal in full-length CPR indicates the E-$FADH_2$-$NADP^+$ complex does not accumulate as an intermediate, presumably due to rapid interflavin electron transfer. For full-length H322Q, and to a much greater degree for H322A, the diminished absorbance signal at 600 nm observed in Figure 4.6 indicates impeded interflavin electron transfer in these variants.

4.3.5 Redox Potentiometry of H322A

Potentiometric analysis of H322A was performed to determine if the removal of the imidazole side chain alters the midpoint potentials of the FAD redox couples. Previous redox titrations with wild-type CPR found that the FAD couples were similar in the full-length enzyme and the isolated NADPH/FAD domain.[66] Thus, the fitting process was simplified by using the $H322A_{FAD}$ alone in the titrations. Under anaerobic conditions, gradual addition of dithionite led to formation of the FAD semiquinone and complete reduction to the FAD hydroquinone. A plot of the absorbance values at 600 nm against the measured potential values that were normalized to the standard hydrogen electron is presented in Figure 4.10.

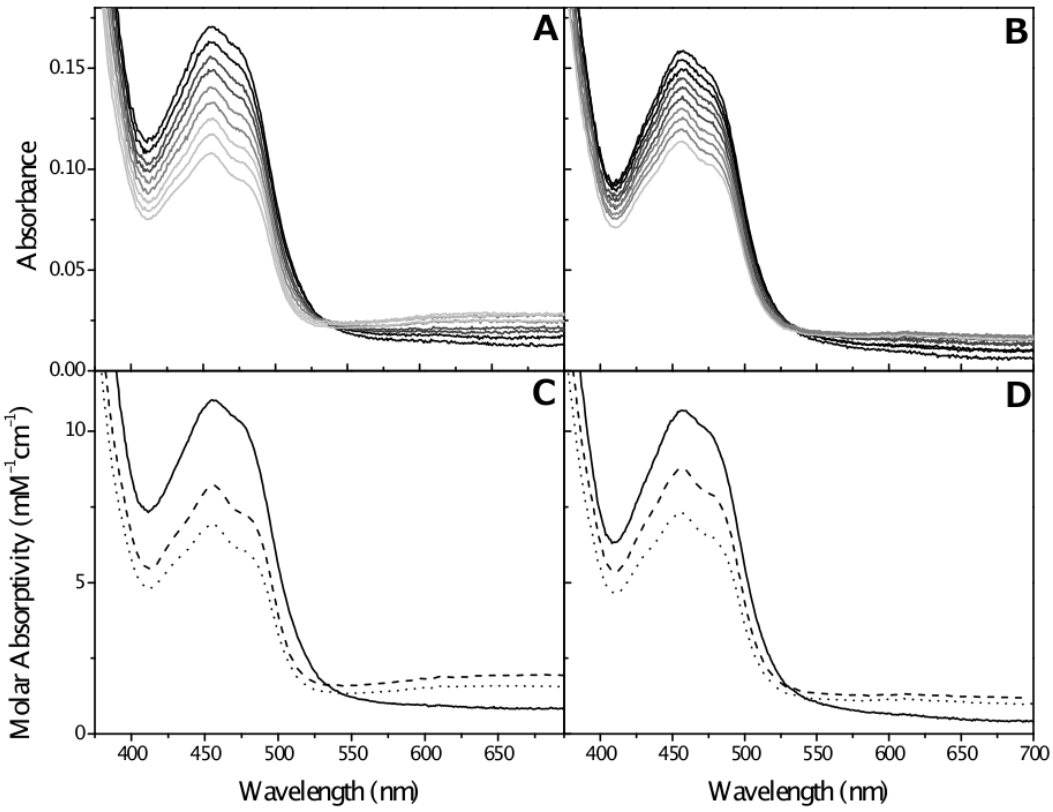

Figure 4.8: Spectral changes upon NADPH reduction of wild-type and H322A FAD domain variants monitored by multi-wavelength stopped-flow spectrophotometry. Conditions: 20 μM enzyme, 10-fold excess NADPH, anaerobic 50 mM Tris-HCl pH 7.5 at 25 °C. Time-dependent spectral changes over a 1 s time frame are shown for wild-type FAD domain (A) and H322A FAD domain (B). Global analysis of SVD-resolved spectra generated deconvoluted spectral intermediates for WT_{FAD} (C) and $H322A_{FAD}$ (D). WT_{FAD} and $H322A_{FAD}$ were best fit to a two-step model with three spectral intermediates (a $\rightarrow$ b $\rightarrow$ c).

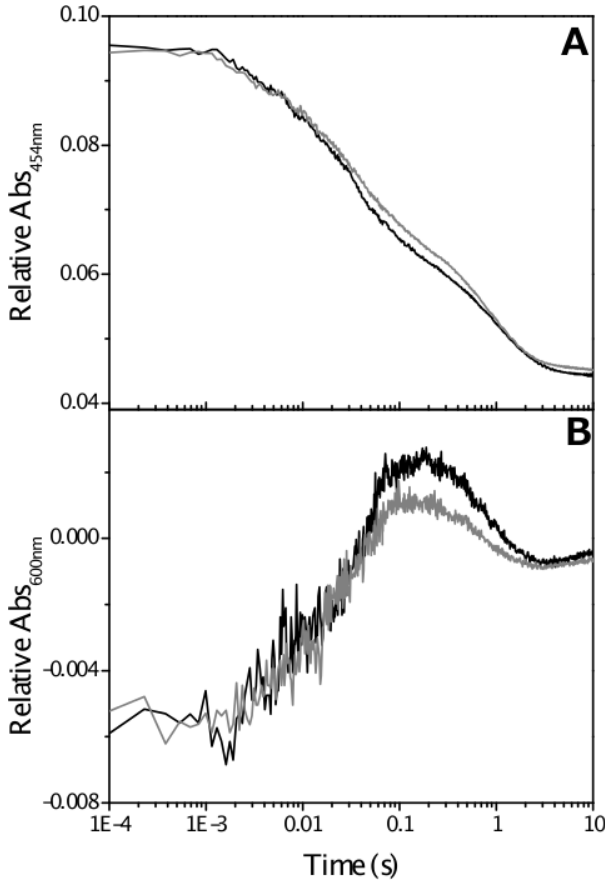

Figure 4.9: Anaerobic reduction of WT_{FAD} (black line) and $H322A_{FAD}$ (gray line) by saturating [NADPH] monitored over 10 s by single wavelength stopped-flow spectrophotometry at 454 and 600 nm. Conditions: 20 μM enzyme, 200 μM NADPH, anaerobic 50 mM Tris-HCl pH 7.5 at 25 °C. The 454 nm spectral data were fit to a double exponential generating a k_{obs1} of 31.9 $\pm$ 0.1 s^{-1} and 31.6 $\pm$ 0.3 s^{-1} and a k_{obs2} of 1.0 $\pm$ 0.1 s^{-1} and 1.2 $\pm$ 0.1 s^{-1} for WT_{FAD} and $H322A_{FAD}$.

A fit of the data in the plot to the Nerst equation generated midpoint potentials of -273 ± 6 mV for the $FAD_{ox/sq}$ couple and -398 ± 20 mV for $FAD_{sq/hq}$. These values compare well to those obtained for WT_{FAD}, indicating that the imidazole side chain does not influence the midpoint potentials of the FAD redox center.

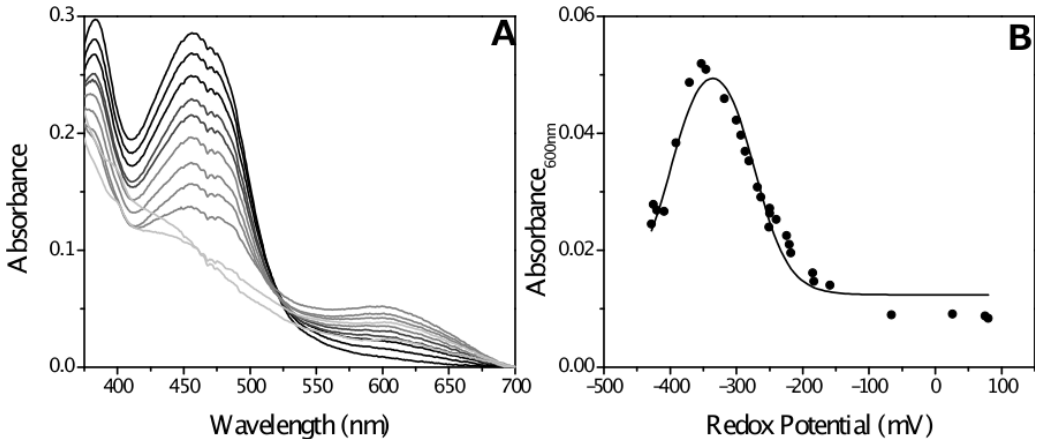

Figure 4.10: Redox titrations of $H322A_{FAD}$. Panel A: Spectral features of $H322A_{FAD}$ after each addition of reductant. Panel B: Plot of absorbance at 600 nm againsts the normalized redox potential. These data were fit to the Nernst equation which yielded a midpoint potential of -273 ± 6 mV for $FAD_{ox]sq}$ and -398 ± 20 mV for $FAD_{sq/hq}$.

4.3.6 Multiple and single wavelength pre-steady state kinetics of MSR variants

Rapid turnover of the MSR variants with saturating amounts of NADPH were followed by anaerobic stopped-flow spectrophotometry. After rapid mixing with NADPH, the spectral changes over 150 s were recorded from 375 to 700 nm. The spectra obtained for A312Q resembles that of wild-type MSR where reduction follows a three-step kinetic model with four distinct spectral species. The first kinetic phase (a → b) represents reduction of the fully oxidized enzyme to the FAD hydroquinone species (E-$FADH_2$-FMN). This is evident by the absorbance bleaching at 454 nm and lack of absorbance change at 600 nm. The first phase occurs with a k_{obs1} that is 1.9-fold slower than that of wild-type MSR but with a similar amplitude change. Conversion of spectral species b to c involves absorbance loss at 454 nm and the emergence of an absorbance peak at 600 nm. Thus, the second phase reports on interflavin electron transfer and formation of the disemiquinone. Complete loss of an absorbance signal across the detected wavelengths corresponds to the enzyme reduction by a second reducing equivalent from NADPH to form the four-electron reduced dihydroquinone (E-$FADH_2$-$FMNH_2$).

Table 4.3: Observed rate constants of the pre-steady state NADPH reduction of MSR A312 variants by stopped-flow spectrophotometry. See Figure 4.11 for details.

MSR	k_{obs1} (s^{-1})	k_{obs2} (s^{-1})	k_{obs3} (s^{-1})
Wild-type	24.9 ± 0.1	0.18 ± 0.01	0.016 ± 0.003
A312Q	13.0 ± 0.1	1.6 ± 0.01	0.10 ± 0.01
A312H	0.76 ± 0.01	0.032 ± 0.001	-

In contrast to wild-type MSR and A312Q, the kinetic profile of A312H reduction under pseudo-first order conditions fits best to a two-step kinetic model. The conversion of spectral species a to b occurs with the loss of absorbance at 454 nm and the appearance of an absorbance signal at 600 nm, as is observed in wild-type CPR. These spectral changes indicate that the hydride and interflavin electron transfer steps are coupled in A312H. However, the rate constant associated with this step is 30-fold slower than the equivalent step in wild-type MSR. To determine if the reduced rate of flavin reduction measured for A312H is due to slower hydride transfer, kinetic isotope effect studies were performed with (R)-[4-^{2}H] NADPH. A KIE of 1.3 was determined for the MSR variant, which is slightly less than the KIE of 1.7 measured for native MSR.[65] Therefore, the hydride transfer step becomes less rate-determining in A312H than in wild-type MSR.

Single wavelength absorption spectrophotometry conducted at 454 and 600 nm allowed for the determination of initial rate constants for A312Q and A312H reduction. Both variants exhibited bleaching of the flavin absorbance maxima at 454 nm and were fitted to a double and single exponential equation for A312Q and A312H. The resulting rate constants were in agreement with those previously determined by global analysis of multiple wavelength data. Both variants also exhibited an 'up' and 'down' phase at 600 nm that reached a maxima at ∼5 - 10 s then decayed over 100 s during the reductive half-reaction. These two kinetic phases were assigned to the formation and decay of the disemiquinone (E-FADH•-FMNH•). Reliable fits of the 600 nm absorbance changes were not possible. Despite a smaller amplitude change of the 600 nm peak in A312Q and A312H, the variants form the disemiquinone over a shorter time frame than wild-type MSR, suggesting that these variants are more efficient at $FADH_2$ to FMN interflavin electron transfer.

4.3.7 Kinetic parameters of the truncated hinge variant of MSR

A variant was constructed with only the first 12 amino acids of the 82 amino acid long hinge region for wild-type MSR. Steady state assays on the MSR hinge variant revealed only a moderate decrease in the rate of cytochrome c^{3+} reduction (k_{cat} = 2.01 ± 0.05 s^{-1}). The ability of the variant to catalyze the reduction of cytochrome c^{3+} indicates

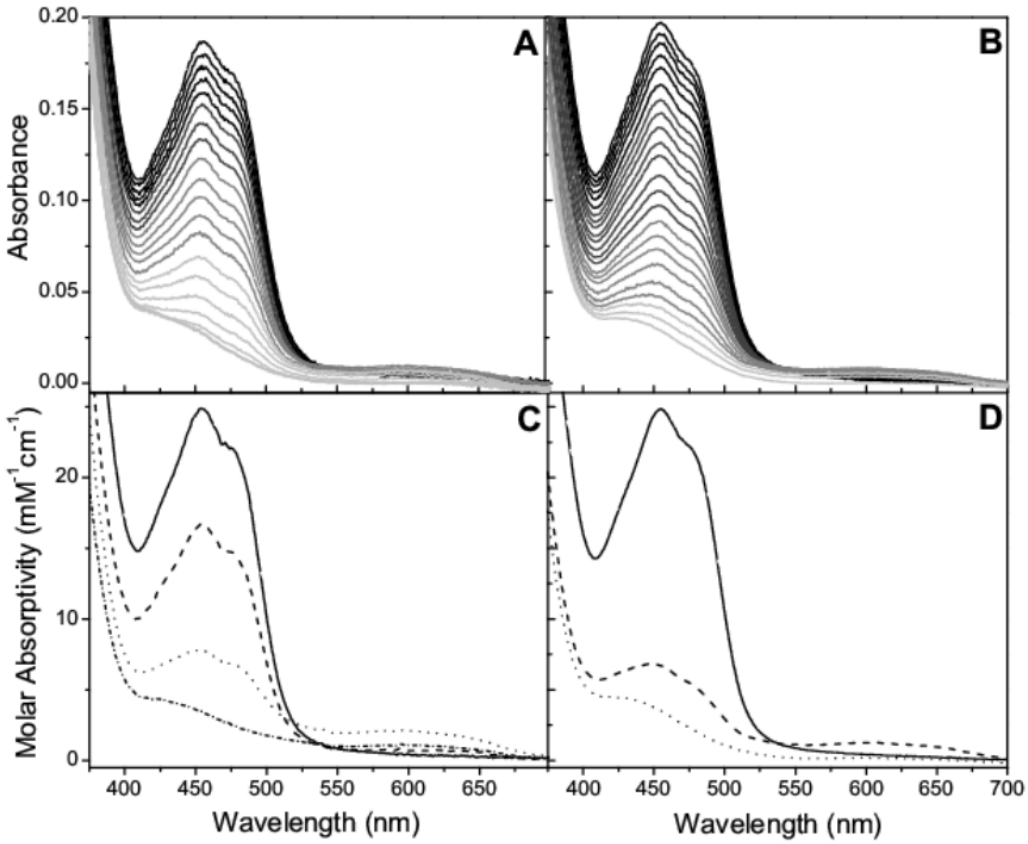

Figure 4.11: Anaerobic multiple wavelength stopped-flow spectrophotometry of NADPH-mediated reduction of MSR A312 variants. Conditions: 20 μM enzyme, 200 μM NADPH, anaerobic 50 mM Tris-HCl pH 7.5 at 25 °C. Absorbance changes from 375 to 700 nm during the course of A312Q (A) and A312H (B) reduction. Global analysis of spectral data revealed a three-step kinetic model for A312Q (C) and a two-step kinetic model for A312H (D).

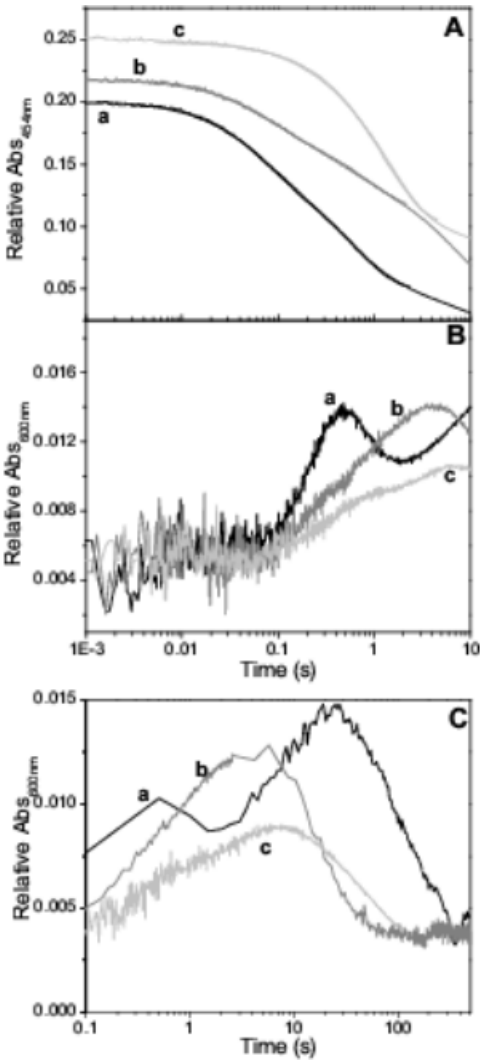

Figure 4.12: Anaerobic reduction of A312Q and A312H by saturating NADPH monitored by single wavelength stopped-flow spectrophotometry at 454 and 600 nm. Conditions: 20 μM enzyme, 200 μM NADPH, anaerobic 50 mM Tris-HCl pH 7.5 at 25 °C. Wild-type MSR (a), A312Q (b) and A312H (c). Rapid absorbance changes over 10 s at 454 nm (Panel A) and 600 nm (Panel B). Panel C shows the absorbance changes occuring at 600 nm over 150 s.

that electron transfer through the variant is still possible. Pre-steady state kinetics of the NADPH-mediated reduction of the MSR hinge variant was monitored by photomultiplier and photodiode array detection, shown in Figure 4.13. Due to low purification yields, a final concentration of only 6 μM of the hinge variant was possible. Pseudo-first order conditions with NADPH were still maintained, however the smaller amplitude changes are attributed to the lower concentration. As expected, the mutation did not affect the rate of FAD reduction (k_{obs1}). However, the second and third rate constant decreased by 10- and 2-fold from wild-type, reporting on hindered interflavin electron.

4.4 Discussion

4.4.1 Active site His322 weakens coenzyme binding

The presence of His322 in the FAD isoalloxazine active site of CPR weakens the binding affinity for the coenzyme. Steady state inhibition assays with $NADP^+$ revealed that exchanging the histidine for an alanine in CPR resulted in tighter coenzyme binding while substituting the equivalent residue in MSR with a histidine resulted in weaker coenzyme binding. To understand the origin of this effect on coenzyme binding by the active site histidine, the crystal structure of the W676X variant is analyzed. This variant, in which the C-terminal residues Trp676 and Ser677 are removed, enables productive binding of the nicotinamide ring which is stacked at a 30°tilt over the FAD isoalloxazine ring. In this position, the carboxamide group of the coenzyme nicotinamide ring forms a strong hydrogen bond ($\sim$2.5 $\mathring{A}$) to the side chain of Asp674. This polar interaction with the coenzyme repositions Asp674, such that the hydrogen bonds with the side chain of Ser457 is severed (over 4 $\mathring{A}$ away). However, His322 remains hydrogen-bonded to Asp674 and potentially competes with the carboxamide group for polar interaction with Asp674. As a consequence of this competitive interaction, the histidine may indirectly weaken NADP(H) binding and promote $NADP^+$ release.

Previous mutagenesis studies by Hubbard *et al.* in rat CPR proposed that the release of oxidized coenzyme is required for interflavin electron transfer and disemiquinone formation.[61] They suggested that disruption of the hydrogen bonding network among the catalytic triad, due to stacking of the nicotinamide ring, prevents deprotonation of $FADH_2$. Supporting this hypothesis are my results for the W676Y and W676F variants. In these variants, interflavin electron transfer was impeded because the nicotinamide ring remained stacked against the $FADH_2$, forming a stable CT species.[144] Since the oxidized coenzyme remains tightly bound in the flavin active site, the hydrogen-bonding network presumably remains disrupted and prevents FAD hydroquinone deprotonation.

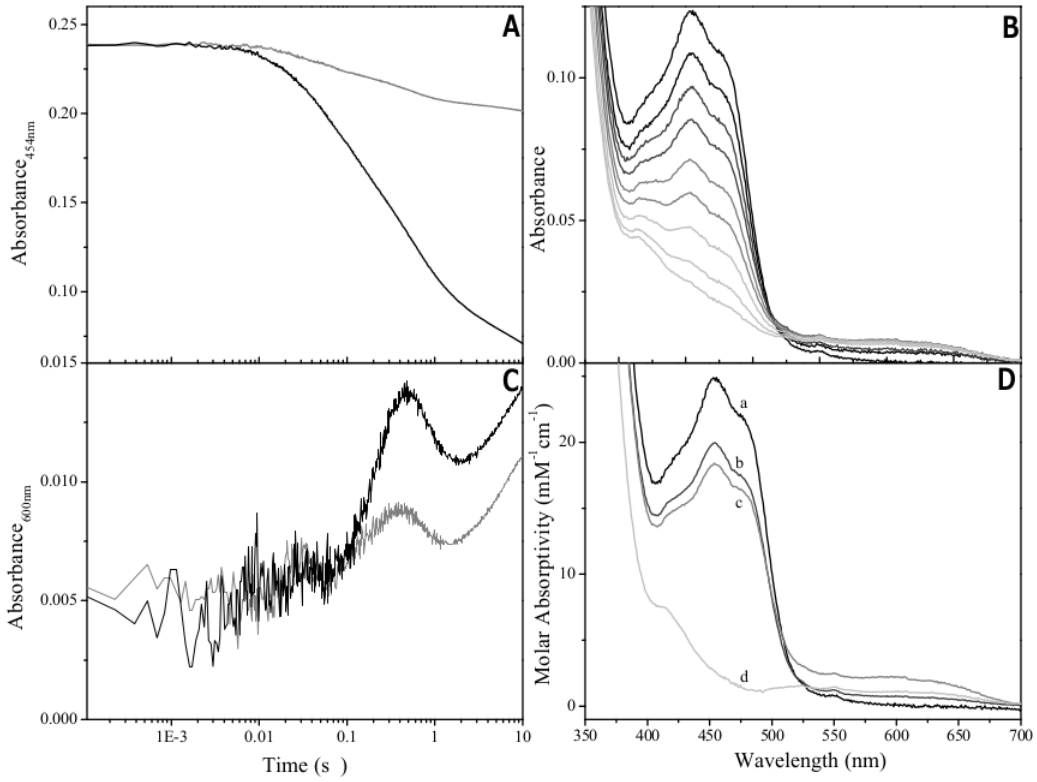

Figure 4.13: Single and multiple wavelength absorbance changes during the anaerobic reduction of the MSR hinge variant. Conditions: 6 μM enzyme, 60 μM NADPH, anaerobic 50 mM Tris-HCl pH 7.5 at 25 °C. Panel *A* and *B* show the 454 and 600 nm absorbance changes over the 10 s rapid reduction of the hinge variant, respectively. Hinge variant is shown in grey and wild-type MSR is in black. Panel *C* shows full spectral changes over 500 s (300 spectral scans reduced to 10 for clarity). Panel *D* shows the deconvoluted spectral profile of the hinge variant following a three-step kinetic model with four spectral species (a→b→c→d) with observed rate constants of k_{obs1} = 25.78 ± 0.01 s^{-1}, k_{obs2} = 0.0200 ± 0.0004 s^{-1} and k_{obs3} = 0.00711 ± 0.0008 s^{-1}.

4.4.2 His322 promotes interflavin electron transfer

My results show that participation of the His322 imidazole side chain in the hydrogen-bonding network around the FAD isoalloxazine ring favours interflavin electron transfer. In H322Q and to a much greater degree in H322A, the interflavin electron transfer is impeded, as evident by the loss of the disemiquinone absorbance signal at 600 nm. Reduction of H322A did not involve any significant buildup of a $NADP^+$-$FADH_2$ CT signal. Thus, unlike the W676 variants, the impeded intramolecular electron transfer in H322A is not due to persistent stacking of the oxidized coenzyme at the FAD active site. Despite the tighter binding affinity observed in H322A, the bulky Trp676 still functions to displace the oxidized nicotinamide ring. Moreover, the equivalent rate constants measured for wild-type and H322A FAD domain variants indicate that hydride transfer is not influenced by the imidazole side chain and is not the origin of the diminished disemiquinone signal. Instead, the 2.5-fold decrease in the k_{obs1} of H322A is likely due to disrupted electron transfer from $FADH_2$ to FMN. Disrupted electron transfer is also evident in the steady state kinetic data for reduction of cytochrome *c* and FeCN, where a larger decrease was observed for the former oxidant compared to the latter. Given that FeCN receives an electron from FAD or FMN and cytochrome *c* receives an electron only from FMN, a mutation that would hinder interflavin electron transfer would be expected to affect cytochrome *c* turnover more significantly than that of FeCN. This was observed for the H322A variant.

The stopped-flow data did however show that, under anaerobic conditions, interflavin electron transfer is possible in H322A since the variant can form the disemiquinone. However, it is only over much longer time domains and only at a fraction of the absorbance signal observed in wild-type. Under aerobic conditions, the disemiquinone absorbance band in H322A is comparable to that of wild-type. Formation of the disemiquinone under these conditions is likely attributed to single electron transfer from $FADH_2$ to O_2, to form FADH• and a superoxide radical.

The definitive mechanism of how His322 promotes interflavin electron transfer is still unclear. However, due to its position at the active site, the influence of His322 on catalysis likely originates from its role in the hydrogen-bonding network around the FAD cofactor. Through the network, His322 contributes to the correct positioning of Asp674 to optimize the hydrogen bond contact with Ser457. A stronger interaction between Asp674 and Ser475 would favour proton abstraction and formation of the FAD semiquinone. It is also possible that the pKa of Asp674 is affected by the non-covalent interaction with His322, thereby influencing the ability of Asp674 to act as a general base.

4.4.3 Differential effect of introducing histidine into MSR active site

In an effort to reconstruct the hydrogen-bonding network observed for CPR in MSR, the A312H and A312Q variants were expressed and analyzed. Substituting an alanine for a glutamine only elicited modest effects on the kinetic and coenzyme binding properties of MSR. Notably, disemiquinone formation did peak at an earlier time in A312Q compared to wild-type MSR. It is possible that the polar side chain of glutamine forms weak polar interactions with Asp695 that partially mimics the interactions of the water molecules found in this position in MSR. Interestingly, reduction of the A312H variant was more similar to wild-type CPR than MSR. The first observable phase involved the absorbance loss at 454 nm along with the emergence of an absorbance band at 600 nm. Like in CPR, the hydride transfer and interflavin electron transfer steps are tightly coupled into one kinetic phase in A312H. However, this kinetic coupling may be a consequence of the dramatically reduced rate of FAD reduction as well as the long delay that precedes flavin reduction observed at 454 nm. Thus, the FAD hydroquinone does not accumulate in this variant. The earlier appearance of the disemiquinone in A312 variants suggests that the more solvent-exposed Asp695 in wild-type MSR is less efficient at deprotonating the N5 nitrogen of the FAD isoalloxazine ring.

4.4.4 Role of the extended hinge in MSR

In an effort to determine if the 82 amino acid extended hinge of MSR adversely affected the rate of intramolecular electron transfer, a variant with a shortened hinge was constructed. The selected amino acid sequence was homologous to the first 12 amino acids of the CPR hinge. MSR and CPR require large-scale conformational motion to alternate between a closed state for intramolecular electron transfer and an open state for intermolecular electron transfer. Since MSR has a much longer hinge region that tethers the FMN domain to the FAD/NADPH domain compared to CPR, the enzyme is expected to have a much greater entropic cost going from the open to closed conformation. Therefore, shortening the hinge was hypothesized to reduce the entropic cost of conformational change and enhance interflavin electron transfer. Kinetic analysis of the hinge variant revealed that the first rate constant associated with hydride transfer was not altered by the mutation however, the second and third rate constants of flavin reduction were significantly slower. A possible explanation for these effects are that the residues specifically involved in the coordinated motion of the FMN domain were removed, thereby disrupting the formation of the closed enzyme state. Furthermore, truncating such a large segment of the primary amino acid sequence may have led to a degree of misfolding in the secondary and tertiary structures of MSR.

4.5 Experimental Procedure

4.5.1 Materials

Unless otherwise stated, all chemical reagents were purchased from Fisher Scientific. NADPH, $NADP^+$, 2',5'-ADP, and cytochrome c^{3+} were obtained from Sigma Aldrich (Oakville, ON, Canada). [4(R)-^{2}H]NADPH (A-side NADPD) was synthesized and isolated as previously described.[144] *Pfu* Turbo DNA polymerase, *Taq* DNA polymerase and Xl1 Blue cell lines were purchased from Agilent Technologies (Mississauga, ON, Canada). Rosetta(DE3)pLysS competent cells were obtained from EMD Biosciences. Protein purification supplies, Resource Q column and glutathionine sepharose 4B resin, were purchased from GE Biosciences.

4.5.2 Generation and expression of MSR and CPR variants

The MSR A312H and A312Q variants and the CPR H322A and H322Q variants were generated from soluble (transmembrane domain cleaved) wild-type CPR plasmid pET-15b and wild-type MSR plasmid pGEX-4T1 using the QuikChange Site-Directed Mutagenesis Kit (Agilent Technologies). Oligonucleotide primers were designed based on the published sequence (Accession number: NM000941 CPR and AF121214 MSR) and purchased from Integrated DNA Technologies (Coralville, Iowa, USA). The primers are tabulated in Table 4.4. NAPS DNA Sequencing Laboratory of the University of British Columbia (Vancouver, Canada) confirmed the desired mutations were made without additional errors. Successful plasmids of both MSR and CPR were then transformed into the *Escherichia coli* strain Rosetta2(DE3)pLysS using the heat shock method. The MSR recombinant GST-fusion proteins were expressed and harvested as previously described in Section 2.5.2. The CPR recombinant His-tagged proteins were expressed and harvested as described in Section 3.4.3.

4.5.3 Generation and expression of the isolated FAD/NADP(H) domain of CPR

The gene encoding for the isolated FAD/NADP(H)-binding and connecting domain of CPR was PCR amplified from the cDNA of wild-type CPR. The primers were designed based on the published sequence (Accession number: NM000941) with flanking NdeI and BamHI restriction sites, Table 4.4. Both the PCR amplified product and the pET15b vector were digested with NdeI and BamHI then ligated together using the T7 DNA ligase and allowed to ligate overnight at 16 °C. Ligation products were then transformed into the XL1-Blue cell strain (Novagen). The plasmid construct (pCPR-FAD) was isolated using the E.Z.N.A Plasmid Mini Kit I from Omega Bio-tek then sent off for sequencing at the NAPS

Table 4.4: The forward (F) and reverse (R) oligonucleotide primers designed for each MSR and CPR variant. Mutation is in bold.

Enzyme Variant	Oligonucleotide Sequence
A312H$_{MSR}$	F 5' CCTATCAGCCTGGAGAT**CAC**TTCAGCGTGATCTGC 3'
A312H$_{MSR}$	R 5' GCAGATCACGCTGAA**GTG**ATCTCCAGGCTGATAGG 3'
A312Q$_{MSR}$	F 5' CTATCAGCCTGGAGAT**CAG**TTCAGCGTGATCTGC 3'
A312Q$_{MSR}$	R 5' GCAGATCACGCTGAA**CTG**ATCTCCAGGCTGATAG 3'
H322A$_{CPR}$	F 5' GTATGAATCTGGGGAC**GCC**GTGGCTGTGTACC 3'
H322A$_{CPR}$	R 5' GGTACACAGCCAC**GGC**GTCCCCAGATTCATAC 3'
H322Q$_{CPR}$	F 5' GTATGAATCTGGGGAC**CAA**GTGGCTGTGTACC 3'
H322Q$_{CPR}$	R 5' GGTACACAGCCAC**TTG**GTCCCCAGATTCATAC 3'
FAD-domain	F 5' GTAGCT**CATATG**CGTCAGTACGAGCTTGT 3'
	R 5' CAAGTC**GGATCC**CTAGCTCCACACGTCC 3'

DNA Sequencing Laboratory at the University of British Columbia (Vancouver, Canada). Successful clones of pCPR-FAD were kept and stored at $-20\,^{\circ}$C. The H322A mutation was made in pCPR-FAD by site-directed mutagenesis then isolated and sent for sequencing. Successfully mutated plasmids were transformed into Rosetta2(DE3)pLysS and expressed as described in Section 3.4.3.

4.5.4 Generation of MSR truncated hinge

To avoid adding more mutations than necessary to the sequence of MSR, recursive PCR was used to synthesize the wild-type FMN-domain with the new hinge sequence. First, an Xbal restriction enzyme site was introduced into the C-terminal end of the hinge region in wild-type MSR using the following primers: Forward 5' GCC TCT CTG AAT ATT CTA GAT TTA CCC CCA GAA TAT TTA C 3', and Reverse 5' G TAA ATA TTC TGG GGG TAA ATC TAG AAT ATT CAG AGA GGC 3'. The mutation was introduced using the recommended reaction mixture concentrations and cycling conditions from the QuikChange Site-Directed Mutagenesis Kit (Agilent Technologies). The mutation was confirmed by the NAPS DNA Sequencing Laboratory of the University of British Columbia (Vancouver, Canada).

Table 4.5: Recursive PCR forward (F) and reverse (R) oligonucleotide primers designed for wild-type MSR FMN-domain with CPR hinge synthesis.

Name	**Oligonucleotide Sequence**
Flanking	
1 (EcoR1 Site)	F 5' GTGCCGCGCGGCGAATTCATGCGCCGCTTTCTGCTGCTGTATGCTACCCAGCAGGG 3'
2 (Xba1 Site)	R 5' CCTGTAAATATTCTGGGGGTAAACCAGGAATATCTAGACGAATGCTGGACTCC 3'
Internal	
1	R 5' GCTCACATATTTCTTCTGCGATGGCCTTTGCCTGTCCCTGCTGGGTAGCATACAG 3'
2	F 5' CGCAGAAGAAATATGTGAGCAAGCTGTGGTACATGGATTTTCTGCAGATCTTC 3'
3	R 5' TCGGTTTTTAGGTCATACTTATCGGATTCACTAATACAGTGAAGATCTGCAGAAAATCCA 3'
4	F 5' GACCTAAAAACCGAAACAGCTCCTCTTGTTGTTGTGGTTTCTACCACGGGCACCGGAG 3'
5	R 5' CTGTATTTCCTTAACAAACTTGCGGGCTGTGTCGGGTGGGTCTCCGGTGCCCGTG 3'
6	F 5' GCAAGTTTGTTAAGGAAATACAGAACCAAACACTGCCGGTTGATTTCTTTGCTCACCTG 3'
7	R 5' GTATTCTGAATCACCGAGACCCAGTAACCCATACCGCAGGTGAGCAAAGAAATCAAC 3'
8	F 5' GTCTCGGTGATTCAGAATACACCTACTTTTGCAATGGGGGGAAGATAATTGATAAACG 3'
9	R 5' GTGTCATAGAAATGCCGGGCTCCAAGCTCTTGAAGTCGTTTATCAATTATCTTCCCCC 3'
10	F 5' CCGGCATTTCTATGACACTGGACATGCAGATGACTGTGTAGGTTTAGAACTTGTGGTTG 3'
11	R 5' CTTTCTGAGGGCTGGCCAGAGTCCAGCAATCCACGGCTCAACCACAAGTTCTAAACC 3'
12	F 5' GCCAGCCCTCAGAAAGCATTTTGGGGTGGAAGCCACTGGCGAGGAGTCCAGCATTCGT 3'

De novo synthesis of the wild-type MSR FMN-domain with the CPR hinge was accomplished through "one pot" recursive PCR.[145]. Fourteen individual oligonuleotide strands with lengths ranging 53-60 bases were designed based on the coding and non-coding nucleotide sequence to form ∼20 bp overlapping complimentary ends for extension during the PCR cycles, see Table 4.5. The existing N-terminal EcoR1 site and the original FMN domain sequence were preserved while the hinge sequence (5'^{463}AGGT...TATT^{726} 3') was exchanged for that of CPR with a terminal Xba1 site (underlined) (5' GGG GTG GAA GCC ACT GGC GAG GAG TCC AGC ATT CGT CTA GA 3').[105] The 50 μL reaction mixture consisted of 5 μL 10× Taq reaction buffer, 1.5 μL dNTP (10 mM each), 0.2 μM of each internal oligo, 2 μM of each flanking oligo, and 2 units of *Taq* DNA polymerase. PCR cycling conditions were as follows: 30 cycles of 1 min at 95 °C, 1 min at 64 °C, and 1 min at 72 °C with a final extension time of 5 min at 72 °C. The resulting PCR product was then amplified using the flanking oligos. Successful, complete gene synthesis was confirmed by the NAPS DNA Sequencing Laboratory using the flanking oligos as primers.

Synthesized gene insert and full length MSR plasmid with introduced Xba1 site vector were purified using a Cycle Pure Kit from Qiagen (Valencia,CA), and digested with EcoR1 and Xba1 restricting enzymes for two hours, or overnight at 37 °C, respectively. The vector was then dephosphorylated with antarctic phosphatase (37 °C for 30 min, followed by 65 °C for 30 min). The insert and vector were again purified using a Cycle Pure Kit from Qiagen. Cut plasmid was isolated using a Gel Extraction Kit (Qiagen). One hundred nanograms of vector and 21 ng of insert were then ligated in a total volume of 20 μL, containing 1 unit of T4 DNA ligase and 2 μL 10× buffer at 16 °C overnight. Ligation products were transformed into *E.coli* Xl1 Blue cell strain onto LB plates containing 100 μg mL^{-1} ampicillin and grown overnight at 37 °C. Successful mutagenesis and ligation without any PCR-induced errors was confirmed through sequencing.

4.5.5 Purification of MSR variants

Purification of the MSR variants followed the procedure previously described in Section 2.5.4.

4.5.6 Purification of CPR variants

Purification of the CPR variants followed the procedure previously described in Section 3.4.5.

4.5.7 Steady state turnover analysis

Steady state turnover assays for the MSR variants were conducted as previously described in Section 2.5.5. CPR variant assays followed the same protocol but were performed in 50 mM KPi pH 7.5 buffer. Steady state reduction of FeCN was also monitored at 420 nm by spectrophotometry (extinction coefficient of 1 020 $M^{-1}cm^{-1}$) with 0.5 mM FeCN, 100 μM NADPH and 10 nM of enzyme.

4.5.8 Pre-steady state kinetic analysis

Pre-steady state kinetic assays for the MSR and CPR variants were conducted as previously described in Section 2.5.6.

4.5.9 Redox Potentiometry

Pre-steady state kinetic assays for the MSR and CPR variants were conducted as previously described in Section 3.4.8. Potentiometric titrations on the isolated FAD/NADPH- and connecting domain of CPR were conducted in 50 mM potassium phosphate pH 7.0 with 20 % glycerol to discourage precipitation.

Chapter 5

Conservation of an aromatic FAD-shielding residue, Trp704, in *Artemisia annua* Cytochrome P450 Reductase

5.1 Summary

In this chapter, the role of the FAD isoalloxazine ring-shielding tryptophan residue (Trp704) in plant CPR derived from *Artemisia annua* is investigated through site-directed mutagenesis. Four mutations are made to the C-terminal Trp704 to reduce and remove the π-π-stacking interaction with the isoalloxazine ring: W704Y, W704F, W704H, and W704S. Aerobic and anaerobic spectrophotometry allowed for the steady state and pre-steady state kinetic characterization of each AaCPR. Through these studies, the Trp704 in AaCPR, as in human CPR, was determined to trigger $NADP^+$ release which is a partially rate-determining step in AaCPR catalysis. However, dissociation of the coenzyme is not as rate-determining in AaCPR as it is in human CPR. The flavin reduction kinetics of AaCPR variants differ notably from those of human CPR and are discussed herein.

5.2 Background

Artemisia annua is a Chinese herb that is harvested for the medicinal chemical artemisinin. Artemisinin, an endoperoxidized sesquiterpene, is a highly effective antimalarial, and artemisinin-based combination therapies are recommended by the World Health Organization as the first-line treatment for the disease.[146] To increase drug affordability and availability, metabolic engineering of microbes has been employed for large-scale semi-synthesis of artemisinin.[147–149] Keaslings and coworkers transformed *Saccharomyces cerevisiae* and *Escherischia coli* with three genes from *A. annua* that encode for enzymes in the artemisinin biosynthetic pathway: amorpha-4,11-diene synthase, CYP71AV1, and cytochrome P450 reductase (AaCPR).[148,149] Amorpha-4,11-diene synthase catalyzes the

first committed step in artemisinin synthesis, the conversion of farnesyl pyrophosphate to amorpha-4,11-diene. The cytochrome P450 monooxygenase CYP71AV1 catalyzes the three-step oxidation of amorpha-4,11-diene to produce the artemisinin precursor, artemisic acid. CYP71AV1 activity requires the sequential transfer of two electrons from AaCPR.

CPR from *Artemisia annua* shares $\sim$ 50% amino acid sequence similarity with human CPR, and the overall catalytic mechanism of the plant enzyme is expected to be similar to that formerly described for human CPR. In an effort to further optimize the engineered biosynthetic pathway for artemisinin production, Simtchouk *et al.* investigated the kinetic and thermodynamic properties of AaCPR.[150] Overall, the catalytic performance of AaCPR is improved compared to human CPR as the plant enzyme reduces cytochrome *c* with a 3-fold faster k_{cat}. Interestingly, it does so with a 30-fold weaker binding affinity for $NADP^+$. Most striking of all is the pre-steady state flavin reduction of AaCPR over the reductive half-reaction. Even with the temperature lowered from 25 °C to 6 °C, flavin reduction is much faster in AaCPR with reduction of the enzyme by the first and second NADPH equivalent occurring at rate constants of >500 and 18 s^{-1}. The improved rates are not attributed to the flavin center redox potentials, as they are similar to those determined in human CPR. However, unlike human CPR, the spectral changes associated with the first kinetic phase include formation of a large absorbance signal in the long wavelengths that is characteristic of a charge-transfer species. This charge-transfer species is assigned to the interaction between FAD and the nicotinamide ring of the coenzyme. A greater propensity for the Trp704-displaced conformation in AaCPR may be the origin of the accelerated observed rates of flavin reduction.

Alternatively, Simtchouk *et al.* also proposed that the accelerated flavin reduction may be due to weaker binding of the oxidized coenzyme. Previous studies with mammalian CPR have found that $NADP^+$ release is necessary for formation of the disemiquinone intermediate and binding of a second NADPH for further flavin reduction; as such $NADP^+$ release has been proposed as the rate-determining step in the reductive half-reaction in mammalian CPR.[60,68,144] These studies revealed an increase in the primary kinetic isotope effect associated with hydride transfer under high ionic strength conditions. These conditions weaken coenzyme binding, such that product release is less rate-determining. This, in turn, unmasks the isotope effect associated with breakage of a C-H/D bond. In low ionic strength conditions (conditions that promote tight coenzyme binding), the intrinsic KIE for hydride transfer is diminished to 1.0, which indicates that other steps (i.e. $NADP^+$ release) are more rate-determining.[151] Furthermore, an elevated primary KIE measured for AaCPR (1.7) in comparison with human CPR (1.1) under the same assay conditions reveal a shift in the rate-determining step from $NADP^+$ release to hydride transfer in AaCPR.[150]

Despite an exceptional difference in coenzyme binding affinity in AaCPR, an amino acid sequence alignment with human CPR shows that the key residues identified for coenzyme binding are conserved in AaCPR. Furthermore, the FAD isoalloxazine ring-stacking aromatic trytophan (Trp704) is also conserved. In light of the regulatory role of the conserved aromatic residue in coenzyme binding and intramolecular electron flow in human CPR and other diflavin oxidoreductases, the potential differential regulatory role of Trp704 in AaCPR was investigated.

The subtle differential regulatory role of the C-terminal Trp704 residue in coenzyme binding and electron flow in AaCPR was determined by mutagenesis. For direct comparison with human CPR, the following mutations were made: W704S, W704H, W704Y, and W704F. Mutation to histidine (W704H), tyrosine (W704Y) and phenylalanine (W704F) were chosen to maintain residue aromaticity, while investigating the role of side chain size and polarity. The effect of reducing side chain size and aromaticity is evaluated from mutation of Trp704 to a serine (W704S). Spectroscopic analysis cytochrome *c* reduction with each variant was used to determine their respective steady state kinetic properties. Pre-steady state flavin reduction under anaerobic conditions with saturating NADPH for each variant was measured by stopped-flow spectrophotometry.

5.3 Results

5.3.1 Steady state kinetic parameters

CPR-catalyzed reduction of cytochrome *c* was used to determine the steady state kinetic properties of each W704 variant. The data are summarized in Table 5.1. Compared to wild-type AaCPR, all W704 variants elicited slower enzymatic turnover with k_{cat} values ranging from 0.11 to 9.21 s^{-1}. The slowest variant is W704S followed by W704F, W704H, and the fastest is W704Y. Under the same assay conditions as wild-type AaCPR, it was not possible to extract an inhibition constant for $NADP^+$ as the necessary [NADPH] values were too low for the detection limits of a 1 cm path length cuvette. The lack of detectable K_i for W704Y and W704F, together with the K_i determined for W704H and W704S, indicates that the coenzyme binding affinity is much higher in the W704 variants.

Table 5.1: Steady state kinetic parameters of AaCPR W704 variants. Conditions: 1 mL reaction volume, 8 μM cytochrome c^{3+}, 2 *p*mole enzyme, varied [NADPH] and [$NADP^+$], 50 mM Tris-HCl pH 7.5 at 25 °C. Assays were done in triplicate and fit to the Michaelis-Menten equation. Inhibition data from four inhibitor concentrations were fit to a competitive inhibition equation.

Enzyme	k_{cat} (s^{-1})	K_m ($M \times 10^{-6}$)	K_i ($M \times 10^{-6}$)	k_{cat}/K_m ($s^{-1}M^{-1} \times 10^{+6}$)
WT	66 ± 1	1.22 ± 0.11	1.59 ± 0.18	54 ± 5
W704Y	22.5 ± 0.4	0.07 ± 0.01	–	132 ± 20
W704F	4.3 ± 0.1	0.15 ± 0.02	–	29 ± 4
W704H	5.8 ± 0.1	0.42 ± 0.04	0.38 ± 0.04	14 ± 2
W704S	0.110 ± 0.001	0.11 ± 0.01	0.24 ± 0.03	1.0 ± 0.1

5.3.2 Multiple and single wavelength pre-steady state kinetics

Pre-steady state reduction of AaCPR variants with saturating NADPH was monitored by anaerobic stopped-flow spectrophotometry. With wild-type AaCPR, initial studies at 25 °C revealed a large loss of spectral data within the dead-time of the stopped-flow.[150] The temperature was then reduced to 6 °C in an effort to capture the first rate of flavin reduction. Thus, for a direct comparison with wild-type AaCPR, all stopped-fow experiments with W704 variants were also performed at 6 °C. Figure 5.1 displays the multiple wavelength spectra of the oxidized variant combined with the spectra recorded over 15 s after rapid mixing with excess NADPH. Like in wild-type AaCPR, some spectral data of W704F and W704Y are lost in the dead-time (1.5 ms), indicating the relatively rapid (>600 s^{-1}) rate of flavin reduction in these variants. An approximate 30 % amplitude change at the flavin absorbance maxima is observed for W704Y, while an amplitude change of ∼ 14% is observed for W704F. Despite the lost spectral data in W704Y and W704F, double exponential fits of single wavelength traces at 454 nm (Figure 5.3) enabled the extraction of a fast k_{obs1} and slow k_{obs2}. The data are summarized in Table 5.2. The k_{obs1} for both W704Y and W704F is > 700 s^{-1}, while the corresponding rate constant in wild-type AaCPR is 500 s^{-1}. These values underestimate the true rate constant, as there was a small loss of absorbance within the dead-time of the stopped-flow.[150] The smaller initial amplitude change associated with k_{obs1} of W704Y and W704F may indicate that a smaller fraction of the population is being initially reduced. The 4- and 6-fold slower k_{obs2} of W704Y and W704F indicates a slower reduction in these variants. No spectral data are lost within the dead-time for W704H and W704S reduction, indicating that flavin reduction is relatively slow in these variants with k_{obs1} of 4 s^{-1} and 0.018 s^{-1}, respectively. The initial reduction of W704S is significantly delayed, as shown in Figure 5.3 and 5.4 *A*.

Like native AaCPR, the spectral profile of the NADPH-dependent reduction of W704Y shows the loss of the flavin absorbance maxima with the simultaneous appearance of a broad absorbance band from 530-700 nm. This broad flat absorbance band is assigned to the accumulation of a charge-transfer species between the nicotinamide and the FAD isoalloxazine rings. The band is fully formed in the dead-time and Figure 5.3 shows that the concentration of the species is constant over the course of the reductive half-reaction, even over a 150 s extended time domain. In Figure 4.5 panel B, the flavin reduction of W704F at 454 nm is also accompanied by a build up of a flat absorbance band at >500 nm that is indicative of a charge-transfer species. Unlike wild-type AaCPR and W704Y, flavin reduction of W704F and formation of the CT species at 600 nm occurs gradually and completes within 15 s. As equilibrium is established over 150 s, the disemiquinone signal is slightly unmasked as a slight peak centered at 600 nm is observed. The overlapping signals of the disemiquinone and the charge-transfer complex complicate the analysis of spectral data at 600 nm. Attempts have been made in *Anabaena* FNR to assign specific spectral features to different charge-transfer complexes, however these analyses are conducted at longer wavelengths (700-1000 nm) which are beyond the limits of the photodiode array used here.[152]

Reduction of W704H is well within the detection limits of the stopped-flow instrument. Like W704F, a gradual decrease in absorbance at 454 nm occurs with the gradual increase in absorbance in the longer wavelengths. While W704H forms the charge-transfer species, it does so at approximately half the amplitude observed in W704F (see 5.1 and 5.3). Substitution of Trp704 with a serine severely disrupted flavin reduction as evident by the minimal spectral changes at 454 and 600 nm over the same time domain as the other W704 variants, shown in Figure 5.3. Figures 5.1 and 5.4 show that even after an extended time domain of 150-300 s, the variant is only partially reduced with a small absorbance signal assigned to the disemiquinone species.

The early 'up' and 'down' phases at 600 nm observed in wild-type AaCPR are not present in any of the variants. In wild-type AaCPR, this peak was assigned to the formation and decay of the disemiquinone intermediate. In the W704 variants, the disemiquinone species may not accummulate and/or the spectral signal may be masked by the greater absorbance signal for the CT species.

5.4 Discussion

A comparison of the Trp704 variants of AaCPR with the Trp676 variants of human CPR was made to assess the potential differential role of the FAD-stacking aromatic residue in CPR catalysis. Recall from Chapter 3 that mutation of W676 to a smaller aromatic

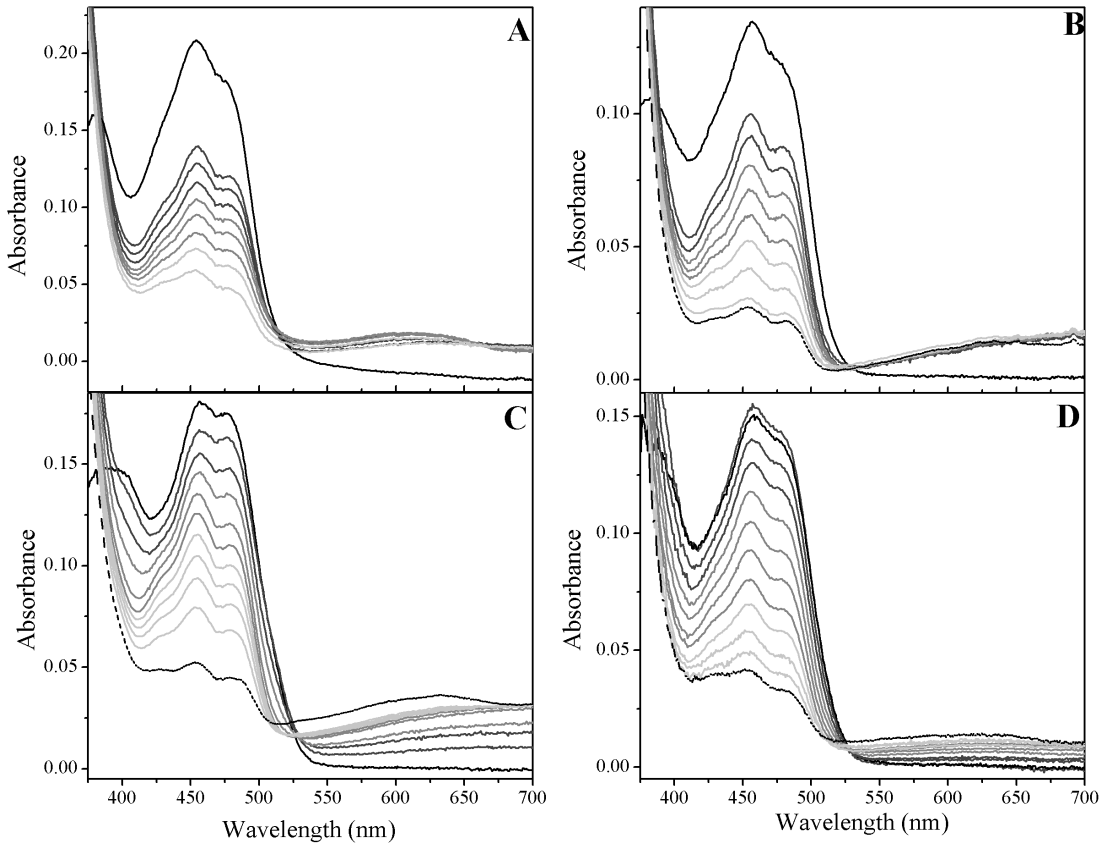

Figure 5.1: Visible spectra of AaCPR W704 variants during reduction by NADPH, monitored by multiple wavelength stopped-flow spectrophotometry. Conditions: 10 μM enzyme, 10-fold excess NADPH, anaerobic 50 mM Tris-HCl pH 7.5 at 6 °C. Spectral scans of wild-type AaCPR (A), W704Y (B), W704F(C) and W704H(D) show the progressive reduction of oxidized enzyme (black) to reduced (light gray) over a 15 s time domain. After 150 s, another trace was recorded (black dashed line).

Table 5.2: Observed rate constants of the pre-steady state reduction of AaCPR variants at 454 nm. Conditions: 10μM enzyme, 100 μM NADPH, anaerobic 50 mM Tris-HCl pH 7.5 at 6 °C. An average of 3-5 traces was taken and the resulting trace was fitted to a double exponential equation.

Enzyme	k_{obs1} (s^{-1})	k_{obs2} (s^{-1})
WT	499 ± 4	18.10 ± 0.04
W704Y	>700	4.76 ± 0.04
W704F	>700	2.78 ± 0.02
W704H	4.4 ± 0.1	0.82 ± 0.01
W704S	0.018 ± 0.007	0.006 ± 0.001

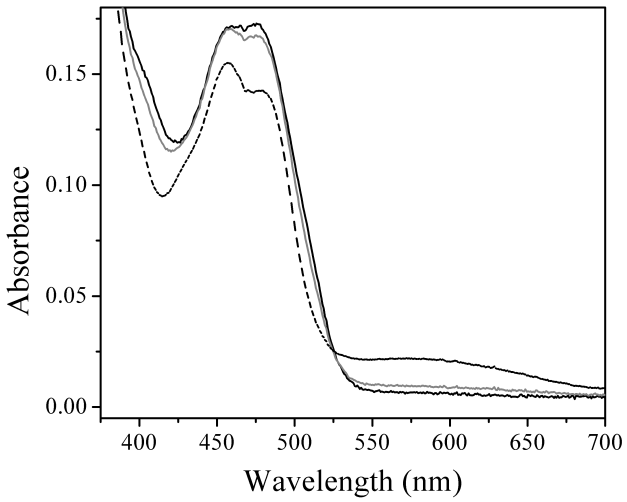

Figure 5.2: Visible spectra of W704S variant during reduction by NADPH, monitored by multiple wavelength stopped-flow spectrophotometry. Conditions: 10 μM enzyme, 10-fold excess NADPH, anaerobic 50 mM Tris-HCl pH 7.5 at 6 °C. Spectral scans of W704S show the oxidized enzyme (black) mixed with NADPH over 15 s (gray). After 150 s, another trace was recorded (black dashed line).

residue led to tighter binding of NADP(H).[144] This was evident in the lower K_i values for $NADP^+$ in the W676F and W676Y variants. By decreasing the size of the isoalloxazine ring-stacking residue, the energetic cost of nicotinamide displacement is presumably lowered and coenzyme binding becomes more energetically favourable. Tighter coenzyme binding was also evident in stopped-flow studies, where a stable $NADP^+$-$FADH_2$ charge-transfer (CT) complex was generated upon reduction of the fully-oxidized enzyme with NADPH. The inability of the smaller aromatic side chains to effectively displace the nicotinamide ring away from the FAD likely leads to the stable formation of this CT complex. As a result, NADPH-mediated reduction of human CPR W676Y and W676F is monophasic (as opposed to biphasic for the native enzyme) leading to a two-electron reduced form of the enzyme. At the completion of the reductive half-reaction, there is a distribution of the NADPH-FAD-FMN and $NADP^+$-$FADH_2$-FMN complexes. The rate constants for flavin reduction in human CPR W676Y and W676F are reduced to 6 and 0.7 s^{-1}, respectively, presumably because tight binding of $NADP^+$ prevents disemiquinone formation, which would otherwise drive the forward flux of electrons to the higher potential FMN cofactor.

Likewise, the W676H variant, reported by Gutierrez and coworkers, also exhibits monophasic flavin reduction to the two-electron level with a slower k_{obs} of 3 s^{-1}.[137] W676H flavin reduction is also accompanied by formation of the CT complex ($NADP^+$-$FADH_2$-

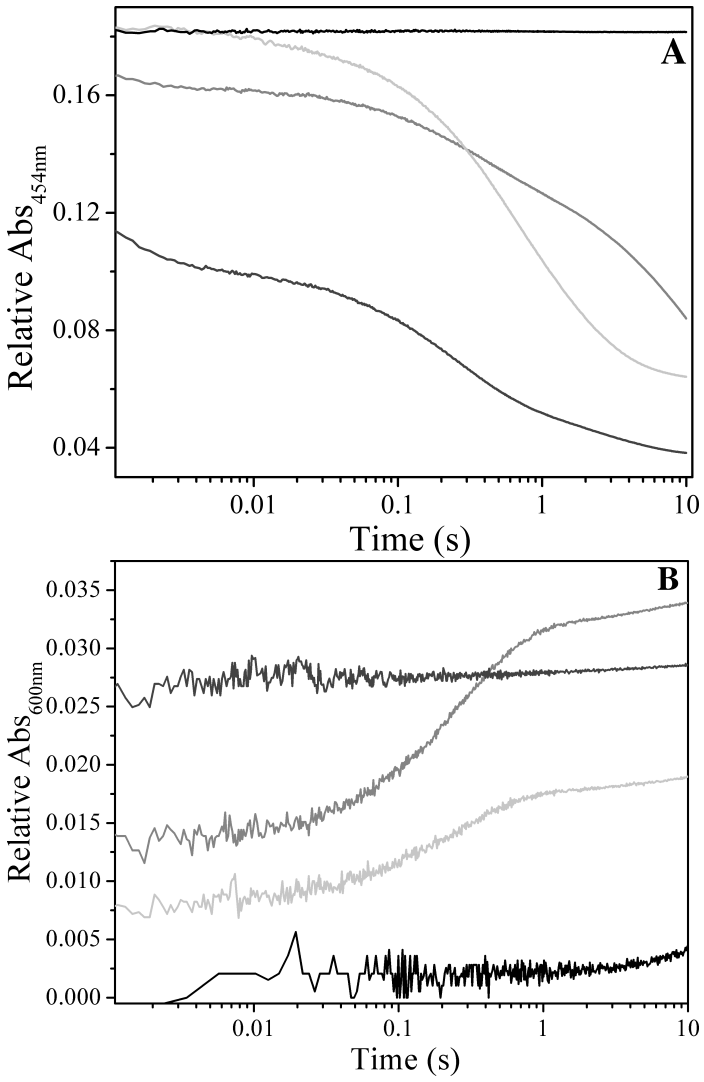

Figure 5.3: Anaerobic single wavelength stopped-flow traces of AaCPR W704 variants. Conditions: 10 μM enzyme, 10-fold excess NADPH, anaerobic 50 mM Tris-HCl pH 7.5 at 6 °C. Panel A: Averaged traces taken at 454 nm over 1 s. Panel B: Averaged traces taken at 600 nm over 10 s. W704Y (dark gray), W704F (gray), W704H (light gray), and W704S (black).

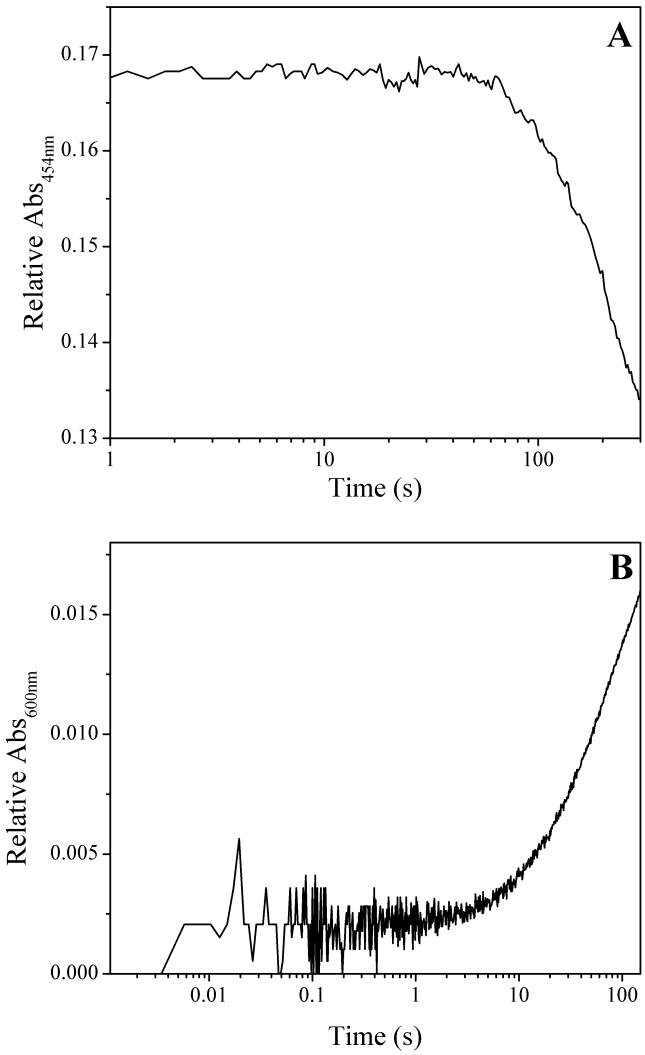

Figure 5.4: Anaerobic flavin reduction of W704S monitored by single wavelength stopped-flow spectrophotometry. Conditions: 10 μM enzyme, 10-fold excess NADPH, anaerobic 50 mM Tris-HCl pH 7.5 at 6 °C. Panel *A*: an average of 3 traces of W704S reduction at 454 nm over 300 s. Panel *B*: an average of 3 traces of W704S reduction at 600 nm over 150 s.

FMN). For W676H, W676Y and W676F, the oxidized coenzyme is essentially 'locked' in the active site, however the CT complex does not form irreversibly since all three variants are capable of reducing cytochrome *c* under steady state conditions, albeit at a slower rate than that of wild-type CPR.

Like the W676Y and W676F variants of human CPR, the corresponding variants of AaCPR elicited a reduction in k_{cat} for cytochrome c^{3+} and a tighter binding affinity for the coenzyme as evident by the lower K_m for the substrate. These data suggest that, as for the human enzyme, the bulky W704 triggers release of $NADP^+$ to make this step less rate-determining in the overall mechanism. That being said, W676 is perhaps more critical for this step of catalysis compared to the AaCPR W704. Since coenzyme binding affinity is much stronger in human CPR, the oxidized coenzyme remains bound in the active site and requires disruptive repulsive interactions to promote its release. For AaCPR, the coenzyme binding affinity is weaker compared to human CPR, therefore release of the oxidized coenzyme may be less rate-determining in the plant species.

This hypothesis is based on stopped-flow data collected for the W704F and W704Y variants of AaCPR, where in contrast to the W676 variants of human CPR, the W704Y variants of AaCPR exhibit biphasic reduction kinetics. Like native AaCPR, there was an initial rapid phase of flavin reductin (k_{obs1}) at >700 s^{-1}, for both W704Y and W704F, followed by a slower k_{obs2} of 5 and 3 s^{-1}, respectively. For W704Y, approximately half of the first kinetic phase is complete within the dead-time of the stopped-flow as there was an ∼58% absorbance loss at 454 nm. This absorbance loss is approximately 38% greater than that observed for native AaCPR, suggesting that reduction by the first NADPH is faster with the W704Y substitution. Also like native AaCPR, a charge-transfer species also fully forms within the dead-time of the stopped-flow, but unlike in human CPR W676Y and W676F variants, this species does not appear to greatly affect further reduction of the enzyme by a second equivalent of NADPH. This is evident by the biphasic nature of flavin reduction in W704Y and W704F. Thus, further reduction suggests that the smaller aromatic side chains are more proficient at displacement of the nicotinamide ring in the AaCPR variants compared to the human CPR variants.

It is unclear as to why the appearance of the charge-transfer complex in AaCPR does not lead to inhibition of further reduction of the enzyme by a second equivalent of NADPH. It is possible that, in AaCPR, more FAD is initially reduced by NADPH and that a fraction of the enzyme population will be converted to the disemiquinone and FMN hydroquinone states upon $NADP^+$ release while the rest remains bound to the coenzyme as $NADP^+$-$FADH_2$-FMN. Further reduction of the FMN hydroquinone (FAD-$FMNH_2$) population by a second molecule of NADPH then forms the four-electron reduced state $FADH_2$-$FMNH_2$ which may also be bound to oxidized coenzyme. Thus, the large CT signal is attributed to a mixture of

two-electron reduced ($NADP^+$-$FADH_2$-FMN) and four-electron reduced ($NADP^+$-$FADH_2$-$FMNH_2$) enzyme species, accounting for the constant high concentration of CT signal in W704Y. Alternatively, the charge-transfer complex may arise from the unproductive binding of NADPH against the various forms of two- and four-electron reduced flavins (NADPH-FADH•-FMNH•, NADPH-FAD-$FMNH_2$, or NADPH-$FADH_2$-$FMNH_2$). The identity of the charge-transfer complexes that form over the course of the reductive half-reaction of AaCPR is key to understanding the catalytic behavior of this enzyme. Recently, some success in this area has been acheived in *Anabaena* FNR however a photodiode array with a wider wavelength range (up to 900-1000 nm) is necessary.[152]

For W704F, the amplitude change associated with k_{obs1} is significantly smaller compared to native AaCPR and W704Y, but like these two forms, the rate constant is >700 s^{-1} and a significant portion of this phase of the reaction occurs in <1 ms. The smaller amplitude change indicates that a smaller fraction of the enzyme is reduced in this first kinetic phase. It is unclear as to why this is, but it may be due to changes in the electronic environment around the FAD cofactor or the greater accumulation of the CT absorbance band in this variant. Further reduction of W704F spans a greater time domain than W704Y and is also multiphasic.

In W704H, the biphasic flavin reduction was slower with k_{obs1} of 4 s^{-1} and k_{obs2} of 0.8 s^{-1}, and the coenzyme binding affinity is moderately stronger in this variant, as evident by the K_i for $NADP^+$. Unlike W704Y and W704F, the initial kinetic phase of W704H reduction is fully captured by stopped-flow spectrophotometry. The reason behind this significantly slower flavin reduction is not immediately clear. Interestingly, the W704H variant also does not form a CT band within the dead-time of the stopped-flow, meaning that placement of the nicotinamide ring against the FAD is inhibited in this variant. This may account for the reduced k_{obs1}.

Exchanging the Trp704 for a serine renders the AaCPR variant catalytically inactive. This is evident by the severely reduced rates for the steady state reduction of cytochrome *c*. Moreover, the severely delayed flavin reduction is no longer under pre-steady state conditions and is likely nonphysiological. Since the serine side chain does not form any π-π-stacking interactions with the FAD isoalloxazine ring, the energetic cost of residue displacement is expected to be reduced significantly. Therefore, nicotinamide ring placement over the hydrophobic isoalloxazine should be favourable. However, there is no spectral evidence of a rapidly formed charge-transfer complex in W704S. Interestingly, mutation of the equivalent Trp704 residue in pea FNR to a serine (Y308) resulted in a much greater active site occupancy of the nicotinamide ring as determined from spectral data, and was captured in Y308S crystal structures.[62] Later theoretical modeling studies on Y303S in *Anabaena* FNR suggest that the active site aromatic Tyr303 residue contributes to the

optimal orientation of the nicotinamide ring to the isoalloxazine ring, thereby influencing the efficiency and mechanism of the reaction.[152–154] Therefore, it is possible that in W704S, the nicotinamide ring may be binding to the active site in a nonproductive way that does not favour formation of the charge-transfer complex or hydride transfer.

5.5 Experimental Procedures

5.5.1 Materials

The reagents NADPH, $NADP^+$, 2',5'-ADP, and cytochrome c^{3+} were ordered from Sigma Aldrich (Oakville, ON, Canada). Agilent Technologies (Mississauga, ON, Canada) provided the *Pfu* Turbo DNA polymerase, *Taq* DNA polymerase and Xl1 Blue cell lines. Rosetta(DE3)pLysS competent cells were purchased from EMD Biosciences. Protein purification supplies, nickel-nitriloacetetic acid, Resource Q column and glutathionine sepharose 4B resin, were obtained from GE Biosciences. All other chemical reagents were purchased from Fisher Scientific.

5.5.2 Generation and expression of AaCPR variants

The W704 variants of *Artemisia annua* CPR were generated from soluble (transmembrane domain cleaved) wild-type AaCPR plasmid pET-15b (pETAaCPR) using the QuikChange Site-Directed Mutagenesis Kit (Agilent Technologies).[150] Oligonucleotide primers were designed from the DNE sequencing results of pETAaCPR and ordered from Integrated DNA Technologies (Coralville, Iowa, USA). See Table 5.3 for the primer sequences. The mutations were confirmed by sequencing from the NAPS DNA Sequencing Laboratory of the University of British Columbia (Vancouver, Canada). We transformed the plasmids using the heat shock method into the *Escherichia coli* strain Rosetta2(DE3)pLysS. The His-tagged recombinant AaCPR variants were expressed and harvested as previously described in Section 3.4.3.

5.5.3 Steady state turnover analysis

Steady state turnover assays for the AaCPR variants were performed as previously described in Section 2.5.5. for MSR, including the same 50 mM Tris-HCl pH 7.5 buffer conditions.

5.5.4 Pre-steady state kinetic analysis

Pre-steady state kinetic assays for the AaCPR variants were performed as previously described in Section 2.5.6.

Table 5.3: The forward (F) and reverse (R) oligonucleotide sequences for W704 variants of AaCPR. Mutations are highlighted in bold.

CPR Variant	Oligonucleotide Sequence
W704S	F 5' CTACCTGCGTGATGTC**TCG**TAAGGATCCGGCTGC 3'
	R 5' GCAGCCGGATCCTTA**CGA**GACATCACGCAGGTAG 3'
W704F	F 5' CTACCTGCGTGATGTC**TTC**TAAGGATCCGGCTGC 3'
	R 5' GCAGCCGGATCCTTA**GAA**GACATCACGCCAGTAG 3'
W704Y	F 5' CTACCTGCGTGATGTC**TAC**TAAGGATCCGGCTGC 3'
	R 5' CTACCTGCGTG**ATG**TCTACTAAGGATCCGGCTGC 3'
W704H	F 5' CTACCTGCGTGATGTC**CAC**TAAGGATCCGGCTGC 3'
	R 5' GCAGCCGGATCCTTA**GTG**GACATCACGCAGGTAG 3'

Chapter 6

Conclusion

MSR and CPR share considerable similarities in structure and function, including 41% amino acid similarity. Large-scale conformational motion allows these dynamic multidomain flavoenzymes to adopt a closed and open conformation to support intra- and intermolecular electron transfer. Catalysis involves transfer of a hydride ion from the obligate two-electron donor NADPH to the bound FAD isoalloxazine ring, followed by the consecutive transfer of single electrons to the FMN isoalloxazine ring, and final one-electron delivery from FMN to an external acceptor. While these general characteristics are shared, their kinetic properties and coenzyme affinity differ. These dissimilarities spurred investigation into the inherent regulatory structures of MSR and CPR using site-directed mutagenesis. Evaluation of the steady state kinetic properties of each generated variant was performed by steady-state kinetic analysis of cytochrome *c* reduction. Dead-end and product inhibition experiments determined the relative substrate binding affinities. Stopped-flow spectroscopy was used to investigate the pre-steady state kinetic properties of the variants. Through these methods, the structural nuances that lead to the distinct catalytic properties of MSR and CPR were uncovered.

In MSR, a large aromatic residue Trp697 forms π-π stacking interactions with the FAD isoalloxazine ring. Steric clash between Trp697 and the nicotinamide ring weakens the binding of the coenzyme.[65] Swapping the tryptophan indole ring for a smaller aromatic side chain improved the rate of cytochrome *c* reduction and accelerated the pre-steady state rate of NADPH-dependent reduction of FAD. An increase in the KIE from 1.7 in native MSR to 2.0 in W697Y and W697F variants suggest that isotopically insensitive steps, such as conformational movement of the aromatic residue, becomes less rate-determining in the variants. Reducing the size of the aromatic side chain weakens the π-π stacking interaction with the isoalloxazine ring and presumably lowers the energetic cost for displacement of the side chain, which, in turn, accelerates hydride transfer. These combined data suggest that displacement of Trp697 by the nicotinamide ring partially gates hydride transfer in MSR.

NADPH initially binds to a polar pocket of MSR through the 2',5'-ADP half of the molecule. The majority of the favourable coenzyme binding energy arises from interactions between the 2'-phosphate group and conserved active site residues. The nicotinamide ring, however, does not contribute favourably to the binding energy because of steric clash be-

tween the nicotinamide ring and Trp697.[65] As expected, aromatic substitution of Trp697 did not affect the 2',5'-ADP binding affinity. However, the substitutions did increase the binding affinity for both NADPH and NADH such that the variants elicited a lower substrate preference for NADPH over NADH compared to the native enzyme. Presumably, reduced steric clash between the nicotinamide ring and the smaller side chains in the variants made the binding of this portion of the nicotinamide ring more favourable, which reduced the differences in binding affinities between the phosphorylated and unphosphorylated coenzyme. Thus, Trp697 contributes to the strong coenzyme preference observed in MSR.

In addition to Trp697, other residues in the FAD/NADPH binding domain have been found to influence the catalytic properties of the enzyme. Weaker coenzyme binding was observed in the A312H variant of MSR. A312 is located within hydrogen bond distance of the catalytic triad that surrounds the FAD isoalloxazine ring. In human CPR, the corresponding residue is a histidine (His322). The histidine residue was proposed to weaken coenzyme association by competing with the nicotinamide ring for hydrogen bond contact with the catalytic triad residue Asp695 (MSR numbering). Flavin reduction was significantly reduced (33-fold slower rate) in the A312H variant. Weaker coenzyme binding affinity potentially contributes to the slow flavin reduction of A312H. Alternatively, given the location of the amino acid variation near the FAD isoalloxazine ring, the substitution may also affect the FAD redox potential.

Mutagenesis studies targeting residues that form electrostatic interactions with the pyrophosphate and 2'phosphate group of NADPH generated variants that improve coenzyme binding affinity and accelerated FAD reduction. Not surprisingly, a substitution at the 2'-phosphate-binding pocket (A622K) elicited the greatest effect, as amino acid interactions with this moiety provides the majority of the coenzyme binding energy. Given that these substitutions were not near the FAD isoalloxazine ring, they were not expected to affect the reduction potential of the cofactor. Thus, increases in flavin reduction are attributed to improved coenzyme binding affinity.

In contrast to MSR, the FAD-shielding Trp676 of human CPR does not pose a thermodynamic barrier to coenzyme binding and hydride transfer. The binding of the nicotinamide ring is not significantly disrupted by Trp676, as evident by the equivalent dissociation constants of 2',5'-ADP and $NADP^+$.[64] As a consequence, reducing the size of the aromatic side chain does not dramatically enhance the coenzyme binding affinity or accelerate flavin reduction, as observed for MSR. CPR catalysis is not limited by Trp676 displacement. Instead, Trp676 acts to displace the oxidized nicotinamide ring. This conclusion is supported by stopped-flow data of Trp676 variants that show the stable formation of the $NADP^+$-$FADH_2$-FMN complex. Since the nicotinamide ring remains planar with the isoalloxazine ring, interflavin electron transfer is hindered. The prolonged interaction between the FAD

hydroquinone and the oxidized nicotinamide ring also leads a shift towards the reverse reaction (hydride transfer to $NADP^+$); this is evident by the inverse KIE of 0.9 measured for W676Y and W676F. Slow flavin reduction is also a product of a greater shift towards the reverse reaction as well as impaired interflavin electron transfer. Thus, the large bulky indole ring of Trp676 is more proficient than other aromatic residues at displacing the oxidized nicotinamide ring from the FAD active site.

Parallel alignment of the nicotinamide ring against the FAD disrupts the hydrogen bond that forms between the Asp674 and Ser457 residues of the catalytic triad (CPR numbering). Asp674 repositions itself to interact with the carboxamide group of the nicotinamide ring. This interaction is likely responsible for optimizing the orientation of the C4 atom of NADPH for hydride transfer. It has been proposed that electron transfer from $FADH_2$ to FMN requires the reformation of the hydrogen bond between Asp674 and Ser457, which enables Asp674 to act as a general base and abstract a proton from the N5 of $FADH_2$ via Ser467.[61,155] Previously, only the three residues of the catalytic triad (Asp674, Ser457, Cys629) were assigned to this hydrogen bond network, however in this work, a neighbouring histidine residue that is within hydrogen bond distance to Asp674 was identified. Substituting the histidine for an alanine revealed that the imidazole weakens coenzyme binding and promotes interflavin electron transfer. Competition between the histidine and the nicotinamide ring for hydrogen bonding with Asp674 likely weakens coenzyme affinity, thereby favouring $NADP^+$ release. Restoration of the hydrogen bond network provides a proton relay pathway for the hydrogen atom of the N5 nitrogen of the isoalloxazine ring and interaction with Ser457 stabilizes the resulting FAD semiquinone, thus enhancing interflavin electron transfer.

$NADP^+$ release is the rate-determining step in CPR catalysis. This conclusion is supported by the K602AV603K variant, which effectively removes a direct salt-bridge interaction with the coenzyme 2'-phosphate group. Coenzyme binding affinity was dramatically weakened and a faster rate constant of flavin reduction was observed. Thus, promoting $NADP^+$ release (by weak coenzyme binding or by bulky Trp676) is important in CPR catalysis.

The different catalytic role of the FAD-stacking tryptophan in MSR and CPR may arise from how the tryptophan is orientated with respect to the FAD in both enzymes. In both substrate-free and substrate-bound MSR, the entire indole ring is positioned over the FAD, maximizing π-π interaction. For CPR, the only available substrate-free crystal structure has an engineered disulfide bond between the FAD and FMN domains.[57] In this structure, Trp676 adopts the same position as that observed in MSR, while in substrate-bound CPR, Trp676 is flipped by 180 degrees and rotated so that only the phenyl group is in van der Waals contact with the isoalloxazine ring. Therefore, a conformational change in Trp676 to

a presumably more stable state upon coenzyme binding is apparently more favourable in CPR than in MSR. Thus, it is possible that the partially stacked position of Trp676 in CPR weakens the flavin-indole contact such that it is easily displaced by the nicotinamide ring. Moreover, previous studies on the conformational dynamics of CPR have shown that binding of 2',5'-ADP and $NADP^+$ confer a shift towards the closed conformation, which shortens the interflavin distance. In the presence of 2',5'-ADP alone, the rate constant associated with interflavin electron transfer is enhanced.[73,75] Recent studies on the conformational behavior of MSR indicate that it exists primarily in the open state, and the conformational distribution is not influenced by the presence of 2',5'-ADP.[156,157] However, in the presence of $NADP^+$, the conformational equilibria is shifted to the closed state. Thus, I propose that subtle interactions at the 2',5'-ADP binding site confer conformational changes to Trp676 to facilitate displacement by the nicotinamide ring in CPR, but not in MSR.

The structural nuances involved in regulating the differential catalytic performance of MSR and CPR have been investigated in this work. Examining these regulatory structures contributes to the overall understanding of diflavin oxidoreductase catalysis and provide a stepping stone for future work on these flavoenzymes. Through mutagenesis studies, I have successfully enhanced MSR catalysis by reducing the size of the FAD-shielding aromatic side chain. In an effort to improve interflavin electron communication as well as FAD reduction, a combination of the W697Y and the A312H mutation would be of interest. For CPR, the presence of the Trp676 and His322 appears to be necessary for rapid flavin kinetics with NADPH. Instead, further mutations aimed to weaken coenzyme binding at the coenzyme-binding cleft may prove to be effective in accelerating flavin reduction. In fact, the double mutant K602AV603K did elicit much faster flavin reduction, however the overall rate of cytochrome *c* reduction remained similar to native CPR. This may be a consequence of disruption to the subtle conformational changes that take place upon 2',5'-ADP binding that influence the conformational dynamics of CPR. Thus, investigation into the participating residues and the mechanism of this relationship would be of interest. Moreover, the aspartic acid loop that extends into the coenzyme-binding site ought to be analyzed for its potential role in regulating coenzyme binding through structural rearrangement. Further analysis of single-amino acid mutations in the isolated FAD/NADPH domain in comparison with full-length MSR and CPR would aid in pinpointing the effect elicited from local versus large-scale structural changes. If the intention is to engineer a NADH-dependent MSR or CPR, then reducing the size of the FAD-shielding aromatic side chain consistently reduced the preference for NADPH over NADH.[132] Use of NADH is favourable for engineered systems because it is relatively inexpensive compared to the phosphorylated counterpart. Smaller aromatic substitutions coupled with mutations at the coenzyme-binding site aimed

to weaken coenzyme affinity, may enhance the overall catalytic performance of CPR or MSR with NADH.

Lastly, there is some ambiguity in the charge-transfer complex assignment among diflavin oxidoreductases. In AaCPR, appropriate identification of the charge-transfer complex that is formed over the reductive half-reaction is important in understanding the catalytic behavior of this plant CPR species. In human CPR, substitution of Trp676 for a smaller aromatic results in the persistent stacking of the oxidized nicotinamide ring over the FAD isoalloxazine ring, thereby impeding further reduction. In contrast, reduction of AaCPR is much more rapid and occurs with the formation of a charge-transfer complex. With mutations that mirror those of human CPR, the charge-transfer complex still forms and does not appear to impede further reduction in the same way as human CPR. Thus, the ability to identify which charge-transfer species are formed or favoured in AaCPR compared to human CPR would be paramount to characterizing the catalytic behavior of these enzymes. This problem has been explored in FNR, and studies have shown some success at distinguishing charge-transfer complexes over longer wavelengths (600 - 1000 nm).[152,158,159]

In the future this research may contribute to improving MSR activity in MS deficient individuals through gene therapy. A small study where patient cell lines were transfected with wild-type *MTRR* minigene constructs *in vitro* resulted in a significant enhancement in MS activity, marked by methionine production.[160] Although this may seem far-fetched at the moment, it may prove to be an attractive treatment option for early neonatal treatment or for individuals that do not benefit from the available therapies today.[161,162] Certainly, the co-expression of mammalian CPR in cytochrome P450 gene-directed enzyme therapy has already been employed in preclinical trials to support cytochrome P450 activity on anticancer prodrugs within target tumor cells.[163–165] Mammalian CPR has also been co-expressed with cytochrome P450s for detoxification of water and soil in transgenic plants, however the system is limited by CPR activity.[166] Cytochrome P450s are also widely employed as biocatalysts for industrial synthesis of numerous chemicals, food ingredients, and pharmaceuticals.[167,168] Thus, strategies to maximize the catalytic efficiency of the cytochrome P450-CPR system are desired to further develop these biocatalysts for commercial and medicinal use. This research thesis provides the structural platform on which to modulate the catalytic performance of MSR and CPR.

Bibliography

1. Colibus, L. D., and Mattevi, A. (2006) New Frontiers in Structural Flavoenzymology. *Current Opinion in Structural Biology 16*, 722–728.

2. Fagan, R. L., and Palfey, B. A. In *Flavin-Dependent Enzymes*; Begley, T. P., Ed.; Comprehensive Natural Products II: Volume 7; Elsevier, 2010; pp 37–114.

3. Ezkurdia, I., Juan, D., Rodriguez, J. M., Frankish, A., Diekhans, M., Harrow, J., Vazquez, J., Valencia, A., and Tress, M. L. (2014) Multiple Evidence Strands Suggest That There May be as Few as 19 000 Human Protein-Coding Genes. *Human Molecular Genetics 23*, 5866–78.

4. Lienhart, W. D., Gudipati, V., and Macheroux, P. (2013) The Human Flavoproteome. *Archives of Biochemistry and Biophysics 535*, 150–162.

5. Macheroux, P., Kappes, B., and Ealick, S. E. (2011) Flavogenomics–a Genomic and Structural View of Flavin-Dependent Proteins. *Federation of European Biochemical Societies Journal 278*, 2625–2634.

6. Tomiki, T., and Saitou, N. (2004) Phylogenetic Analysis of Proteins Associated in the Four Major Energy Metabolism Systems: Photosynthesis, Aerobic Respiration, Denitrification, and Sulfur Respiration. *Journal of Molecular Evolution 59*, 158–176.

7. Jorns, M. S., Wang, B., and Jordan, S. (1987) DNA Repair Catalyzed by *Escherichia coli* DNA Photolyase Containing Only Reduced Flavin: Elimination of the Enzyme's Second chromophore by Reduction with Sodium Borohydride. *Biochemistry 26*, 6810–6816.

8. Sancar, A. (2004) Regulation of the Mammalian Circadian Clock by Cryptochrome. *Journal of Biological Chemistry 279*, 34079–34082.

9. van Berkel, W. J. H., and Joosten, W. (2007) Flavoenzymes. *Current Opinion in Chemical Biology 11*, 195–202.

10. Gropper, S., and Smith, J. L. *Advanced Nutrition and Human Metabolism*, sixth ed.; Wadsworth Publishing: Belmont, California, 2012.

11. Blyth, A. W. *A Manual of Practical Chemistry: The Analysis of Foods and the Detection of Poisons*; Charles Griffin and Company, 1879.

12. Karrer, P., Salomon, H., Schopp, K., Benz, F., and Becker, B. (1935) Synthesen Von Drei Weiteren Stereoisomeren Des Lactoflavins (German)[Syntheses of Three Stereoisomers of Lactoflavins]. *Helvetica Chimica Acta 18*, 908–910.

13. Kuhn, R., Reinemund, K., and Weygand, F. (1934) Synthese des Lumi-Lactoflavins (German)[Synthesis of Lumi-lactoflavins]. *Berichte der Deutschen Chemischen Gesellschaft (A and B Series) 67*, 1460–1462.

14. Massey, V. (2000) The Chemical and Biological Versatility of Riboflavin. *Biochemical Society Transactions 28*, 283–296.

15. Warburg, O., and Christian, W. (1933) Uber Das Gelbe Ferment und Seine Wirkungen (German) [About the Yellow Enzyme and its Effects]. *Biochemische Zeitschrift 266*, 377–411.

16. Theorell, H. (1935) Preparation in Pure State of the Effect Group of Yellow Enzymes. *Biochemische Zeitschrift 275*, 344–346.

17. Warburg, O., and Christian, W. (1938) Isolierung Der Prosthetischen Gruppe Der D-Aminosaureoxydase (German)[Isolation of the Prosthetic Group of D-Aminosaureoxydase]. *Biochemische Zeitschrift 298*, 81.

18. Powers, H. J. (2003) Riboflavin (Vitamin B2) and Health. *The American Journal of Clinical Nutrition 77*, 1352–1360.

19. Koser, S. A. *Vitamin Requirements of Bacteria and Yeasts.*; Charles C. Thomas: Springfield, IL, 1968.

20. Bender, D. A. *Nutritional Biochemistry of the Vitamins*, second edition ed.; Press Syndicate of the University of Cambridge: Cambridge, United Kingdom, 2003.

21. Said, H. M., and Mohammed, Z. M. (2006) Intestinal Absorption of Water-Soluble Vitamins: An Update. *Current Opinion in Gastroenterology 22*, 140–146.

22. Moriyama, Y. (2011) Riboflavin Transporter is Finally Identified. *Journal of Biochemistry 150*, 341–343.

23. White, H., and Merrill, A. (1988) Riboflavin-Binding Proteins. *Annual Review of Nutrition 8*, 279–299.

24. Miura, R. (2001) Versatility and Specificity in Flavoenzymes: Control Mechanisms of Flavin Reactivity. *Chemical Record (New York, N.Y.) 1*, 183–194.

25. Muller, F., Grande, H. J., Harding, L. J., Dunham, W. R., Visser, A. J., Reinders, J. H., Hemmerich, P., and Ehrenberg, A. (1981) On the Molecular and Submolecular Structure of the Semiquinone Cations of Alloxazines and Isoalloxazines as Revealed by Electron-Paramagnetic-Resonance Spectroscopy. *European Journal of Biochemistry 116*, 17–25.

26. Hefti, M. H., Vervoort, J., and van Berkel, W. J. H. (2003) Deflavination and Reconstitution of Flavoproteins. *Federation of European Biochemical Societies Journal 270*, 4227–4242.

27. Mewies, M., McIntire, W. S., and Scrutton, N. S. (1998) Covalent Attachment of Flavin Adenine Dinucleotide (FAD) and Flavin Mononucleotide (FMN) to Enzymes: The Current State of Affairs. *Protein Science 7*, 7–20.

28. Thorpe, C., and Kim, J. J. (1995) Structure and Mechanism of Action of the Acyl-CoA Dehydrogenases. *Federation of American Societies for Experimental Biochemistry Journal 9*, 718–725.

29. Tishkov, V. I., and Khoronenkova, S. V. (2005) D-Amino Acid Oxidase: Structure, Catalytic Mechanism, and Practical Application. *Biochemistry 70*, 40–54.

30. Khoronenkova, S., and Tishkov, V. (2008) D-Amino Acid Oxidase: Physiological Role and Applications. *Biochemistry (Mosc) 73*, 1511–1518.

31. Ghisla, S., Pollegioni, L., and Molla, G. (2011) Revisitation of the βCl-Elimination Reaction of D-Amino Acid Oxidase: New Interpretation of the Reaction That Sparked Flavoprotein Dehydrogenation Mechanisms. *Journal of Biological Chemistry 286*, 40987–40998.

32. Entsch, B., Cole, L. J., and Ballou, D. P. (2005) Protein Dynamics and Electrostatics in the Function of p-Hydroxybenzoate Hydroxylase. *Archives of Biochemistry and Biophysics 433*, 297–311.

33. Gatti, D., Palfey, B., Lah, M., Entsch, B., Massey, V., Ballou, D., and Ludwig, M. (1994) The Mobile Flavin of 4-OH Benzoate Hydroxylase. *Science 266*, 110–114.

34. Carell, T., Burgdorf, L. T., Kundu, L. M., and Cichon, M. (2001) The Mechanism of Action of DNA Photolyases. *Current Opinion in Chemical Biology 5*, 491–498.

35. Lucas-Lledo, J. I., and Lynch, M. (2009) Evolution of Mutation Rates: Phylogenomic Analysis of the Photolyase/Cryptochrome Family. *Journal of Biology and Evolution 26*, 1143–1153.

36. Park, H., Kim, S., Sancar, A., and Deisenhofer, J. (1995) Crystal Structure of DNA Photolyase From *Escherichia coli*. *Science 268*, 1866–1872.

37. Weber, S. (2005) Light-Driven Enzymatic Catalysis of DNA Repair: A Review of Recent Biophysical Studies on Photolyase. *Biochimica et Biophysica Acta - Bioenergetics 1707*, 1–23.

38. Watson, J. A., McTamney, P. M., Adler, J. M., and Rokita, S. E. (2008) Flavoprotein Iodotyrosine Deiodinase Functions Without Cysteine Residues. *Chembiochem 9*, 504–506.

39. Stanbury, J. B. (1960) Deiodination of the Iodinated Amino Acids. *Annals of the New York Academy of Sciences 86*, 417–439.

40. Bianco, A. C., Salvatore, D., Gereben, B., Berry, M. J., and Larsen, P. R. (2002) Biochemistry, Cellular and Molecular Biology, and Physiological Roles of the Iodothyronine Selenodeiodinases. *Endocrine Reviews 23*, 38–89.

41. Hu, J., Chuenchor, W., and Rokita, S. E. (2014) A Switch Between One- and Two-Electron Chemistry of the Human Flavoprotein Iodotyrosine Deiodinase is Controlled by Substrate. *Journal of Biological Chemistry*

42. Avron, M., and Jagendorf, A. T. (1956) A TPNH Diaphorase from Chloroplasts. *Archives of Biochemistry and Biophysics 65*, 475–490.

43. Arnon, D. I. (1965) Ferredoxin and Photosynthesis. *Science 149*, 1460–1470.

44. Karplus, P., Daniels, M., and Herriott, J. (1991) Atomic Structure of Ferredoxin-NADP+ Reductase: Prototype for a Structurally Novel Flavoenzyme Family. *Science 251*, 60–66.

45. Correll, C. C., Ludwig, M. L., Bruns, C. M., and Karplus, P. A. (1993) Structural Prototypes for an Extended Family of Flavoprotein Reductases: Comparison of Phthalate Dioxygenase Reductase with Ferredoxin Reductase and Ferredoxin. *Protein Science 2*, 2112–2133.

46. Aliverti, A., Pandini, V., Pennati, A., de Rosa, M., and Zanetti, G. (2008) Structural and Functional Diversity of Ferredoxin-NADP+ Reductases. *Archives of Biochemistry and Biophysics 474*, 283–291.

47. Zeghouf, M., Fontecave, M., Macherel, D., and Coves, J. (1998) The Flavoprotein Component of the *Escherichia coli* Sulfite Reductase: Expression, Purification, and Spectral and Catalytic Properties of a Monomeric Form Containing Both the Flavin Adenine Dinucleotide and the Flavin Mononucleotide Cofactors. *Biochemistry 37*, 6114–6123.

48. Narhi, L. O., and Fulco, A. J. (1987) Identification and Characterization of Two Functional Domains in Cytochrome P450BM3, a Catalytically Self-Sufficient Monooxygenase Induced by Barbiturates in *Bacillus megaterium*. *Journal of Biological Chemistry 262*, 6683–6690.

49. Wang, M., Roberts, D. L., Paschke, R., Shea, T. M., Masters, B. S., and Kim, J. J. (1997) Three-Dimensional Structure of NADPH-Cytochrome P450 Reductase: Prototype for FMN- and FAD-Containing Enzymes. *Proceedings of the National Academy of Sciences of the United States of America 94*, 8411–8416.

50. Masters, B. S., McMillan, K., Sheta, E. A., Nishimura, J. S., Roman, L. J., and Martasek, P. (1996) Neuronal Nitric Oxide Synthase, a Modular Enzyme Formed by Convergent Evolution: Structure Studies of a Cysteine Thiolate-Liganded Heme Protein That Hydroxylates L-Arginine to Produce NO as a Cellular Signal. *Federation of American Societies for Experimental Biology Journal 10*, 552–558.

51. Stuehr, D. J. (1997) Structure-Function Aspects in the Nitric Oxide Synthases. *Annual Review of Pharmacology and Toxicology 37*, 339–359.

52. Olteanu, H., and Banerjee, R. (2001) Human Methionine Synthase Reductase, a Soluble P450 Reductase-like Dual Flavoprotein, is Sufficient for NADPH-Dependent Methionine Synthase Activation. *Journal of Biological Chemistry 276*, 35558–35563.

53. Paine, M. J. I., Garner, A. P., Powell, D., Sibbald, J., Sales, M., Pratt, N., Smith, T., Tew, D. G., and Wolf, C. R. (2000) Cloning and Characterization of a Novel Human Dual Flavin Reductase. *Journal of Biological Chemistry 275*, 1471–1478.

54. Porter, T. D., and Kasper, C. B. (1986) NADPH-Cytochrome P450 Oxidoreductase: Flavin Mononucleotide and Flavin Adenine Dinucleotide Domains Evolved From Different Flavoproteins. *Biochemistry 25*, 1682–1687.

55. Phillips, A. H., and Langdon, R. G. (1962) Hepatic Triphosphopyridine Nucleotide-Cytochrome c Reductase: Isolation, Characterization, and Kinetic Studies. *Journal of Biological Chemistry 237*, 2652–2660.

56. Zhao, Q., Modi, S., Smith, G., Paine, M., Mcdonagh, P. D., Wolf, C. R., Tew, D., Lian, L.-Y., Roberts, G. C. K., and Driessen, H. P. C. (1999) Crystal Structure of the FMN-Binding Domain of Human Cytochrome P450 Reductase at 1.93 Angstrom Resolution. *Protein Science 8*, 298–306.

57. Xia, C., Hamdane, D., Shen, A. L., Choi, V., Kasper, C. B., Pearl, N. M., Zhang, H., Im, S. C., Waskell, L., and Kim, J. J. (2011) Conformational Changes of NADPH-Cytochrome P450 Oxidoreductase are Essential for Catalysis and Cofactor Binding. *Journal of Biological Chemistry 286*, 16246–16260.

58. Andersen, J. F., Utermohlen, J. G., and Feyereisen, R. (1994) Expression of Housefly CYP6A1 and NADPH-Cytochrome P450 Reductase in *Escherichia coli* and Reconstitution of an Insecticide-Metabolizing P450 System. *Biochemistry 33*, 2171–2177.

59. Hamdane, D., Xia, C., Im, S. C., Zhang, H., Kim, J. J., and Waskell, L. (2009) Structure and Function of an NADPH-Cytochrome P450 Oxidoreductase in an Open Conformation Capable of Reducing Cytochrome P450. *Journal of Biological Chemistry 284*, 11374–11384.

60. Shen, A. L., Sem, D. S., and Kasper, C. B. (1999) Mechanistic Studies on the Reductive Half-Reaction of NADPH-Cytochrome P450 Oxidoreductase. *Journal of Biological Chemistry 274*, 5391–5398.

61. Hubbard, P. A., Shen, A. L., Paschke, R., Kasper, C. B., and Kim, J.-J. P. (2001) NADPH-Cytochrome P450 Oxidoreductase: Structural Basis for Hydride and Electron Transfer. *Journal of Biological Chemistry 276*, 29163–29170.

62. Deng, Z., Aliverti, A., Zanetti, G., Arakaki, A. K., Ottado, J., Orellano, E. G., Calcaterra, N. B., Ceccarelli, E. A., Carrillo, N., and Karplus, P. A. (1999) A Productive NADP+ Binding Mode of Rerredoxin-NADP+ Reductase Revealed by Protein Engineering and Crystallographic Studies. *Nature Structural Biology 6*, 847–853.

63. Piubelli, L., Aliverti, A., Arakaki, A. K., Carrillo, N., Ceccarelli, E. A., Karplus, P. A., and Zanetti, G. (2000) Competition Between C-Terminal Tyrosine and Nicotinamide Modulates Pyridine Nucleotide Affinity and Specificity in Plant Ferredoxin-NADP+ Reductase. *Journal of Biological Chemistry 275*, 10472–10476.

64. Grunau, A., Paine, M. J., Ladbury, J. E., and Gutierrez, A. (2006) Global Effects of the Energetics of Coenzyme Binding:NADPH Controls the Protein Interaction Properties of Human Cytochrome P450 Reductase. *Biochemistry 45*, 1421–1434.

65. Wolthers, K. R., Lou, X., Toogood, H. S., Leys, D., and Scrutton, N. S. (2007) Mechanism of Coenzyme Binding to Human Methionine Synthase Reductase Revealed Through the Crystal Structure of the FNR-like Module and Isothermal Titration Calorimetry. *Biochemistry 46*, 11833–11844.

66. Munro, A. W., Noble, M. A., Robledo, L., Daff, S. N., and Chapman, S. K. (2001) Determination of the Redox Properties of Human NADPH-Cytochrome P450 Reductase. *Biochemistry 40*, 1956–1963.

67. Gutierrez, A., Lian, L.-Y., Wolf, C. R., Scrutton, N. S., and Roberts, G. C. K. (2001) Stopped-Flow Kinetic Studies of Flavin Reduction in Human Cytochrome P450 Reductase and its Component Domains. *Biochemistry 40*, 1964–1975.

68. Oprian, D. D., and Coon, M. J. (1982) Oxidation-Reduction States of FMN and FAD in NADPH-Cytochrome P450 Reductase During Reduction by NADPH. *Journal of Biological Chemistry 257*, 8935–8944.

69. Iyanagi, T., Makino, N., and Mason, H. (1974) Redox Properties of the Reduced Nicotinamide Adenine Dinucleotide Phosphate-Cytochrome P450 and Reduced Nicotinamide Adenine Dinucleotide-Cytochrome b5 Reductases. *Biochemistry 13*, 1701–1710.

70. Sadeghi, S. J., Fantuzzi, A., and Gilardi, G. (2011) Breakthrough in P450 Bioelectrochemistry and Future Perspectives. *Biochimica et Biophysica Acta 1814*, 237–248.

71. Das, A., Grinkova, Y. V., and Sligar, S. G. (2007) Redox Potential Control by Drug Binding to Cytochrome P450 3A4. *Journal of the American Chemical Society 129*, 13778–13779.

72. Das, A., and Sligar, S. G. (2009) Modulation of the Cytochrome P450 Reductase Redox Potential by the Phospholipid Bilayer. *Biochemistry 48*, 12104–12112.

73. Ellis, J., Gutierrez, A., Barsukov, I. L., Huang, W.-C., Grossmann, J. G., and Roberts, G. C. K. (2009) Domain Motion in Cytochrome P450 Reductase: Conformation Equilibria Revealed by NMR and Small-Angle X-Ray Scattering. *Journal of Biological Chemistry 284*, 36628–36637.

74. Vincent, B., Morellet, N., Fatemi, F., Aigrain, L., Truan, G., Guittet, E., and Lescop, E. (2012) The Closed and Compact Domain Organization of the 70-kDa Human Cytochrome P450 Reductase in its Oxidized State as Revealed by NMR. *Journal of Molecular Biology 420*, 296–309.

75. Pudney, C., Khara, B., Johannissen, L., and Scrutton, N. (2011) Coupled Motions Direct Electrons Along Human Microsomal P450 Chains. *Public Library of Science Biology 9*.

76. Huang, W., Ellis, J., Moody, P., Raven, E., and Roberts, G. (2013) Redox-Linked Domain Movements in the Catalytic Cycle of Cytochrome P450 Reductase. *Structure 21*, 1581–1589.

77. Enoch, H. G., and Strittmatter, P. (1979) Cytochrome b5 Reduction by NADPH-Cytochrome P450 Reductase. *Journal of Biological Chemistry 254*, 8976–8981.

78. Ono, T., and Bloch, K. (1975) Solubilization and Partial Characterization of Rat Liver Squalene Epoxidase. *Journal of Biological Chemistry 250*, 1571–1579.

79. Schacter, B. A., Nelson, E. B., Marver, H. S., and Masters, B. S. (1972) Immunochemical Evidence for an Association of Heme Oxygenase With the Microsomal Electron Transport System. *Journal of Biological Chemistry 247*, 3601–3607.

80. Omura, T., and Sato, R. (1962) A New Cytochrome in Liver Microsomes. *Journal of Biological Chemistry 237*, PC1375–PC1376.

81. Strobel, H., Hodgson, A., and Shen, S. *Cytochrome P450: Structure, Mechanism and Biochemistry*, second edition ed.; Plenum Press: New York, 1995.

82. Nelson, D. R., Schuler, M. A., Paquette, S. M., Werck-Reichhart, D., and Bak, S. (2004) Comparative Genomics of Rice and *Arabidopsis*. Analysis of 727 Cytochrome P450 genes and Pseudogenes from a Monocot and a Dicot. *Plant Physiology 135*, 756–772.

83. Wilkinson, G. R. (2005) Drug Metabolism and Variability Among Patients in Drug Response. *New England Journal of Medicine 352*, 2211–2221.

84. Meunier, B., Visser, S. P. D., and Shaik, S. (2004) Mechanism of Oxidation Reactions Catalyzed by Cytochrome P450 Enzymes. *Chemical Reviews 104*, 3947–3980.

85. Sono, M., Roach, M. P., Coulter, E. D., and Dawson, J. H. (1996) Heme-Containing Oxygenases. *Chemical Reviews 96*, 2841–2888.

86. Guengerich, F. P. (1992) Characterization of Human Cytochrome P450 Enzymes. *Federation of American Societies for Experimental Biology Journal 6*, 745–748.

87. De Montellano, P. R. O. *Cytochrome P450: Structure, Mechanism, and Biochemistry*; Springer, 2005.

88. Groves, J. T., and McClusky, G. A. (1976) Aliphatic Hydroxylation Via Oxygen Rebound. Oxygen Transfer Catalyzed by Iron. *Journal of the American Chemical Society 98*, 859–861.

89. Hasemann, C. A., Kurumbail, R. G., Boddupalli, S. S., Peterson, J. A., and Deisenhofer, J. (1995) Structure and Function of Cytochromes P450:A Comparative Analysis of Three Crystal Structures. *Structure 3*, 41–62.

90. Williams, P. A., Cosme, J., Sridhar, V., Johnson, E. F., and McRee, D. E. (2000) Mammalian Microsomal Cytochrome P450 Monooxygenase: Structural Adaptations for Membrane Binding and Functional Diversity. *Molecular Cell 5*, 121–131.

91. Nelson, D. R. (2009) The Cytochrome P450 Homepage. *Human Genomics 4*, 59–65.

92. Mao, G., Seebeck, T., Schrenker, D., and Yu, O. (2013) CYP709B3, a Cytochrome P450 Monooxygenase Gene Involved in Salt Tolerance in *Arabidopsis thaliana*. *BioMedCentral Plant Biology 13*, 169.

93. Anzenbacher, P., and Anzenbacherova, E. (2001) Cytochromes P450 and Metabolism of Xenobiotics. *Cellular and Molecular Life Sciences 58*, 737–747.

94. Scott, R. R., and Miller, W. L. (2008) Genetic and Clinical Features of P450 Oxidoreductase Deficiency. *Hormone Research in Pediatrics 69*, 266–275.

95. Pandey, A. V., and Fluck, C. E. (2013) NADPH P450 Oxidoreductase: Structure, Function, and Pathology of Diseases. *Pharmacology & Therapeutics 138*, 229–254.

96. Zhang, X., Li, L., Ding, X., and Kaminsky, L. S. (2011) Identification of Cytochrome P450 Oxidoreductase Gene Variants That are Significantly Associated with the Interindividual Variations in Warfarin Maintenance Dose. *Drug Metabolism and Disposition 39*, 1433–1439.

97. Hart, S. N., Wang, S., Nakamoto, K., Wesselman, C., Li, Y., and Zhong, X. (2008) Genetic Polymorphisms in Cytochrome P450 Oxidoreductase Influence Microsomal P450-Catalyzed Drug Metabolism. *Pharmacogenetics and Genomics 18*, 11–24.

98. Huang, N., Pandey, A. V., Reardon, W., Lapunzina, P. D., Mowat, D., Jabs, E. W., Vliet, G. V., Sack, J., and Fluck, C. E. (2005) Diversity and Function of Mutations in P450 Oxidoreductase in Patients with Antley-Bixler Syndrome and Disordered Steroidogenesis. *The American Journal of Human Genetics 76*, 729–749.

99. Miller, W. L. (2004) P450 Oxidoreductase Deficiency: A New Disorder of Steroidogenesis With Multiple Clinical Manifestations. *Trends in Endocrinology and Metabolism 15*, 311–315.

100. Henderson, C. J., Otto, D. M., Carrie, D., Magnuson, M. A., McLaren, A. W., Rosewell, I., and Wolf, C. R. (2003) Inactivation of the Hepatic Cytochrome P450 System by Conditional Deletion of Hepatic Cytochrome P450 Reductase. *Journal of Biological Chemistry 278*, 13480–13486.

101. Shen, A. L., O'Leary, K. A., and Kasper, C. B. (2002) Association of Multiple Developmental Defects and Embryonic Lethality with Loss of Microsomal NADPH-Cytochrome P450 Oxidoreductase. *Journal of Biological Chemistry 277*, 6536–6541.

102. Gu, J., Weng, Y., Zhang, Q.-Y., Cui, H., Behr, M., Wu, L., Yang, W., Zhang, L., and Ding, X. (2003) Liver-Specific Deletion of the NADPH-Cytochrome P450 Reductase Gene Impact on Plasma Cholesterol Homeostasis and the Function and Regulation of Microsomal Cytochrome P450 and Heme Oxygenase. *Journal of Biological Chemistry 278*, 25895–25901.

103. Leclerc, D., Wilson, A., Dumas, R., Gafuik, C., Song, D., Watkins, D., Heng, H. H., Rommens, J. M., Scherer, S. W., Rosenblatt, D. S., and Gravel, R. A. (1998) Cloning and Mapping of a cDNA for Methionine Synthase Reductase, a Flavoprotein Defective in Patients With Homocystinuria. *Proceedings of the National Academy of Sciences of the United States of America 95*, 3059–3064.

104. Froese, D. S., Wu, X., Zhang, J., Dumas, R., Schoel, W. M., Amrein, M., and Gravel, R. A. (2008) Restricted Role for Methionine Synthase Reductase Defined by Subcellular Localization. *Molecular Genetics and Metabolism 94*, 68–77.

105. Wolthers, K. R., Basran, J., Munro, A. W., and Scrutton, N. S. (2003) Molecular Dissection of Human Methionine Synthase Reductase: Determination of the Flavin Redox Potentials in Full-Length Enzyme and Isolated Flavin-Binding Domains. *Biochemistry 42*, 3911–3920.

106. Jarrett, J. T., Hoover, D. M., Ludwig, M. L., and Matthews, R. G. (1998) The Mechanism of Adenosylmethionine-Dependent Activation of Methionine Synthase: A Rapid Kinetic Analysis of Intermediates in Reductive Methylation of Cob(II)alamin Enzyme. *Biochemistry 37*, 12649–12658.

107. Yamada, K., Gravel, R. A., Toraya, T., and Matthews, R. G. (2006) Human Methionine Synthase Reductase is a Molecular Chaperone for Human Methionine

Synthase. *Proceedings of the National Academy of Sciences of the United States of America 103*, 9476–9481.

108. Banerjee, R. V., and Matthews, R. G. (1990) Cobalamin-Dependent Methionine Synthase. *Federation of American Societies for Experimental Biology 4*, 1450–1459.

109. Fujimori, D. (2013) Radical SAM-Mediated Methylation Reactions. *Current Opinion in Chemical Biology 17*, 597–604.

110. Boldyrev, A. A. (2009) Molecular Mechanisms of Homocysteine Toxicity. *Biochemistry (Mosc) 74*, 589–598.

111. Evans, J. C., Huddler, D. P., Hilgers, M. T., Romanchuk, G., Matthews, R. G., and Ludwig, M. L. (2004) Structures of the N-Terminal Modules Imply Large Domain Motions During Catalysis by Methionine Synthase. *Proceedings of the National Academy of Sciences of the United States of America 101*, 3729–3736.

112. Drennan, C. L., Huang, S., Drummond, J. T., Matthews, R. G., and Ludwig, M. (1994) How a Protein Binds B12: A 3.0 Angstrom X-Ray Structure of B12-Binding Domains of Methionine Synthase. *Science 266*, 1669–1674.

113. Wolthers, K. R., and Scrutton, N. S. (2007) Protein Interactions in the Human Methionine Synthase-Methionine Synthase Reductase Complex and Implications for the Mechanism of Enzyme Reactivation. *Biochemistry 46*, 6696–6709.

114. Olteanu, H., Munson, T., and Banerjee, R. (2002) Differences in the Efficiency of Reductive Activation of Methionine Synthase and Exogenous Electron Acceptors Between the Common Polymorphic Variants of Human Methionine Synthase Reductase. *Biochemistry 41*, 13378–13385.

115. Olteanu, H., Wolthers, K. R., Munro, A. W., Scrutton, N. S., and Banerjee, R. (2004) Kinetic and Thermodynamic Characterization of the Common Polymorphic Variants of Human Methionine Synthase Reductase. *Biochemistry 43*, 1988–1997.

116. van der Linden, I. J., den Heijer, M., Afman, L. A., Gellekink, H., Vermeulen, S. H. H. M., Kluijtmans, L. A. J., and Blom, H. J. (2006) The Methionine Synthase Reductase 66AG Polymorphism is a Maternal Risk Factor for Spina Bifida. *Journal of Molecular Medicine 84*, 1047–1054.

117. Coppede, F., Bosco, P., Lorenzoni, V., Denaro, M., Anello, G., Antonucci, I., Barone, C., Stuppia, L., Romano, C., and Migliore, L. (2014) The MTRR 66AG Polymorphism and Maternal Risk of Birth of a Child with Down Syndrome in

Caucasian Women: A CaseControl Study and a Meta-Analysis. *Molecular Biology Reports 41*, 5571–5583.

118. Ouyang, S., Li, Y., Liu, Z., Chang, H., and Wu, J. (2013) Association Between MTR A2756G and MTRR A66G Polymorphisms and Maternal Risk for Neural Tube Defects: A Meta-Analysis. *Gene 515*, 308–312.

119. Bosco, P., Gueant-Rodriguez, R.-M., Anello, G., Barone, C., Namour, F., Caraci, F., Romano, A., Romano, C., and Gueant, J.-L. (2003) Methionine Synthase (MTR) (AG) Polymorphism, Double Heterozygosity Methionine Synthase AG Methionine Synthase Reductase (MTRR) 66 AG, and Elevated Homocysteinemia are Three Risk Factors for Having a Child with Down Syndrome. *American Journal of Medical Genetics Part A 121A*, 219–224.

120. Wilson, A., Platt, R., Wu, Q., Leclerc, D., Christensen, B., Yang, H., Gravel, R. A., and Rozen, R. (1999) A Common Variant in Methionine Synthase Reductase Combined with Low Cobalamin (Vitamin B12) Increases Risk for Spina Bifida. *Molecular Genetics and Metabolism 67*, 317–323.

121. Watkins, D., and Rosenblatt, D. S. (1988) Genetic Heterogeneity Among Patients with Methylcobalamin Deficiency. Definition of Two Complementation Groups, cblE and cblG. *The Journal of Clinical Investigation 81*, 1690–1694.

122. Wilson, A., Leclerc, D., Rosenblatt, D. S., and Gravel, R. A. (1999) Molecular Basis for Methionine Synthase Reductase Deficiency in Patients Belonging to the cblE Complementation Group of Disorders in Folate/Cobalamin Metabolism. *Human Molecular Genetics 8*, 2009–2016.

123. Elmore, C. L., Wu, X., Leclerc, D., Watson, E. D., Bottiglieri, T., Krupenko, N. I., Krupenko, S. A., Cross, J. C., Rozen, R., Gravel, R. A., and Matthews, R. G. (2007) Metabolic Derangement of Methionine and Folate Metabolism in Mice Deficient in Methionine Synthase Reductase. *Molecular genetics and metabolism 91*, 85–97.

124. Wald, D. S., Law, M., and Morris, J. K. (2002) Homocysteine and Cardiovascular Disease: Evidence on Causality from a Meta-Analysis. *British Medical Journal 325*, 1202.

125. Castro, R., Rivera, I., Blom, H. J., Jakobs, C., and de Almeida, I. T. (2006) Homocysteine Metabolism, Hyperhomocysteinaemia and Vascular Disease: An Overview. *Journal of Inherited Metabolic Disease 29*, 3–20.

126. van der Put, N. M., van Straaten, H. W. M., Trijbels, F. J. M., and Blom, H. J. (2001) Folate, Homocysteine and Neural Tube Defects: An Overview. *Experimental Biology and Medicine 226*, 243–270.

127. Zhang, J., Martsek, P., Paschke, R., Shea, T., Masters, B. S. S., and Kim, J.-J. P. (2001) Crystal Structure of the FAD/NADPH-Binding Domain of Rat Neuronal Nitric-Oxide Synthase: Comparisons With NADPH-cytochrome P450 Oxidoreductase. *Journal of Biological Chemistry 276*, 37506–37513.

128. Sem, D. S., and Kasper, C. B. (1992) Geometric Relationship Between the Nicotinamide and Isoalloxazine Rings in NADPH-Cytochrome P450 Oxidoreductase: Implications for the Classification of Evolutionarily and Functionally Related Flavoproteins. *Biochemistry 31*, 3391–3398.

129. Orellano, E. G., Calcaterra, N. B., Carrillo, N., and Ceccarelli, E. A. (1993) Probing the Role of the Carboxyl-Terminal Region of Ferredoxin-NADP+ Reductase by Site-Directed Mutagenesis and Deletion Analysis. *Journal of Biological Chemistry 268*, 19267–19273.

130. Adak, S., Sharma, M., Meade, A. L., and Stuehr, D. J. (2002) A Conserved Flavin-Shielding Residue Regulates NO Synthase Electron Transfer and Nicotinamide Coenzyme Specificity. *Proceedings of the National Academy of Sciences of the United States of America 99*, 13516–13521.

131. Konas, D. W., Zhu, K., Sharma, M., Aulak, K. S., Brudvig, G. W., and Stuehr, D. J. (2004) The FAD-Shielding Residue Phe1395 Regulates Neuronal Nitric Oxide Synthase Catalysis by Controlling NADP+ Affinity and a Conformational Equilibrium Within the Flavoprotein Domain. *Journal of Biological Chemistry 279*, 35412–35425.

132. Dohr, O., Paine, M. J. I., Friedberg, T., Roberts, G. C. K., and Wolf, C. R. (2001) Engineering of a Functional Human NADH-Dependent Cytochrome P450 System. *Proceedings of the National Academy of Sciences of the United States of America 98*, 81–86.

133. Wolthers, K. R., and Scrutton, N. S. (2004) Electron Transfer in Human Methionine Synthase Reductase Studied by Stopped-Flow Spectrophotometry. *Biochemistry 43*, 490–500.

134. Batie, C. J., and Kamin, H. (1986) Association of Ferredoxin-NADP+ Reductase with NADP(H) Specificity and Oxidation-Reduction Properties. *Journal of Biological Chemistry 261*, 11214–11223.

135. Murataliev, M. B., and Feyereisen, R. (2000) Interaction of NADP(H) With Oxidized and Reduced P450 Reductase During Catalysis. Studies With Nucleotide Analogues. *Biochemistry 39*, 5066–5074.

136. Meints, C. E., Gustafsson, F. S., Scrutton, N. S., and Wolthers, K. R. (2011) Tryptophan 697 Modulates Hydride and Interflavin Electron Transfer in Human Methionine Synthase Reductase. *Biochemistry 50*, 11131–11142.

137. Gutierrez, A., Doehr, O., Paine, M., Wolf, C. R., Scrutton, N. S., and Roberts, G. C. K. (2000) Trp-676 Facilitates Nicotinamide Coenzyme Exchange in the Reductive Half-Reaction of Human Cytochrome P450 Reductase:Properties of the Soluble W676H and W676A Mutant Reductases. *Biochemistry 39*, 15990–15999.

138. Gutierrez, A., Paine, M., Wolf, C. R., Scrutton, N. S., and Roberts, G. C. K. (2002) Relaxation Kinetics of Cytochrome P450 Reductase:Internal Electron Transfer is Limited by Conformational Change and Regulated by Coenzyme Binding. *Biochemistry 41*, 4626–4637.

139. Viola, R., Cook, P., and Cleland, W. (1979) Stereoselective Preparation of Deuterated Reduced Nicotinamide Adenine Nucleotides and Substrates by Enzymatic Synthesis. *Analytical Biochemistry 96*, 334–340.

140. Dutton, P. (1978) Redox Potentiometry: Determination of Midpoint Potentials of Oxidation-Reduction Components of Biological Electron Transfer Systems. *Methods in Enzymology 54*, 411–435.

141. Haque, M., Bayachou, M. A., Fadlalla, D. D., and Stuehr, D. J. (2013) Charge-Pairing Interactions Control the Conformational Setpoint and Motions of the FMN Domain in Neuronal Nitric Oxide Synthase. *Biochemical Journal 450*, 607–617.

142. Jenner, M., Ellis, J., Huang, W.-C., LloydRaven, E., Roberts, G. C. K., and Oldham, N. J. (2011) Detection of a Protein Conformational Equilibrium by Electrospray Ionisation-Ion Mobility-Mass Spectrometry. *Angewandte Chemie International Edition 50*, 8291–8294.

143. Dumit, V. I., Essigke, T., Cortez, N., and Ullmann, G. M. (2010) Mechanistic Insights Into FerredoxinNADP(H) Reductase Catalysis Involving the Conserved Glutamate in the Active Site. *Journal of Molecular Biology 397*, 814–825.

144. Meints, C. E., Simtchouk, S., and Wolthers, K. R. (2013) Aromatic Substitution of the FAD-Shielding Tryptophan Reveals its Differential Role in Regulating Electron

Flux in Methionine Synthase Reductase and Cytochrome P450 Reductase. *Federation of European Biological Societies Journal 280*, 1460–1474.

145. Prodromou, C., and Pearl, L. H. (1992) Recursive PCR: A Novel Technique For Total Gene Synthesis. *Protein Engineering 5*, 827–829.

146. World Health Organization, *World Malaria Report 2008*; Nonserial Publication Series; World Health Organization, 2008.

147. Zeng, Q., Qiu, F., and Yuan, L. (2008) Production of Artermisinin by Genetically-Modified Microbes. *Biotechnology Letters 30*, 581–592.

148. Ro, D. K., Paradise, E. M., Ouellet, M., Fisher, K. J., Newman, K. L., Ndungu, J. M., Ho, K. A., Eachus, R. A., Ham, T. S., Kirby, J., Chang, M. C., Withers, S. T., Shiba, Y., Sarpong, R., and Keasling, J. D. (2006) Production of the Antimalarial Drug Precursor Artemisinic Acid in Engineered Yeast. *Nature 440*, 940–943.

149. Chang, M. C., Eachus, R. A., Trieu, W., Ro, D. K., and Keasling, J. D. (2007) Engineering *Escherichia coli* for Production of Functionalized Terpenoids using Plant P450s. *Nature Chemical Biology 3*, 274–277.

150. Simtchouk, S., Eng, J. L., Meints, C. E., Makins, C., and Wolthers, K. R. (2013) Kinetic Analysis of Cytochrome P450 Reductase from *Artemisia annua* Reveals Accelerated Rates of NADPH-Dependent Flavin Reduction. *Federation of European Biochemical Societies Journal 280*, 6627–6642.

151. Sem, D. S., and Kasper, C. B. (1995) Effect of Ionic Strength on the Kinetic Mechanism and Relative Rate Limitation of Steps in the Model NADPH-Cytochrome P450 Oxidoreductase Reaction with Cytochrome C. *Biochemistry 34*, 12768–74.

152. Peregrina, J., Sanchez-Azqueta, A., Herguedas, B., Martinez-Julvez, M., and Medina, M. (2010) Role of Specific Residues in Coenzyme Binding, Charge-Transfer Complex Formation, and Catalysis in *Anabaena* Ferredoxin NADP+-Reductase. *Biochimica et Biophysica Acta 1797*, 1638–46.

153. Lans, I., Medina, M., Rosta, E., Hummer, G., Garcia-Viloca, M., Lluch, J., and Gonzalez-Lafont, A. (2012) Theoretical Study of the Mechanism of the Hydride Transfer Between Ferredoxin-NADP+ Reductase and NADP+: The Role of Tyr303. *Journal of the American Chemical Society 134*, 20544–53.

154. Lans, I., Peregrina, J., Medina, M., Garcia-Viloca, M., Gonzalez-Lafont, A., and Lluch, J. (2010) Mechanism of the Hydride Transfer Between *Anabaena* Tyr303Ser FNR(rd)/FNR(ox) and NADP+/H. A Combined Pre-Steady State Kinetic/Ensemble Averaged Transition-State Theory With Multidimensional Tunneling Study. *Journal of Physical Chemistry 114*, 3368–79.

155. Meints, C. E., Parke, S. M., and Wolthers, K. R. (2014) Proximal FAD Histidine Residue Influences Interflavin Electron Transfer in Cytochrome P450 Reductase and Methionine Synthase Reductase. *Archives of Biochemistry and Biophysics 547*, 18–26.

156. Haque, M., Bayachou, M., Tejero, J., Kenney, C., Pearl, N., Im, S., Waskell, L., and Stuehr, D. (2014) Distinct Conformational Behaviors of Four Mammalian Dual-Flavin Reductases (Cytochrome P450 Reductase, Methionine Synthase Reductase, Neuronal Nitric Oxide Synthase, Endothelial Nitric Oxide Synthase) Determine Their Unique Catalytic Profiles. *Federation of European Biological Societies Journal 281*, 5325–5340.

157. Rigby, S. E., Lou, X., Toogood, H. S., Wolthers, K. R., and Scrutton, N. S. (2011) ELDOR Spectroscopy Reveals That Energy Landscapes in Human Methionine Synthase Reductase are Extensively Remodelled Following Ligand and Partner Protein Binding. *Chembiochem 12*, 863–867.

158. Tejero, J., Martinez-Julvez, M., Mayoral, T., Luquita, A., Sanz-Aparicio, J., Hermoso, J. A., Hurley, J. K., Tollin, G., Gmez-Moreno, C., and Medina, M. (2003) Involvement of the Pyrophosphate and the 2'-Phosphate Binding Regions of Ferredoxin-NADP+ Reductase in Coenzyme Specificity. *Journal of Biological Chemistry 278*, 49203–14.

159. Tejero, J., Perez-Dorado, I., Maya, C., Martinez-Julvez, M., Sanz-Aparicio, J., Gomez-Moreno, C., Hermoso, J., and Medina, M. (2005) C-Terminal Tyrosine of Ferredoxin-NADP+ Reductase in Hydride Transfer Processes with NAD(P)+/H. *Biochemistry 44*, 13477–90.

160. Zavadakova, P., Fowler, B., Suormala, T., Novotna, Z., Mueller, P., Hennermann, J., Zeman, J., Vilaseca, M., Vilarinho, L., Gutsche, S., Wilichowski, E., Horneff, G., and Kozich, V. (2005) cblE Type of Homocystinuria Due to Methionine Synthase Reductase Deficiency: Functional Correction by Minigene Expression. *Human Mutation 25*, 239–47.

161. Watkins, D., and Rosenblatt, D. S. (2011) Inborn Errors of Cobalamin Absorption and Metabolism. *American Journal of Medical Genetics Seminars in Medical Genetics 157*, 33–44.

162. Waddington, S., Kennea, N., Buckley, S., Gregory, L., Themis, M., and Coutelle, C. (2004) Fetal and Neonatal Gene Therapy: Benefits and Pitfalls. *Gene Therapy 11*, S92–7.

163. Jounaidi, Y., and Waxman, D. (2001) Frequent, Moderate-Dose Cyclophosphamide Administration Improves the Efficacy of Cytochrome P450/Cytochrome P450 Reductase-Based Cancer Gene Therapy. *Cancer Research 61*, 4437–44.

164. Chen, L., and Waxman, D. (2002) Cytochrome P450 Gene-Directed Enzyme Prodrug Therapy (GDEPT) for Cancer. *Current Pharmaceutical Design 8*, 1405–16.

165. Roy, P., and Waxman, D. (2006) Activation of Oxazaphosphorines by Cytochrome P450: Application to Gene-Directed Enzyme Prodrug Therapy For Cancer. *Toxicology In Vitro 20*, 176–86.

166. Kumar, S., Jin, M., and Weemhoff, J. (2012) Cytochrome P450-Mediated Phytoremediation Using Transgenic Plants: A Need for Engineered Cytochrome P450 Enzymes. *Journal of Petroleum and Environmental Biotechnology 3*, 1000127.

167. Guengerich, F. (2002) Cytochrome P450 Enzymes in the Generation of Commercial Products. *Nature Reviews Drug Discovery 1*, 359–66.

168. Urlacher, V., Lutz-Wahl, S., and Schmid, R. (2004) Microbial P450 enzymes in Biotechnology. *Applied Microbiology and Biotechnology 64*, 317–25.